The background of the cover is a grayscale micrograph showing the internal structure of a hardening cementitious material. It features a central, large, roughly circular region with a fine, granular texture, surrounded by a network of darker, interconnected lines and patches, representing the complex microstructure of the material during its curing process.

**Microstructure and transport
phenomena in visco-elastic
modelling of hardening
cementitious materials**

H.W.M. van der Ham

**Microstructure and transport phenomena
in visco-elastic modelling
of hardening cementitious materials**

To my unborn child

Microstructure and transport phenomena in visco-elastic modelling of hardening cementitious materials

Proefschrift

ter verkrijging van de graad van doctor
aan de Technische Universiteit van Delft,
op gezag van de Rector Magnificus prof. ir. K.C.A.M. Luyben,
voorzitter van het College voor Promoties,
in het openbaar te verdedigen op

maandag 7 februari 2011 om 15.00 uur
door

Herbert Wenceslaus Maria VAN DER HAM

civiel ingenieur
geboren te Teteringen

Dit proefschrift is goedgekeurd door de promotor:

Prof. dr. ir. K. van Breugel

Copromotor: Dr. ir. E. A. B. Koenders

Samenstelling promotiecommissie:

Rector Magnificus

Prof. dr. ir. K. van Breugel

Dr. ir. E.A.B. Koenders

Prof. J.E. Jonasson

Prof. dr. ir. L. Taerwe

Prof. dr. ir. L. J. Sluys

Dr. P. Acker

Dr. ir. A. de Boer

Prof. dr. ir. E.M. Haas

Voorzitter

Technische Universiteit Delft, promotor

Technische Universiteit Delft, copromotor

Lulea University of Technology, Sweden

Universiteit Gent, Belgium

Technische Universiteit Delft

Lafarge Cement Research Center, France

Ministry of infrastructure and environment

Technische Universiteit Delft, reservelid

ISBN 978-94-6108-132-2

Keywords: Hardening concrete, modelling, visco-elastic behaviour, moisture transport

Copyright © 2011 by Herbert van der Ham

All rights reserved. No part of the material protected by this copyright notice may be reproduced or utilised in any form or by any means, electronic or mechanical, including photocopying, recording or by any information storage and retrieval system, without written permission from the author. Printed by Gildeprint, The Netherlands.

Table of contents

1	INTRODUCTION	1
1.1	GENERAL	1
1.2	AIM OF THIS RESEARCH	5
1.3	RESEARCH QUESTION	5
1.4	STARTING POINT AND SCOPE LIMITATIONS	5
1.5	SCOPE AND THESIS SET-UP	6
2	INITIAL STATE	9
2.1	GENERAL	9
2.2	HYDRATION AND MICROSTRUCTURAL DEVELOPMENT	10
2.2.1	<i>Pixel-based model</i>	12
2.2.2	<i>Particle-based model</i>	13
2.2.3	<i>Evaluation of hydration simulation software</i>	14
2.3	VISCO-ELASTICITY	15
2.3.1	<i>Basic expressions</i>	21
2.3.2	<i>Rheological models</i>	23
2.3.3	<i>Solidification theory</i>	25
2.4	DISCUSSION	33
3	PROPOSED MODEL FOR TIME-DEPENDENT BEHAVIOUR	35
3.1	GENERAL	35
3.2	HOLLOW SHELLS	35
3.3	INTERACTION BETWEEN SHELL AND CORE OF HYDRATING CEMENT GRAINS	37
3.4	FLOW ASPECTS OF THE MODEL	39
3.4.1	<i>Pressure transfer of load bearing water due to particle loading</i>	43
3.4.2	<i>Permeability of CSH-gel</i>	49
3.5	TIME DEPENDENT DEFORMATION OF THE SHELL	50
3.6	CEMENT PASTE	54
3.6.1	<i>Influence of age and degree of hydration at loading</i>	57
3.6.2	<i>Influence of the water/cement ratio</i>	59
3.6.3	<i>Influence of cement fineness</i>	59
3.7	VALIDATION GRID	61
3.8	DISCUSSION	63
4	MOISTURE MOVEMENTS AT MICROLEVEL	65
4.1	MOISTURE STATE IN MICROSTRUCTURES	65
4.2	MODELLING MOISTURE STATE	66
4.3	CONSERVATION OF VOLUME	68
4.3.1	<i>Source and sink</i>	68
4.3.2	<i>Transport components</i>	71
4.4	BALANCE EQUATION	75
4.5	CALCULATED EFFECTS OF MOISTURE MOVEMENTS ON CONCRETE PROPERTIES	77
4.5.1	<i>Influence of moisture transport</i>	77
4.5.2	<i>Transport from ITZ into the bulk paste</i>	78
4.5.3	<i>Influence of water/cement-ratio</i>	79
4.5.4	<i>Influence of cement fineness</i>	83

4.6	VALIDATION GRID	83
4.7	INFLUENCE OF CAPILLARY WATER TRANSPORT ON VISCO-ELASTIC BEHAVIOUR	86
5	EXPERIMENTS AND VALIDATION OF THE PROPOSED MODEL	89
5.1	AIM OF THE EXPERIMENTAL RESEARCH	89
5.2	CEMENT PROPERTIES, CONCRETE MIX COMPOSITION AND MIXING PROCEDURE	91
5.3	EXPERIMENTAL SET-UP	92
5.3.1	<i>Autogenous Deformation Testing Machine</i>	94
5.3.2	<i>Temperature Stress Testing Machine</i>	94
5.4	SUSTAINED LOADING EXPERIMENTS	96
5.4.1	<i>Influence of cement fineness</i>	99
5.4.2	<i>Influence of load sign</i>	101
5.5	RELAXATION EXPERIMENTS	104
5.6	SIMULATION OF EXPERIMENTAL RESULTS	105
5.7	RELIABILITY OF STRESS PREDICTIONS	110
5.8	DISCUSSION	112
6	CONCLUSIONS	113
6.1	EVALUATION	113
6.2	CONCLUSIONS	115
6.3	RECOMMENDATIONS AND OUTLOOK	116
	REFERENCES	119
	APPENDIX A FINITE ELEMENT APPROACH	127
	APPENDIX B DEFORMATIONS OF A HOLLOW SHELL	137
	APPENDIX C HOLLOW SHELLS AND MICROSTRUCTURAL DEVELOPMENT	143
	APPENDIX D PRACTICAL APPLICATION	147
	SUMMARY	167
	SAMENVATTING	169
	ACKNOWLEDGEMENTS	171
	CURRICULUM VITAE	173

1 Introduction

1.1 General

The initial phase of structures, as far as the material properties are considered, is considered as the phase at which the prime properties are “born”. It is also the state at which the consistency of concrete changes from a highly flowable material into a hardened material with a load bearing capacity. One of the major issues that play a role during the initial phase of concrete is the hardening process. During the hardening process of concrete, material properties develop, like strength and stiffness. At the same time, hydration induced deformations may develop, which can be partly restrained. In case of restrained deformations, micro cracks may develop. Depending on the external hardening conditions macro-cracking may develop as well (Figure 1.1). Formation of cracks is of particular importance for the durability of concrete since it may harm the concrete cover layer that protects the reinforcement against the intrusion of aggressive substances (chlorides, CO₂, etc.). Crack free concrete protects the reinforcement from corrosion better than cracked concrete and will improve the durability of a concrete structure. It contributes to a longer service-life which is strongly correlated with the presence of cracks in a structure. Taking into consideration that about 50% of the total budget for infrastructure is spent on monitoring, maintenance and repair of concrete structures [Breugel, 2007], it is evident that there is a strong demand for improving the initial quality of concrete structures.

Controlling and reducing the risk of cracking could contribute to this improvement to a large extent. Reliable predictions of the risk of cracking, however, are still very difficult. The reason for this is that concrete is a very complex material.

Introduction

In general, concrete is a mixture of gravel, sand, cement and water. In most concretes, also additives are added to the mixture to control workability of the fresh mixture and to control the moment at which the properties of the hardened material will start to develop. After many years of research, it is possible to predict strength and stiffness of hardened concrete with sufficient accuracy and reliability. However, the prediction of stresses and the probability of cracking of hardening concrete is still difficult. It has appeared that there is a lack of knowledge about the rheological and time dependent properties and on how to predict these properties. During the reaction between cement and water, a multi-phase transition process takes place. The hydration process liberates heat that, on its turn, leads to an expansion of the concrete. When the hydration process slows down and less heat is produced than is lost to the environment, the temperature in the structure will decrease, resulting in thermal contraction (shrinkage) of the concrete. If restrained, cracking of a structural element may occur (Figure 1.2, top). Besides this, other mechanisms play a role simultaneously. The volume of the formed hydration product is smaller than the volume of the original constituents, i.e. cement and water (chemical shrinkage). This results in a volume reduction of the hardening concrete. Due to the consumption of water by the hydration process, pores will be emptied which results in a reduction of the degree of saturation. This reduction of saturation in the pore structure causes an internal drying (self-desiccation) and an external volume change (autogenous deformations). If internally driven deformations of the hardening concrete (Figure 1.2, middle) are (partly) restraint, for instance if a fresh concrete wall is cast on an already existing slab, tensile stresses will occur. This may significantly harm the durability and the service-life prospect. In the primary stage of hardening, when the hydration heat is liberated and the temperature in the structure increases, predominantly compressive stresses occur, generally without causing harm to the concrete. After the heating stage, the structure cools down. Restraining the deformations on cooling will introduce tensile stresses in the structure and, since concrete has a very low tensile strain capacity, cracks are very likely to occur. The result of this phenomenon is shown in Figure 1.1.



Figure 1.1 Example of water leakage of a cracked concrete wall casted on an existing concrete slab

After many years of research by many researchers, models and calculation procedures have been developed to calculate the stresses during hardening. However, there still exists a significant scatter in performances of models for different mixtures. Hereafter a gap exists between predicted and measured stresses (Figure 1.2, bottom). As a result of this, the reliability of predictions of probability of cracking is still low. This situation shows the need for new research in this field and provides the motivation to evaluate the current state of the art of visco-elastic models and to come up with ideas for improvement of the reliability of crack predictions in hardening concrete.

Introduction

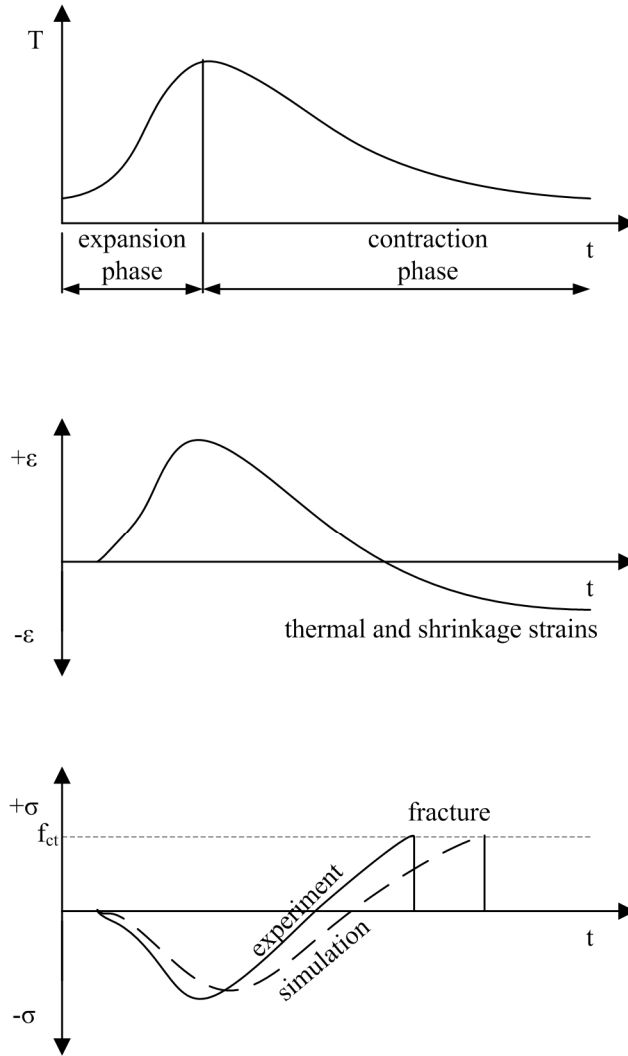


Figure 1.2 Early-age temperature development (top), strains (middle) and stresses measured by experiment versus simulated stresses (bottom)

1.2 Aim of this research

The aim of this research project is to increase the accuracy and the reliability of the calculation of stresses and of the probability of cracking of hardening concrete. With the help of the research results, it must be possible to take justified decisions about measures to avoid or control cracks in hardening concrete and to avoid unnecessary spending of public money on maintenance and repair. The design of concrete mixtures, structures and the building process should be adjusted in order to reduce the probability of cracking in a hardening concrete structure and/or to make a crack free structure that is better capable to withstand chemical and environmental attacks during its service life-time.

1.3 Research question

The durability of reinforced concrete structures depends, among other things, on the quality of the concrete and the presence of cracks. In case of durability predictions, it is necessary to calculate the probability of cracking as accurately and as reliably as possible. Since still a significant gap exists between stresses during hardening predicted by simulation models and measured from experiments, the main research question to be examined in this thesis is therefore:

How can the accuracy of stress prediction in hardening concrete be improved by a more detailed description of microstructure and transport phenomena?

1.4 Starting point and scope limitations

Starting point for this research is an evaluation of existing visco-elastic models. Many models were proposed in the past and will be evaluated in this thesis and are considered as a starting point for the development of an improved model that contributes to more reliable stress predictions. Existing models vary from very basic expressions to complex solidification theories, which take into account the

Introduction

formation of new hydration products by continuing hydration explicitly. The model results provided in this research project will be validated by using the Temperature-Stress Testing Machine (TSTM) [Rilem, 1982]. The experiments will be chosen such that they are complimentary to previous research conducted on this subject. This thesis only covers the topic of hardening concrete. No research has been done on hardened concrete.

1.5 Scope and thesis set-up

The structure of this thesis is shown in Figure 1.3. In the first introductory chapter the research problem and aim are outlined. The second chapter will summarize how the microstructure changes during hardening and how this can be modelled. The state of the art of visco-elastic models is discussed and the specific features of existing models are evaluated. In chapter three the time-dependent behaviour of hardening concrete is linked to the moisture state in the system. In chapter four, the state of capillary water, which is considered a very important parameter in concrete properties, is discussed. Chapter five describes the experiments conducted on hardening concrete. Several influencing factors are tested explicitly and will be discussed in detail. The experiments are used to validate the proposed visco-elastic model. It is shown that the accuracy and reliability of calculated stresses in hardening concrete elements are increased. Chapter six summarizes the results of this thesis. An evaluation of the research results is elaborated. The research question will be addressed again and it is discussed to what extent the research aim has been reached. Furthermore, suggestions will be done on how the remaining gap between simulations and measurements of stresses in hardening concrete can be improved in future research.

Preliminary research	
Chapter 1 Introduction	Problem description and research strategy
Chapter 2 Initial state	Explanation of microstructural development and visco-elasticity in hardening concrete
Model development	
Chapter 3 Proposed model for time-dependent behaviour	Modeling time-dependent behaviour by coupling it to microstructural developments and the moisture state
Chapter 4 Moisture movements at microlevel	Moisture transport through the microstructure is modelled and the influence on concrete properties is presented
Validation	
Chapter 5 Experiments and validation	Measured stresses during hardening of concrete under restrained deformations, influence of parameters and comparison between experiments and simulations
Conclusions	
Chapter 6 Conclusions	The research question will be answered, the conclusions of the research are presented and recommendations are made for future research
Appendices	
Appendix A	Finite element approach
Appendix B	Deformations of a hollow shell
Appendix C	Hollow shells and microstructural development
Appendix D	Practical application

Figure 1.3 Thesis overview

2 Initial state

2.1 General

The initial stage of a structure made of concrete is the stage when properties of the concrete develop. The initial liquid state of the mixture of gravel, sand, cement, water and eventually additives changes into a hardened system due to the hydration of cement. During this initial stage, properties like strength and stiffness gradually increase with increasing degree of hydration. The hardening phase is accompanied by phenomena which can cause stresses in the system. These phenomena are thermal deformations and hardening deformations (chemical shrinkage and autogenous deformations). Restraining these deformations will result in elastic stress increments:

$$\Delta\sigma(t) = \Delta[\varepsilon_T(\alpha) + \varepsilon_{cs(\alpha)} + \varepsilon_{as(\alpha)}] \cdot E(t)_{(\alpha)} \cdot R \quad [2.1]$$

with:

- $\Delta\sigma$ = stress increment [MPa]
- t = age of the concrete [hrs]
- α = degree of hydration [-]
- $\Delta\varepsilon_T$ = increment of thermal deformation [-]
- $\Delta\varepsilon_{cs}$ = increment of chemical shrinkage [-]
- $\Delta\varepsilon_{as}$ = increment of autogenous deformation [-]
- E = modulus of elasticity [MPa]
- R = degree of restraint (0 - 1) [-]

The time dependent behaviour of stresses can be taken into account by multiplying the stress increments with a relaxation factor $\psi(t, \tau)$:

$$\Delta\sigma(t, \tau) = \Delta\sigma(t) \cdot \psi(t, \tau) \quad [2.2]$$

with:

Initial state

$\Delta\sigma(t,\tau)$ = time dependent stress increment [MPa]

$\Delta\sigma(t)$ = elastic stress increment [MPa]

$\psi(t,\tau)$ = relaxation factor [-]

t = age of the concrete [hrs]

τ = age of the concrete at loading [hrs]

The stress development in the concrete can now be calculated by superposition of the stress increments:

$$\sigma(t) = \sum_{i=0}^j \Delta\sigma(t, \tau) \quad [2.3]$$

with:

$\sigma(t)$ = stress development in time [MPa]

$\Delta\sigma(t,\tau)$ = time dependent stress increment [MPa]

Models which describe these volumetric changes (thermal, chemical, autogenous), development of modulus of elasticity and the visco-elasticity of the system can be based on microstructural simulation models, which simulate the cement hydration (degree of hydration) and the development of the microstructure.

2.2 Hydration and microstructural development

Hydration is the chemical reaction between cement and water. Immediately after mixing water and cement, the chemical components of the cement (C_3S , C_2S , C_3A and C_4AF) start to react with the water. To keep the concrete workable for a longer time, gypsum is added. Gypsum and C_3A react and form ettringite, long needles, which initiate the first stiffening of the mixture. Second, the C_2S and C_3S hydrate.

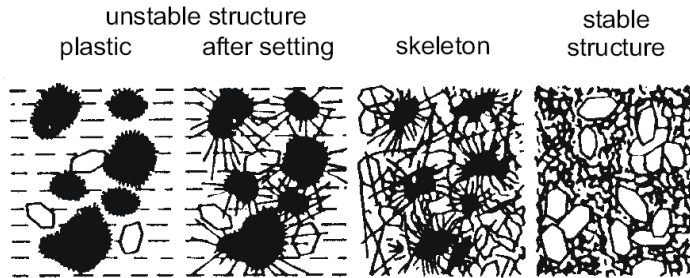


Figure 2.1 Development of cement structure during the hardening process, from an unstable plastic structure to a stable structure [Locher, 1976]

This hydration initially forms short CSH fibres which build a skeleton. Later this skeleton is filled with short CSH fibres. Finally the C_4AF and C_3A react with ettringite forming monosulphate and $C_4(AF)H_{13}$. The reaction products transform the initially plastic paste into a stable structure after setting (Figure 2.1).

To be able to predict concrete properties which depend on the degree of hydration, there was need of models which simulate the hydration of cement. The development of simulation models that describe the cement hydration at the microlevel started with the introduction of the ‘single particle model’ [Jander, 1927] and [Pommersheim, 1980]. Those models describe the hydration of a single cement grain by the formation of hydration products, for example CSH, on the particle surface explicitly. Outer and inner hydration products were distinguished. Outer products are assumed to grow from the original particle surface in outward direction. Inner products are assumed to grow from the original particle surface to the centre of the particle. In order to account for the interaction between the surrounding particles and the formation of microstructure between the different particles, morphology-based microstructural simulation models were developed, which describe the hydration process and the formation of structure for a system of hydrating cement particles. In general terms it can be said that two main streams of microstructural simulation models have been developed, i.e. the Pixel-based models and the particle-based models. In terms of hydration modelling, both models have their unique characteristic features.

2.2.1 Pixel-based model

The pixel-based digital-image model as developed at the National Institute of Standardisation (NIST) in Washington USA by Bentz and Garboczi [Bentz, 1996] is an advanced microlevel hydration model. A well-known version of this model is named CEMHY3D. The model is a 3D model that operates at the (sub-)micro level where each cement particle is represented by a collection of digital elements (pixels). Cement hydration is simulated by running the entire digitized frame of pixels using a set of cellular-automata-like rules as illustrated in Figure 2.2. This enables to account for a direct representation of the hydration process of a multisize, multiphase and, a non-spherical grading of cement particles.

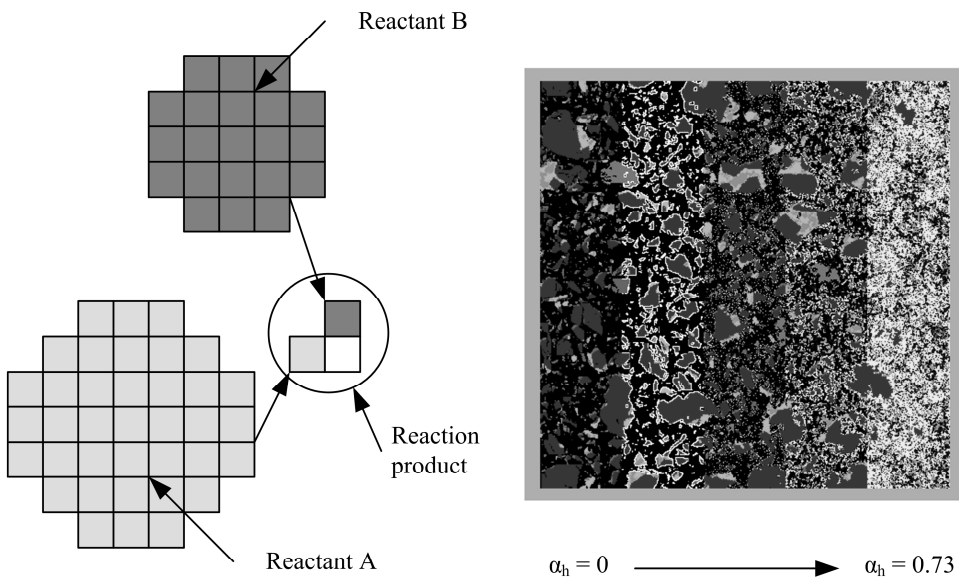


Figure 2.2 Schematical representation of the Pixel-model of NIST (left) and illustration of various steps in the digital-image based cement hydration model showing initial cement particles ($\alpha_h = 0$) to hydrated image ($\alpha_h = 0.73$) (right) [Bentz, 1997]

Depending on the identity of each individual pixel, whenever coming into solution, a pixel is able to diffuse and to react with other pixels and to form new reaction products that precipitate in the close vicinity of the hydrating particles or in a water rich space. A digital SEM image can be used as input for the hydration model. The model considers all of the major phases present in cement. The pixel representation of the microstructure is mapped onto a finite-difference or finite-element grid. It is trivial that there can be a simple one-to-one mapping between pixels and finite elements. The strongest point of this approach lies in the fact that the particle size distribution, the phase volume fractions and the surface area fractions of the real cement powder are preserved in the reconstructed images. A limitation of digital-image-based models is the resolution. Since each pixel is typically $1 \mu\text{m}^3$ in volume, features smaller than this cannot be resolved. However, since most cements contain particles that cover a range between 1 and $70 \mu\text{m}$ in diameter, almost all cements can be represented very accurately in a computational volume of $100 \times 100 \times 100$ pixels. Disadvantage of this model is the large CPU-time it requires to simulate cement hydration.

2.2.2 Particle-based model

A typical particle-based model is the HYMOSTRUC model (acronym for HYdration, MORphology and STRUCture), The model uses spherical particles to simulate the particle size distribution of the cement grains. Hydration of the spheres is initially described by a phase-boundary reaction, and whenever having exceeded a certain thickness of the transition zone, the reaction process alters into a diffusion controlled reaction [Breugel, 1997]. With the volume of the reaction products exceeding the volume of the dissolving cement by a factor 2.2, the hydrating cement grains are modelled as gradually growing spheres. During hydration, smaller particles become gradually embedded in the outer shell of bigger particles (Figure 2.3) under the formation of a load bearing microstructure.

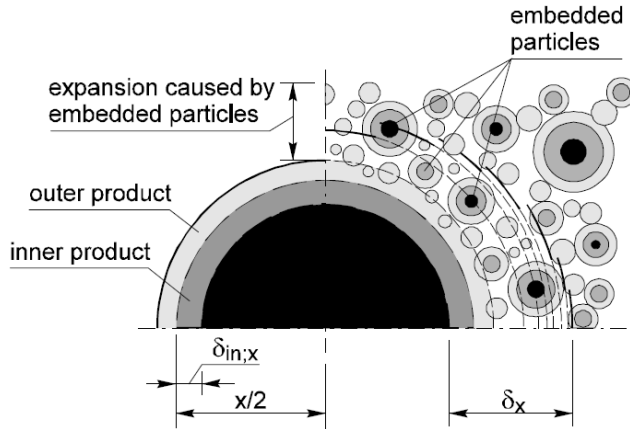


Figure 2.3 Interaction mechanism for expanding particles. Free expansion (left) and embedding of particles (right) [Breugel, 1997]

The expansion process is modelled according to the particle growth model. The embedding process represents the formation of the microstructure and is based on the following assumptions:

- Reaction products precipitate in the close vicinity of dissolving cement grains;
- Dissolution and growth of the cement particles occurs concentrically, taking particle interaction into account;
- Under isothermal conditions, the density of the reaction product is constant throughout the hydration process and independent of the place where the products are formed;
- Particles of the same size hydrate at the same rate.

2.2.3 Evaluation of hydration simulation software

The development of hydration simulation software introduced the possibility to couple the results and information from the simulations with the property development of hardening concrete. Properties like strength, stiffness, porosity and permeability are simulated accurately with elapse of time (degree of hydration). On its turn, these properties are used in simulation software, which determine the stress

development in hardening concrete structures. However, an important property in stress simulations, the visco-elastic behaviour of hardening concrete, is still under development to relate it explicitly to microstructural simulation models [Lokhorst, 2001] [Mabrouk, 2004].

2.3 Visco-elasticity

Visco-elasticity is a very important property in hardening concrete, since it relates stress development to time dependent deformations. If a concrete structure is deformed elastically, elastic stresses will arise immediately in the structure (time-independent). Keeping the deformations constant, visco-elastic behaviour results in relaxation of the stresses (time-dependent) (Figure 2.4, top). If an element is loaded by a sustained load, the deformations gradually increase with time (creep) (Figure 2.4, bottom). Creep is linked to relaxation by the formula [Wittmann, 1974]:

$$\psi(.) = \exp[-\varphi(.)] \quad [2.4]$$

with:

$\Psi(.)$ = relaxation factor [-]

$\Phi(.)$ = creep factor [-]

The visco-elastic phenomenon of concrete is affected by a number of factors that influence the magnitude and rate of the deformations. Some important conditions have been summarized by Byfors [Byfors, 1980]. For a given concrete mixture these are the loading time, age at loading, stress level, temperature and relative humidity (Figure 2.5).

Initial state

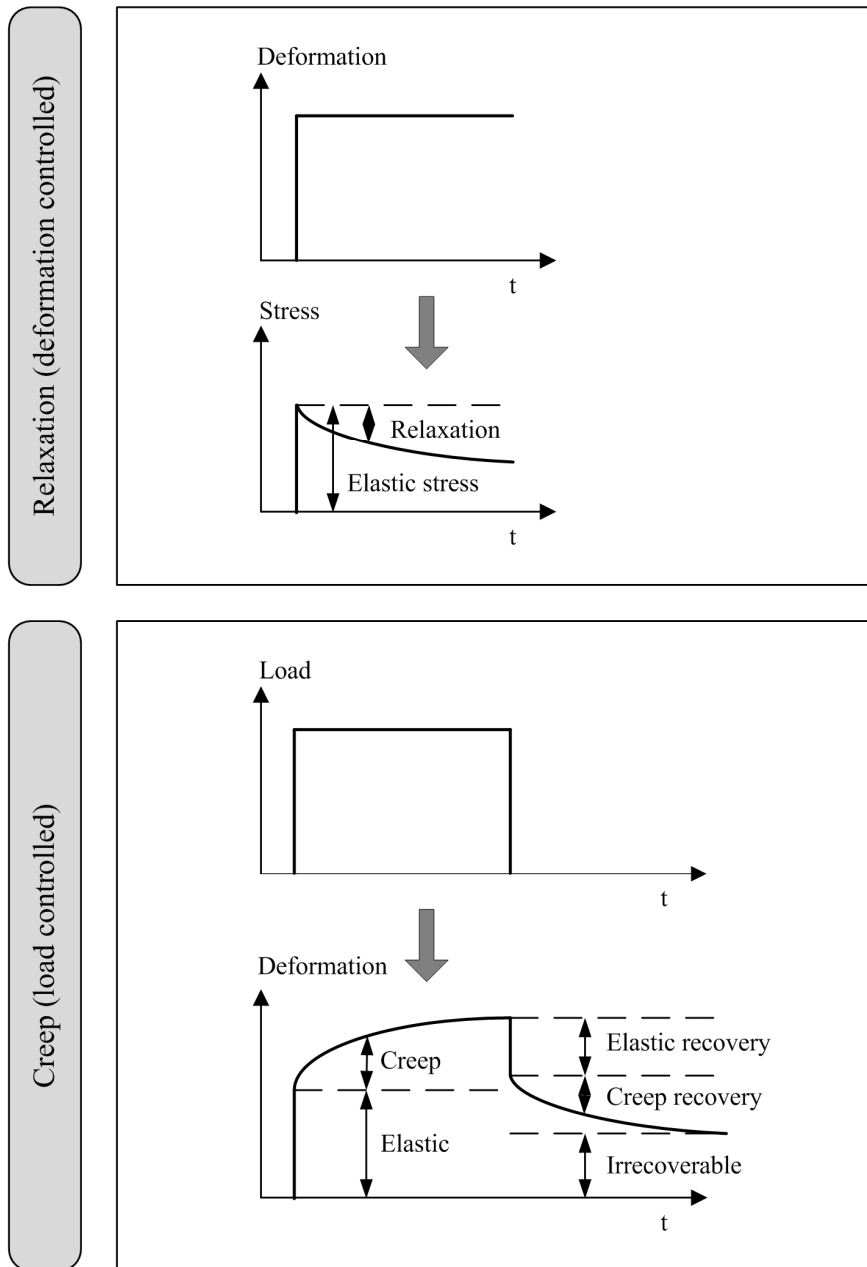


Figure 2.4 Relaxation of stresses (top) and creep of deformations (bottom) of a specimen under sustained loading

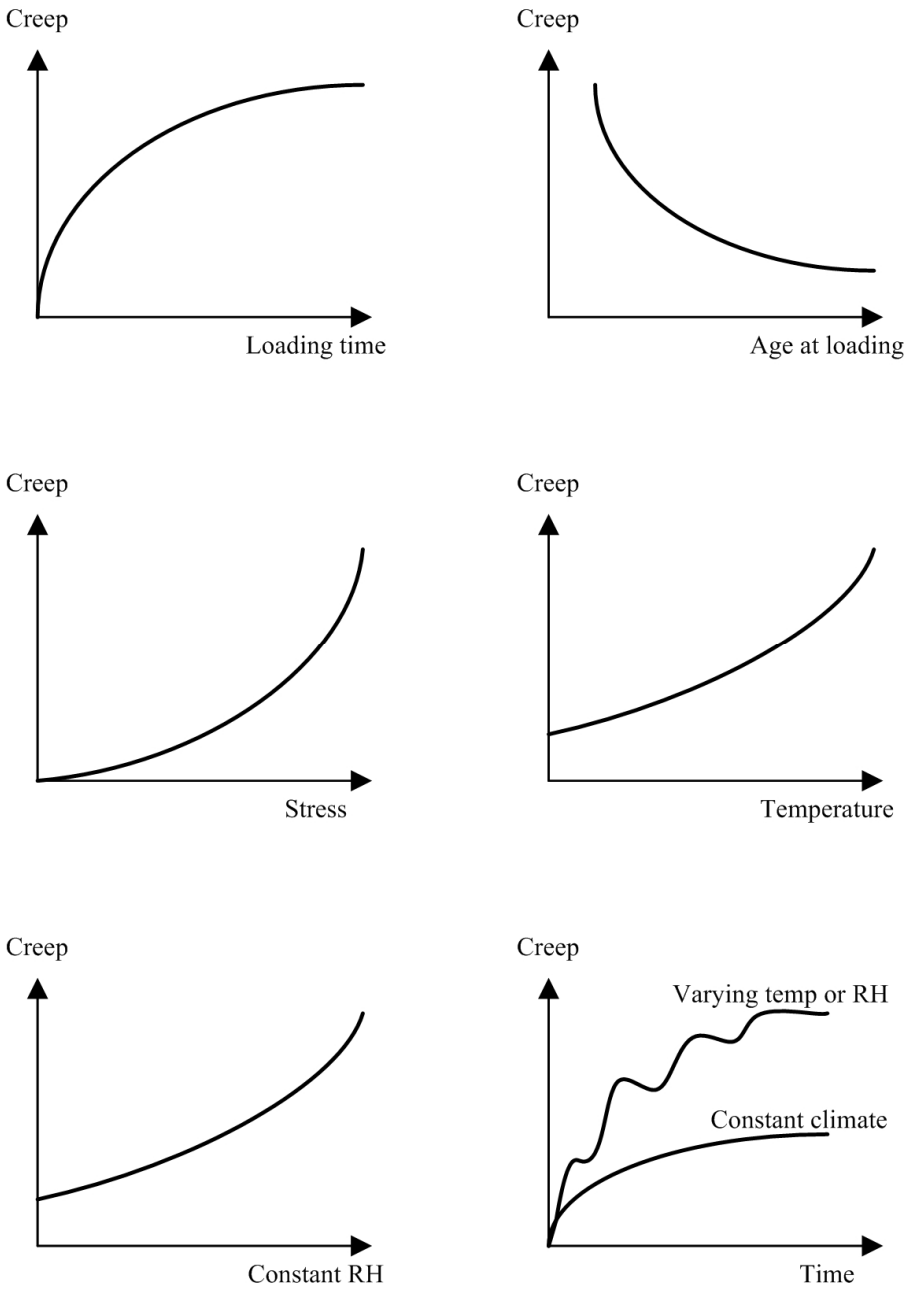


Figure 2.5 Conditions influencing creep deformations [Byfors, 1980]

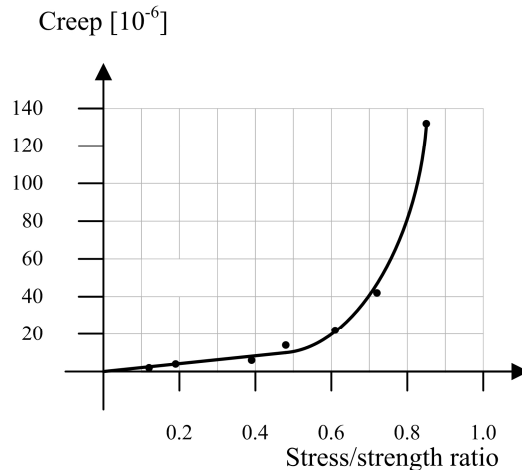


Figure 2.6 Compressive creep related to the stress/strength-ratio after Neville [Neville, 1970]

Besides the conditions summarized by Byfors several other generally accepted mixture-dependent factors are mentioned in literature; stiffer aggregates and/or a higher content of aggregates will restrain the deformations. An increase of the water/cement-ratio will increase the visco-elastic deformations significantly as well [Lorman, 1940]. The visco-elastic deformations of silica fume concrete were found to be larger than that of concrete without silica fume. This behaviour seems to be typical for loading at early ages [Igarashi, 1999], [Kovler, 1999] and [Igarashi, 2002]. From a wide range of experimental results there is substantial evidence for a linear relation between creep and the applied stress, except in specimens loaded at very early ages [Neville, 1970]. At a very early age, there is an upper limit for the linear relation at a stress/strength ratio of about 0.4 to 0.6 (Figure 2.6). Above this stress/strength ratio internal microcracking dominates the deformational behaviour of the concrete. Once the cracking has started, the creep behaviour also changes. The upper limit for a linear relation was confirmed by Altrushi [Altrushi, 2003].

Inter alia with the number of factors influencing the visco-elastic behaviour of hardening concrete, many mechanisms are proposed to describe the visco-elastic

behaviour of (hardening) concrete. Neville summarized for following mechanisms on a phenomenological basis [Neville 1970]:

- **Mechanical deformation-theory.** Freyssinet stated that under a load, capillaries are deformed and the water meniscus will displace to a point where the capillary diameter is different, so that the tension under which the capillary water is held is changed. To maintain equilibrium with the tension in the capillary water, the stress in the solid phase changes too. The resultant deformation is called creep. This process is completely reversible if a load is removed. An irrecoverable part was introduced by deformations due to the tendency of hydrated cement paste toward maximum stability under a sustained load, but the influence of all factors on creep is not explained by the mechanical deformation theory.
- **Plastic theory.** According to the plastic theory, creep of concrete may be in the nature of crystalline flow. Plastic deformations should take place only if the applied stress exceeds a yield point. However, there is no value for this stress below which no non-elastic deformations occur. Besides this, no volume changes can take place by plastic deformations, while creep of concrete leads to a definite reduction in volume.
- **Viscous and viscous-elastic theory.** A cement flow through the aggregates is proposed due to loading on the concrete [Thomas, 1937]. The flow is resisted by the presence of aggregates, which become more highly stressed while the stress on the cement paste decreases in time. Several arguments against this mechanism can be found (no volume changes, creep Poisson's ratio is equal to zero for this mechanism).
- **Elastic after-effect theory.** Drying of concrete causes non-uniform volume changes which produce transient stresses. These, combined with the stresses due to external loading, give rise to a distribution and magnitude of stresses much different from those in a non-shrinking companion specimen [Picket, 1942].
- **Solid solution theory.** The pressure of water in the cement gel is affected by the applied stress, with a result that the water content of the gel and its volume are altered (transport of water between the gel pores and the capillary pores). [Lea, 1946].

Initial state

- **Seepage theory.** Seepage is a viscous flow of the dispersion medium through and ahead of the disperse phase, introduced by Lynam [Lynam, 1934]. The decrease of volume under a stress is characterized by a partial immediate recovery after stress removal. Creep in concrete is taken to be due to seepage of gel water under pressure. The rate of seepage depends on the moisture gradient. As water is squeezed out, the stress on the solid increases and the pressure on the water correspondingly decreases.
- **Micro cracking theory.** Micro cracking is assumed to be responsible for the irrecoverable part of the deformation associated with the sustained load.

Several creep hypotheses are developed which integrated two or more visco-elastic mechanisms into one hypothesis, e.g. Kesler's hypothesis (seepage, delayed elasticity and viscous flow) [Ali, 1963] or Ishai's hypothesis (redistribution of stresses due to diffusion of loaded water) [Ishai, 1968]. However, these do not correspond to the general view that the visco-elastic behaviour of hardening concrete has its origin in hydrating cement paste and, at high stress state, also in failure of the paste-aggregate bond. It is generally believed that the visco-elastic behaviour is related to internal movement of adsorbed or inter-crystalline water (internal seepage) [Neville 1970].

Creep hypotheses describe the thoughts behind the phenomenon of visco-elastic behaviour of hardening concrete; however, they do not quantify the visco-elastic behaviour of hardening concrete. Several models have been proposed for quantification of the visco-elastic behaviour of hardening concrete. These models can generally be divided into three groups:

- Basic expressions
- Rheological models
- Solidification theory

The first group includes the basic expressions for creep. These expressions formulate the creep process in the form of an experimentally-based analytical equation. The second group are the rheological models, based on some form of curve fitting using the mathematical formulation of Maxwell or Kelvin chains. The

third group couples the visco-elastic behaviour to physical phenomena like moisture transport or microstructure formation of cement paste.

2.3.1 Basic expressions

Basic expressions are used to describe the average values of the time dependent behaviour of hardened concrete on the macroscale level. However, these equations do not couple the materials behaviour to the development of the microstructure. For hardening concrete, data fitting is used to find agreement between experimental results and results of simulations.

2.3.1.1 Power laws

Very practical and frequently used equations for describing the visco-elastic behaviour of a particular concrete are power laws. A basic power function is the single power law, based on the activation energy approach, where the activation energy corresponds to the average coupling energy of gel particles in the xerogel of hardening cement paste [Wittmann, 1974]:

$$\varepsilon_c(t, t') = a(t') \cdot (t - t')^p \cdot \sigma(t') \quad [2.5]$$

with:

$\varepsilon_c(t, t')$ = creep strain at time t [-]

$a(t')$ = aging factor [-]

t' = age at loading [hrs]

p = constant [-]

σ = applied stress [MPa]

By the single power law, the continuously changing microstructure of the hardening concrete was already taken into account by the aging factor. The single power law evolved into a double power law [Bazant, 1976] and a modified double power law, which was more suitable for young hardening concrete:

$$J(t, t') = \frac{1}{E_0} + \frac{\varphi_0}{E_0} \left[(t')^{-d} (t - t')^p \right] \quad [2.6]$$

Initial state

with:

$J(t,t')$ = creep compliance [1/MPa]

E_0 = modulus of elasticity at age at loading [MPa]

t' = age at application of the load [hrs]

φ_0, d, p = material parameters [-]

Finally the modified double power law evolved into a triple power law. Reason for the evolution to the triple power law was to get a better fit to experimental data of especially very short creep duration, very early age concrete and high performance concrete [Westman, 1999]:

$$J(t,t') = \frac{1}{E_0} + \frac{\varphi_0}{E_0} (t'^{-d} + \alpha) \left[(t-t')^p - B(t,t';p) \right] + \frac{\Psi_1(t')}{E_0} + \frac{\Psi_2(t,t')}{E_0} \quad [2.7]$$

In this function, $B(t,t';p)$ reduces the long-term creep rate, $\Psi_1(t')$ describes the strong age-dependency of the instantaneous deformation and $\Psi_2(t,t')$ describes the increase of early age creep after the load has been applied. The disadvantage of the power laws is the lack of predictive potential because all parameters are fitted to experimental data and vary from case to case [Altrushi, 2003].

2.3.1.2 Exponential formula

Van Breugel proposed a relaxation formula based on the evolution of the degree of hydration and the water-cement-ratio [Breugel, 1980]. The influence of cement type and load sign is taken into account explicitly by the factors d and n .

$$\varphi(\tau_i, t, \alpha_{\tau_i}) = \frac{\alpha_h(t)}{\alpha_h(\tau_i)} - 1 + 1.34 \cdot \omega^{1.65} \cdot \tau_i^{-d} \cdot (t - \tau_i)^n \cdot \frac{\alpha_h(t)}{\alpha_h(\tau_i)} \quad [2.8]$$

with:

α_h = degree of hydration [-]

τ = age at loading [hrs]

ω = water/cement ratio [-]

d = parameter dependent on cement type (0.3 - 0.4) [-]

n = parameter dependent on load sign (0.3 - 0.6) [-]

Besides the influence of the cement type on the degree of hydration, an influence is prescribed on the creep of hardening concrete. Increasing parameter d (increasing the fineness of the cement) results in less creep compared to lower values of d (coarser cement types).

Originally the load sign (concrete loaded in tension or compression) is taken into account by parameter n . A value of 0.3 is taken for concrete loaded in compression, 0.6 is taken for concrete loaded in tension. Recently, better results are obtained by taking this value 0.3 both for concrete loaded in compression and tension [Lura, 2001].

Czerny concluded that for simulations using the exponential formula fit better to experimental results for concrete loaded after 72 hours than concrete loaded before an age of 72 hours [Czerny, 2004].

2.3.2 Rheological models

Creep models based on rheological models are specially developed for materials with changing microstructures, like hydrating cement-based systems. A rheological model is defined as a combination of elements, each of them representing a specific deformational characteristic of a given component or phase of concrete [Neville, 1973]. The idealized deformations are elastic, viscous or plastic, and are represented by basic mechanical elements like a spring, a dashpot or a friction element, respectively. Simple models (Figure 2.7) are developed to describe the behaviour of concrete under sustained loading. Components of which concrete is composed of (e.g. aggregates, sand, cement, water) are homogenised into one element. The simplest rheological models used to build more complex systems are the Kelvin-Voigt model and the Maxwell model.

Initial state

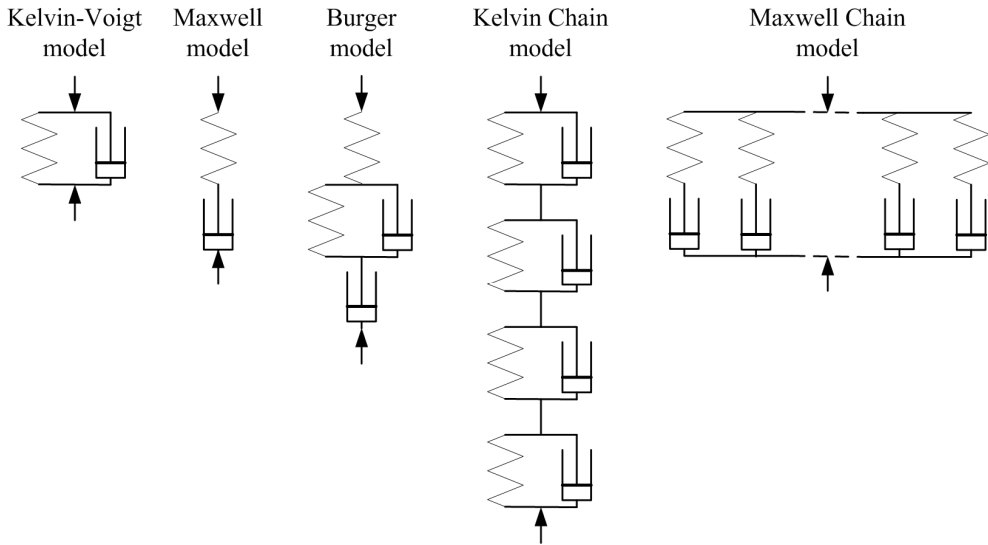


Figure 2.7 Simple rheological models: Kelvin-Voigt model, Maxwell model, Burger model, Kelvin Chain model, Maxwell Chain model.

The Kelvin-Voigt model is a parallel system of a spring and a dashpot. Since the spring and the dashpot are a parallel system, the system is not able to describe elastic behaviour. The constitutive relation is expressed as a linear first-order differential equation:

$$\sigma(t) = E(t) \cdot \epsilon(t) + C(t) \cdot \frac{\partial \epsilon(t)}{\partial t} \quad [2.9]$$

The Maxwell model is a serial system of a spring and a dashpot, which is able to describe an elastic behaviour combined with plastic behaviour. The model can be represented by the following equation:

$$\frac{\partial \epsilon_{\text{total}}(t)}{\partial t} = \frac{\partial \epsilon_D}{\partial t} + \frac{\partial \epsilon_S}{\partial t} = \frac{\sigma}{C(t)} + \frac{1}{E(t)} \cdot \frac{\partial \sigma(t)}{\partial t} \quad [2.10]$$

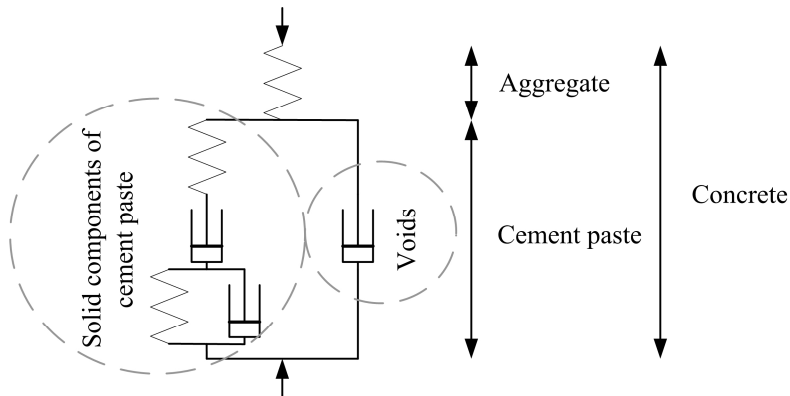


Figure 2.8 Hansen's model, deformational behaviour of concrete divided into behaviour of its physical components [Hansen, 1958].

More extended rheological models describe the behaviour of components of a material under sustained loading (Hansen's model, Figure 2.8). By Hansen's model, an attempt is made to correlate the behaviour of aggregates, the solid components of cement paste and voids in the cement paste to the deformational behaviour of concrete. In principle, rheological models can accomplish any desired level of accuracy in fitting experimental curves by adding more of the basic elements in a chain.

2.3.3 Solidification theory

Solidification theories are developed to describe visco-elastic behaviour of hydrating microstructures. These theories are based on the concept that new hydration products are formed by continuing hydration. The hydration products, formed in a single time step, are represented by a single layer. All layers that solidified at different times are coupled in parallel. For constant stress, strain varies in time. This causes a transfer of load (stress) to new layers and, as the total stress must remain constant, this means a stress reduction in the existing layers (Figure 2.9).

Initial state

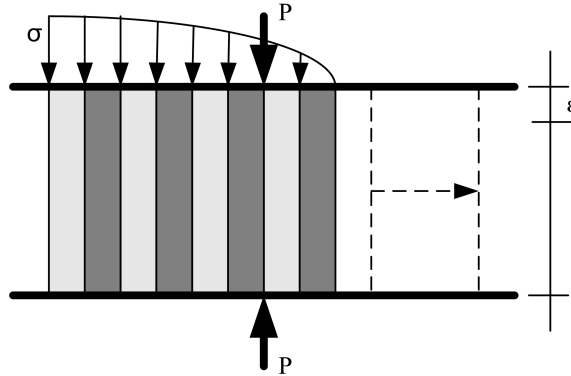


Figure 2.9 Solidification model with parallel arrangement of constituent layers. New layers are added stress free [Carol, 1993]

2.3.3.1 Microprestress solidification theory

The microprestress solidification theory is a theory based on physics, in which aging is explained and modelled by the volume growth (into the pores of hardened Portland cement paste) of a non-aging visco-elastic constituent (cement gel) [Bazant, 2004]. The model for creep consists of three components (Figure 2.10).

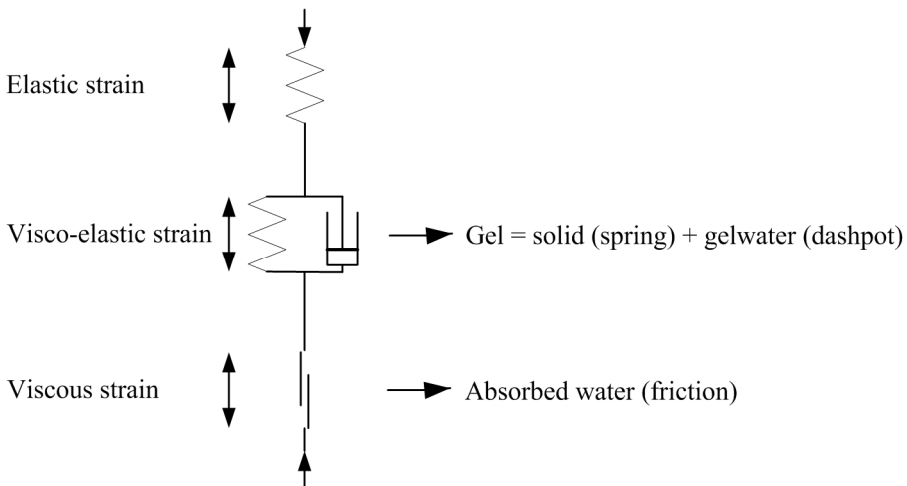


Figure 2.10 Microprestress solidification theory

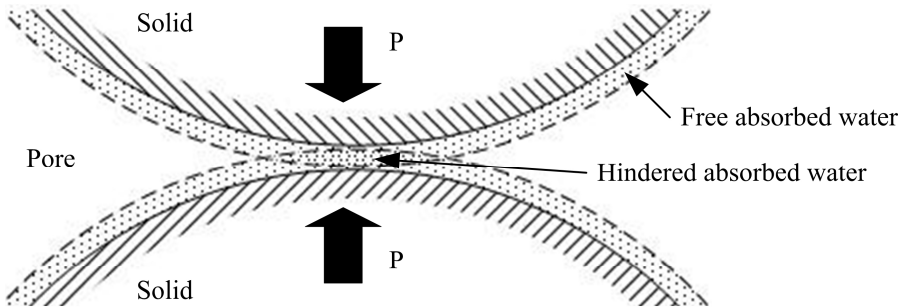


Figure 2.11 Idealized free and hindered absorbed water

First is the elastic strain, which appears immediately after applying a load. Second is the aging visco-elastic strain rate, which accounts for the visco-elastic strain in calcium silicate hydrates. The third part is a purely viscous strain which is the completely irrecoverable part of the creep strain. It is modelled by a viscous dashpot representing the hindered adsorbed water layers (Figure 2.11) in the microstructure of the cement paste. Each solid in the microstructure has a layer of free absorbed water around it. If two solids come in contact with each other, the overlap of free absorbed water has to move. This overlap is defined as hindered absorbed water. Modification of the model was needed to describe early age creep. The model is modified by adding a parameter which may be regarded as a structural setting time [Østergaard, 2001].

2.3.3.2 Unified solidification model

A similar but more detailed physical model is the unified solidification model of hardening concrete composite (Figure 2.12). This model is based on the movement of water through the pore system of a hardening concrete [Mabrouk, 2004].

The model is divided into four parts (Figure 2.13):

First part is the elastic strain which is represented by a spring.

Second is the visco-elastic strain which takes into account the movement of capillary water through the capillary pores and is represented by a Kelvin-chain of an elastic spring and a dashpot. The dashpot constant is determined by the capillary porosity of the paste, the degree of saturation of the capillary pores, the viscosity of the water and several fitted constants (without physical meaning).

Initial state

The third part, which is the visco-plastic strain part, is assumed to be totally irreversible as it is mainly related to the movement of water from the gel pores to the capillary pores. The rate of gel deformation is determined by the dashpot constant, which is determined by the gel porosity, the saturation of the gel pores, the viscosity of the water in the micro pores and some fitted constants.

Finally there is the fourth part, the viscous strains, which are related to the movement of water through the interlaying pores. The movement of water through the interlaying parts is described by a fitted constant.

A similar phenomena is described by Acker, who described the influence of loaded gel water on the visco-elastic behaviour of cement paste [Acker, 2001].

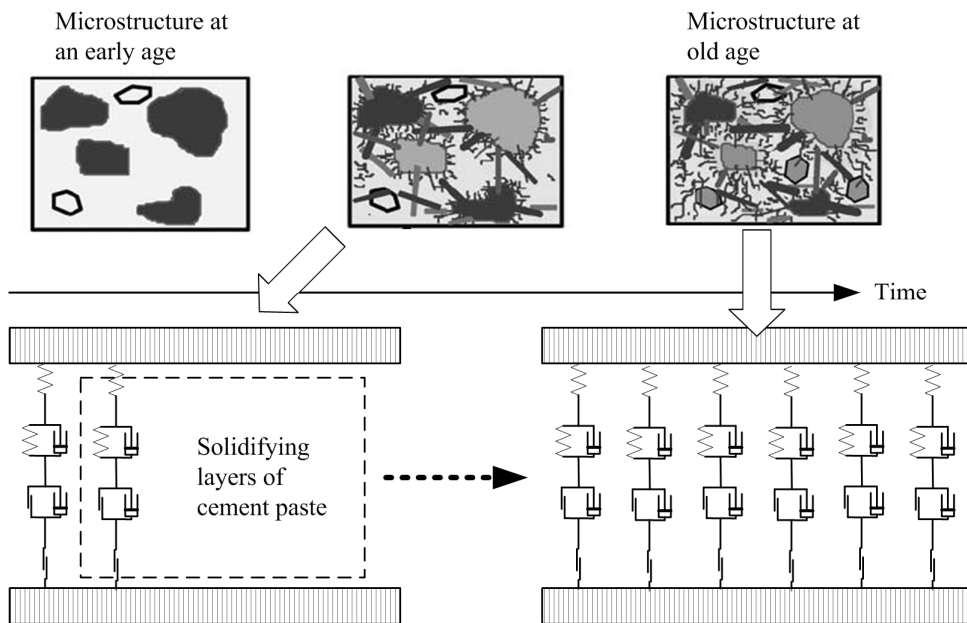


Figure 2.12 Solidifying layers of cement paste and aging of the microstructure [Mabrouk, 2004]

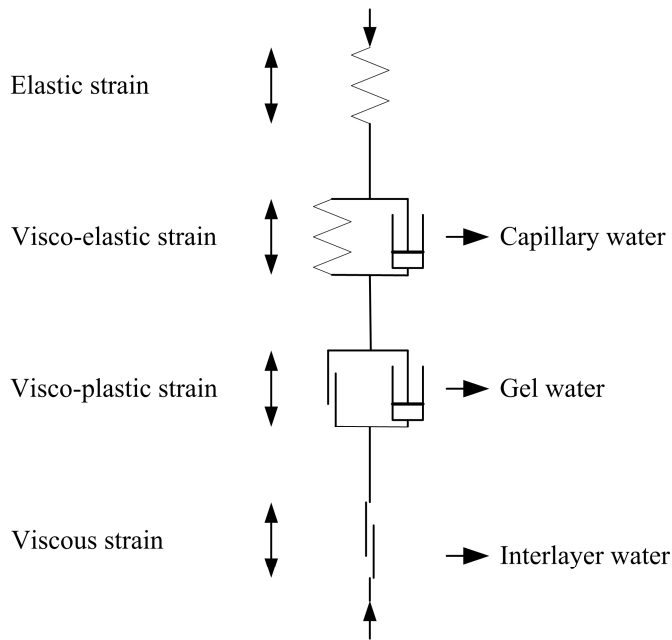


Figure 2.13 Unified solidification model

2.3.3.3 Bar model

The Bar model is proposed to describe the visco-elastic behaviour of a hardening cement paste, based on the microstructural development of the hardening cement paste [Lokhorst, 2001]. The model consists of three components. Initially there is the mixture of anhydrous cement grains and water. When the cement starts hydrating, a layer of cement gel will surround the anhydrous cement grains. In the model, this is represented by horizontal layers on the anhydrous cement component. When hydration continues the cement grains start to develop a connecting network. These connecting particles are represented by vertical bars representing cement gel. The Bar model is shown in Figure 2.14. The stiffness of the system of bars and layers is determined directly by the stiffness of the individual components.

Initial state

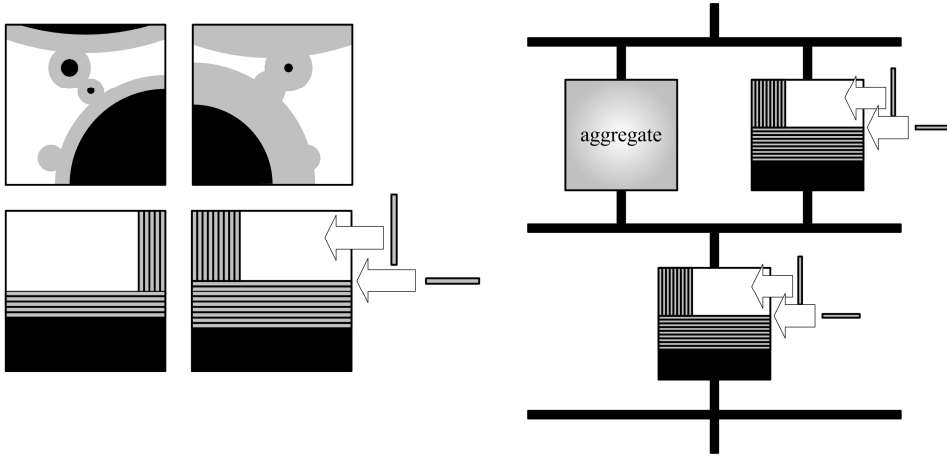


Figure 2.14 Microstructural development and Bar model for hardening cement paste (left). Composite Bar model for concrete (right) [Lokhorst, 2001]

The visco-elastic behaviour of the Bar model is described by a time-dependent behaviour of the cement gel component based on an activation energy based creep formula proposed by Wittmann [Wittmann, 1977] with:

$$\varepsilon_c(t) = a \cdot V(T) \cdot \frac{(t - \tau)}{t_0} \cdot \sigma(\tau) \quad [2.11]$$

$$V(T) = \exp\left(\frac{Q}{R} \cdot \frac{T - T_0}{T \cdot T_0}\right) \quad [2.12]$$

with:

- $\varepsilon_c(t)$ = time-dependent strain at time t [-]
- $t - \tau$ = time under load [hrs]
- t_0 = reference time, 1 [h]
- T = concrete temperature [K]
- Q = activation energy of cement gel, 20.000 [J/mol]
- $\sigma(\tau)$ = stress applied at age τ [MPa]

a	= creep constant [mm ² /N]
n	= power (default value 0.3) [-]
R	= universal gas constant, 8.31 [J/mol.K]
T ₀	= reference temperature, 293 [K]

The creep constant “a” is fitted to experiments on different concrete mixtures loaded in tension or compression and varies for the Portland cement based mixture between $a = 0.5 \cdot 10^{-5}$ (tension) and $a = 1.0 \cdot 10^{-5}$ (compression) and for blast furnace slag based mixture between $a = 1.0 \cdot 10^{-5}$ (tension) and $a = 4.5 \cdot 10^{-5}$ (compression) [Lokhorst, 2001]. An increase of constant “a” results linearly in an increase of time-dependent strains.

2.3.3.4 Hollow shell mode

Already in 1973, Gosh mentioned the influence of an “annular space” on the visco-elastic behaviour of hardening concrete. The annular space, or hollow shell, is defined as a zone between an anhydrous cement grain and the gel shell (transition zone, Figure 2.15). Gosh stated that due to the transport of ions through the gel layer an osmotic pressure is built up. As long as osmotic pressure exists, it will exert a positive dilating pressure on the gel phase surrounding the annular space. The pressure weakens the structure and causes premature rupture of the system. When external mechanical loads are applied to it the rupture results in a lower modulus of elasticity and bigger deformations [Gosh, 1973].

Lokhorst included hollow shells into his creep hypothesis to describe another phenomenon. He stated that two possibilities tend to be possible in a system of hydrating cement particles [Lokhorst, 2001]:

1. Full interactions exist between the anhydrous cement grain and the surrounding shell of cement gel. A load will be transferred via the shell of cement gel and the grain as shown in Figure 2.16 (left).
2. No interactions exist between the anhydrous cement grain and the surrounding shell of cement gel. A load will be transferred via the shell only as shown in Figure 2.16 (right).

Initial state

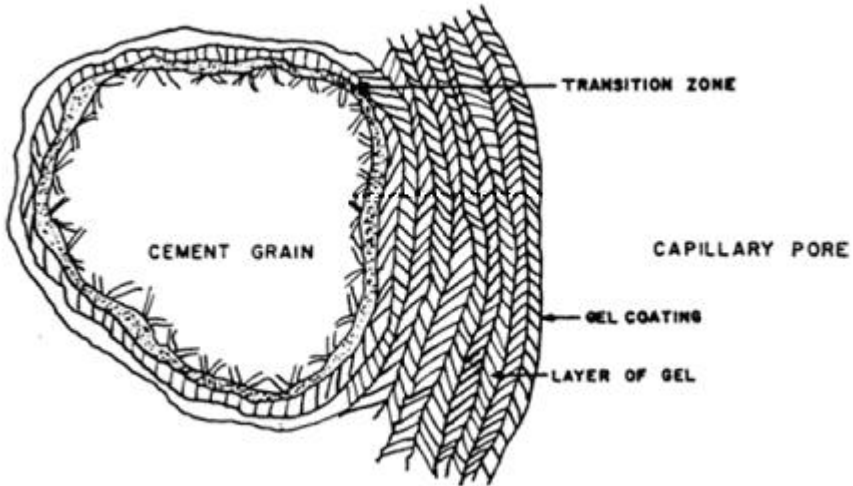


Figure 2.15 Illustration of hydrating cement grain (not to scale) [Ghosh, 1973]

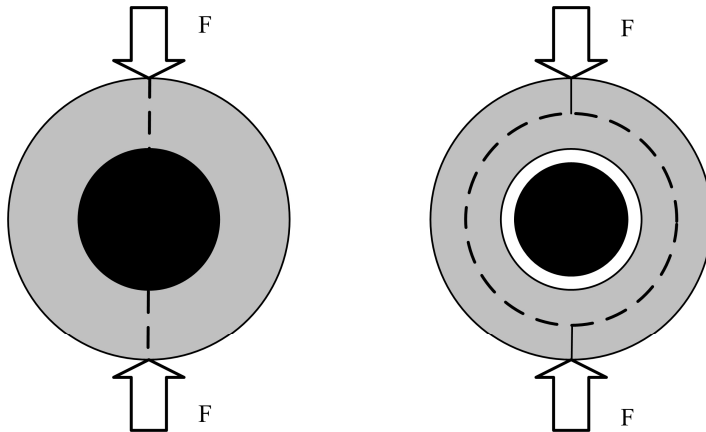


Figure 2.16 Fully interaction between shell and core (left) and No interaction between Shell and core (right)

Both possibilities are implemented in Lokhorst's Bar model. He assumed that the two ways of load transfer are upper and lower bound values for the effective stiffness. In reality, the solution must be somewhere between the system with full interaction and the system with no interaction. For this purpose, a fitting parameter K was introduced (Table 2.1), which interpolates between both systems and is fitted to experimental data [Lokhorst, 2001]. For $K = 0$, the effective stiffness is determined by the system with full interaction between anhydrous cement grain and the shell of cement gel and for $K = 1$, the effective stiffness is determined by the system with no interaction between the anhydrous cement grain and the shell of cement gel.

Table 2.1 Fitting parameter 'K' proposed by Lokhorst [Lokhorst, 2001]

Type of cement	Compression	Tension
BFS Cement	1.0	0.7
Portland cement	0.85	0.5

2.4 Discussion

In the past decennia, visco-elastic models evolved from basic expressions to complex computational models which are based on the physical behaviour of concrete and which are able to predict visco-elastic behaviour better and better. The evolution of visco-elastic models is accompanied by the evolution of (experimental) knowledge of about 20 influencing parameters [Altrushi, 2003].

From model developments and experiments, it became clear that dominating parameters for accurate and reliable visco-elastic models are the microstructural development and moisture movements in a hardening concrete. The continuing hydration of a hardening cement paste causes a continuously changing microstructure and changing moisture distribution. To obtain a reliable description of the visco-elastic behaviour, it is essential to base it on both the microstructural development of the hardening cement paste and physical phenomena like moisture movements in the system. The microprestress solidification theory and the unified solidification model both included the physical phenomenon of moisture transport. However, the physical phenomenon is used at a macroscopic level to determine purely mechanical dashpot constants. Spring constants and dashpot constants are

Initial state

fitted to experimental results of creep experiments. The Bar model is a model based on the microstructural development of hardening concrete; however, in order to increase the accuracy and reliability, there is a need to couple the Bar model to the influence of the actual moisture state in the system on the visco-elastic behaviour, instead of the activation energy approach based creep formula.

In this thesis, it will be endeavoured to make a step forward in understanding and explicit modelling of visco-elastic behaviour of hardening concrete, by taking into account the micro-structural development of hardening cement paste and moisture movements in order to make stress predictions in hardening concrete elements more accurate and reliable.

3 Proposed model for time-dependent behaviour

3.1 General

From literature evaluation about modelling of the visco-elastic behaviour of hardening concrete (chapter two) it is clear that changes in the state of moisture have to be considered explicitly in the solidification theory. It is a step forward in understanding the visco-elastic behaviour of hardening concrete. The consideration of an accurate description of the state of moisture in an evolving solidifying microstructure will increase the reliability of stress predictions and will result in a smaller gap between simulated and measured stresses in hardening concrete elements (Figure 1.2). In this thesis, use is made of the HYMOSTRUC model to model the hydration of cement [Breugel, 1997], the Ribbon model to model the hydration of a tube filled with cement paste [Koenders, 1997] and the Bar model to model the modulus of elasticity of a hardening cement paste, and hardening concrete [Lokhorst, 2001].

3.2 Hollow shells

In this thesis, the moisture state is modelled explicitly in the solidification theory by including hollow permeable shells (Figure 3.1, left) in a microstructural hydration model. This model is called the Shell Deformation Model 'SDM'. Incorporating hollow shells in hydrating cement results in a three phase system. This three phase system is presented for a single hydrating cement particle in Figure 3.1 (right). In the centre an anhydrous cement grain is situated, surrounded by a shell of cement gel (hydration product). Between the anhydrous cement grain and the shell of cement gel, an annular space of about $1\mu\text{m}$ is identified [Ghosh, 1973], [Dalgleish, 1982], [Kjellsen, 1997], [Diamond, 2004] & [Head, 2006]. If this three phase system is loaded, the shell tends to deform. This deformation is

Proposed model for time-dependent behaviour

restraint by the water accumulated in the annular space and results in “load-bearing water”. Due to this, the water pressure in the annular space will change in comparison with the unloaded situation. The permeability of the shell of cement gel allows for the transport of water between the water inside the shells and the water in the capillary pores. This interaction will affect or determine, the time-dependent behaviour of the system. Due to the loading, the water in the annular space will move into the capillary pores (if loaded in compression) and the original shape of the sphere will transform into an oblate spheroid (Figure 3.2).

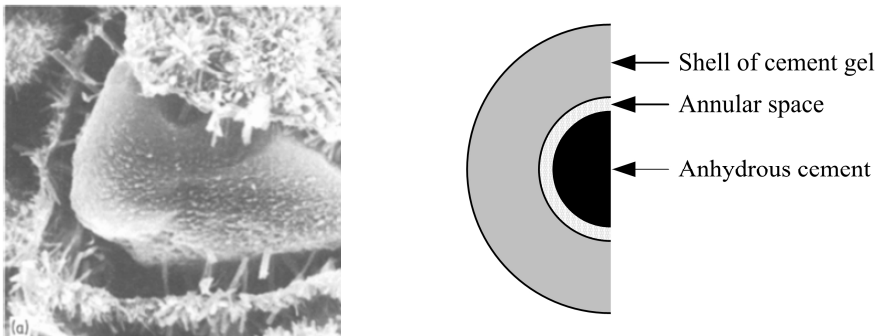


Figure 3.1 A hollow shell in a one-day old cement paste (left) [Dalglish, 1982] and schematized hollow shell (right)

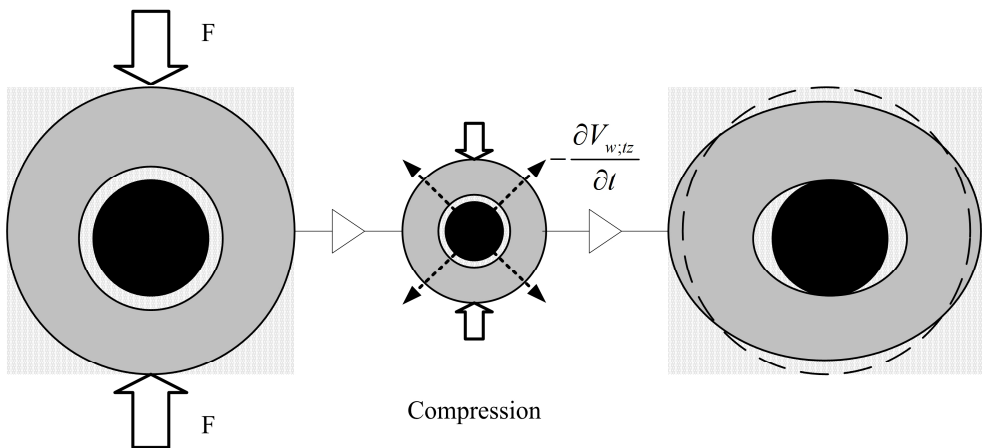


Figure 3.2 General time dependent deformation for a hollow shell in compression

3.3 Interaction between shell and core of hydrating cement grains

A physical interaction between the shell of cement gel and the anhydrous cement grain is conceivable, since the space between the shell of cement gel and the anhydrous cement grain is filled with water. Two extreme conditions can be distinguished to take this interaction into account (Figure 3.3). The first extreme condition assumes a full interaction between shell and core. If this system is loaded, the load will be transferred directly through the shell to the core and through the shell again. Second extreme condition assumes no direct interaction between shell and core. In this loaded system, the load will be transferred through the shell only, and the core will remain stress-free. Both cases are classified as upper and lower boundaries.

For both boundaries, a modulus of elasticity is determined. For the full interaction modulus, this is called the “elastic modulus” and for no interaction this modulus is called the “hollow shell elastic modulus”. The elastic modulus and the hollow shell elastic modulus are determined by the Bar model (Figure 3.4) [Lokhorst, 2001]. The volume of pores, cement gel and anhydrous cement are determined as a function of the degree of hydration using HYMOSTRUC. In reality, the solution will be a situation in-between the upper and lower boundary. This solution can be determined by interpolating between these two extreme conditions:

$$E_{\text{eff}} = (1 - \text{IF}) \cdot H_c + \text{IF} \cdot E_c \quad [3.13]$$

with:

E_{eff} = effective modulus of elasticity [MPa]

IF = interaction factor [-]

H_c = hollow shell elastic modulus (no interaction with core) [MPa]

E_c = elastic modulus (full interaction with core) [MPa]

The interaction factor ‘IF’ is assumed to be related to the transport of water between the annular space and the capillary pores. The determination is based upon the following steps:

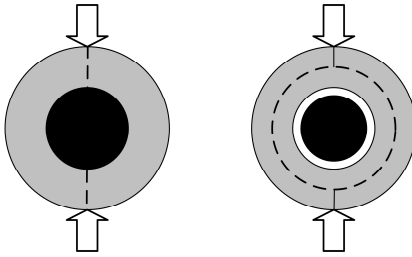


Figure 3.3 Fully interaction (left) and no interaction (right) between core and shell [Lokhorst, 2001]

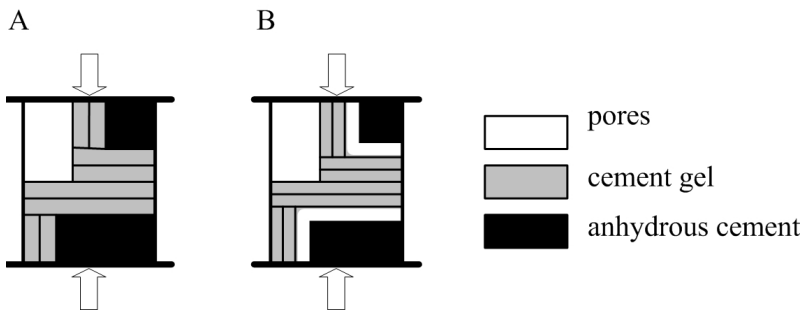


Figure 3.4 Bar model for determination of modulus of elasticity with full interaction (A) and no interaction (B)

- When a grain is loaded, a pressure gradient will develop between the water inside the annular space and the water in the capillary pores. The water in the annular space is classified as load bearing water and full interaction is assumed between shell and anhydrous cement grain ($IF = 1$) (Figure 3.5, step 1).
- During a certain (sustained) loading time, water will be transported through the shell due to the pressure gradient between the water inside the annular space and the water in the capillary pores. (Figure 3.5, step 2).
- The pressure gradient will decrease until the pressure inside the annular space and in the capillary pores will be in equilibrium. Simultaneously the volume of the annular space will decrease. If no pressure gradient exists anymore, the shell will carry the complete load and it is assumed that there is no interaction between shell and core ($IF = 0$) (Figure 3.5, step 3).

- The interaction factor will be calculated from the deformations, determined in step 3. The interaction factor is assumed to be the ratio between the time dependent deformation of the shell of cement gel and the final deformation of the shell (Figure 3.5, step 4):

$$IF_{(t)} = 1 - \frac{\partial u_{(t)}}{\partial u_{\text{final}}} \quad [3.14]$$

With:

IF = Interaction Factor [-]

$\partial u_{(t)}$ = deformation [m]

$\partial u_{\text{final}}$ = final deformation [m]

3.4 Flow aspects of the model

If the three phase system (core of unhydrated cement grain, annular space and shell of cement gel) is loaded, the water inside the annular space will be loaded as well. The water in the capillary pores is ‘relatively free’ to move into the empty pores, while the water inside the annular space is hindered to move. This results in a pressure difference between the water inside the hollow shell and the water in the capillary pores. This pressure difference will induce a water flow through the shell of cement gel. Assuming a very slow laminar water flow and completely saturated gel pores, the rate of the water flow can be calculated by use of Darcy’s Law:

$$v_w = \frac{k_w \cdot \Delta P_w}{\gamma_w \cdot \Delta x} \quad [3.15]$$

with:

v_w = superficial (or bulk) fluid flow rate through the medium [m/s]

k_w = permeability of the medium for water [m/s]

ΔP_w = pressure difference over the medium [Pa]

γ_w = specific density of water [N/m³]

Δx = thickness of the medium (shell of cement gel) [m]

Proposed model for time-dependent behaviour

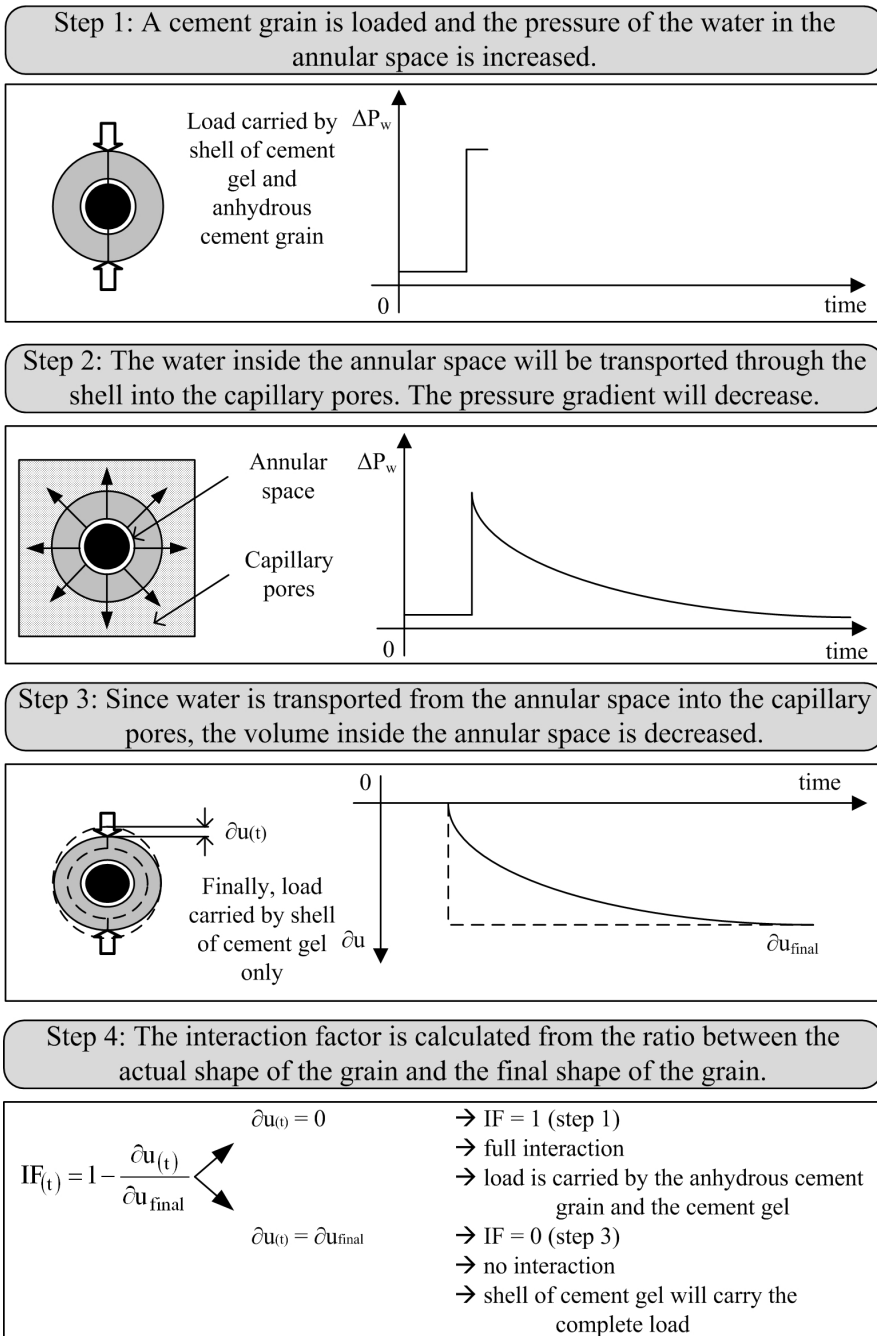


Figure 3.5 Schematic determination of the interaction factor 'IF'

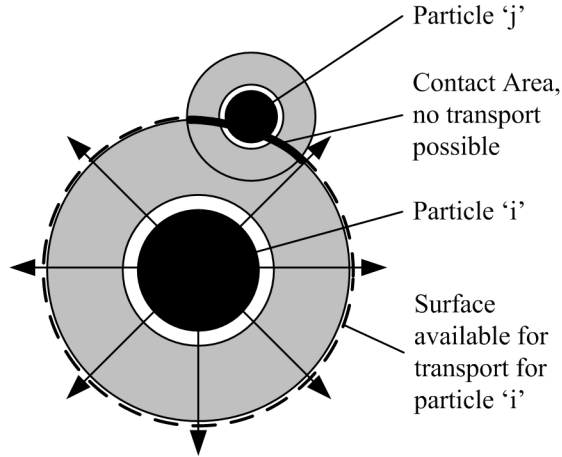


Figure 3.6 Contact area of particle 'i' with neighbour particle 'j'

The pressure difference, which is the driving force for the water movement, is the difference in pressure inside the hollow shell and the pressure in the capillary pores. Multiplying the speed of the water flow by the spherical surface area of the shell of cement gel that is in contact with the surrounding pores, gives the volume of transported water through the shell in time. This flow of water enables the shell of cement gel to deform. The surface of the shell that is in contact with the surrounding pores can be calculated by the outer surface of particle 'i' itself (A_i), minus the contact surface with the neighbour particle 'j' ($A_{\text{contact};j}$) (Figure 3.6).

Which particles will be taken into account to calculate connected surfaces is determined directly after building the microstructure of cement grains. During hydration, the volume of solids increases. If due to this growth a surrounding particle 'j' is (partly) encapsulated in the growing outer shell of the particle 'i', the particle 'j' is considered a neighbour of the particle 'i'. For each grain 'i', all neighbour particles are determined, by assuming all grains completely hydrated (Figure 3.7).

Proposed model for time-dependent behaviour

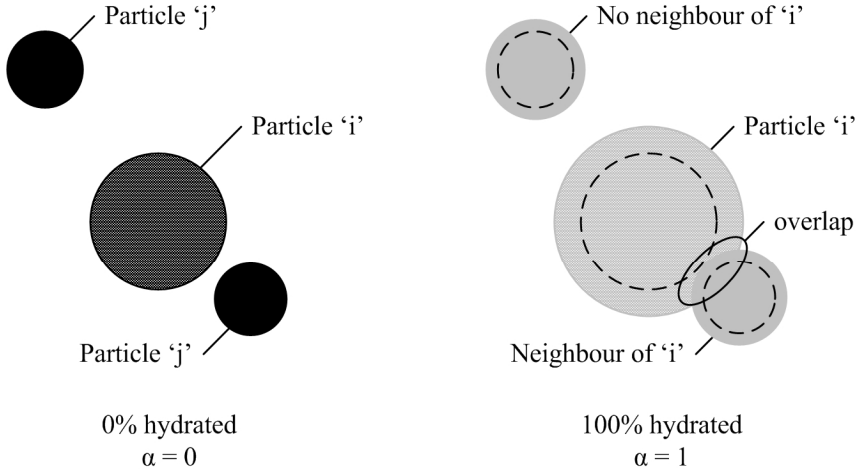


Figure 3.7 Determining neighbour particles 'j' of particle 'i'

The area of the shell of cement gel 'A_t' available for transport of water between the annular space and the capillary pores is now calculated by the difference between the total area of the shell 'A_i' and the contact area with neighbour particles 'A_{contact;j}':

$$A_t = A_i - A_{\text{contact};j} \quad [3.16]$$

with:

$$A_i = \text{total outer area of the shell of cement gel, } A_i = 4\pi r^2 \text{ [m}^2\text{]} \quad [3.17]$$

$$r = \text{mean radius of the shell of cement gel [m]}$$

$$A_{\text{contact};j} = \text{contact area with neighbour particles [m}^2\text{]}$$

The area available for transport of water between the annular space and the capillary pores can be added to Darcy's law (equation 3.15):

$$\frac{\partial V_{\text{annular}(t)}}{\partial t} = \frac{k_w \cdot \Delta P_w}{\gamma_w \cdot \Delta x} \cdot (A_i - A_{\text{contact};j}) \quad [3.18]$$

Now Darcy's law can be used to calculate the volume of water which will be transported between the annular space and the capillary pores in a time step ' ∂t ', due to a pressure gradient (driving force).

3.4.1 Pressure transfer of load bearing water due to particle loading

The driving force for the flow of load bearing water between the annular space (space between the anhydrous cement grain and the shell of cement gel) and the pore system of the bulk paste is the pressure difference between the load bearing water and the pore water pressure in this system. Input for the calculation of the pressure in the annular space is the elastic volume change of the spherical hollow shell. For an unloaded situation, all particles are assumed to be perfectly spherically shaped. The initially spherically shaped three-phase system will deform after loading into an oblate ellipsoid system, which is accompanied by a volume change (Figure 3.8 left and middle).

The sphere (with volume V_{sphere}) will deform into an oblate ellipsoid (with volume V_{oe})

$$V_{\text{sphere}} = \frac{4}{3} \cdot \pi \cdot r^3 \quad \rightarrow \quad V_{\text{sphere}} = \frac{4}{3} \cdot \pi \cdot a \cdot b \cdot c \quad [3.19]$$

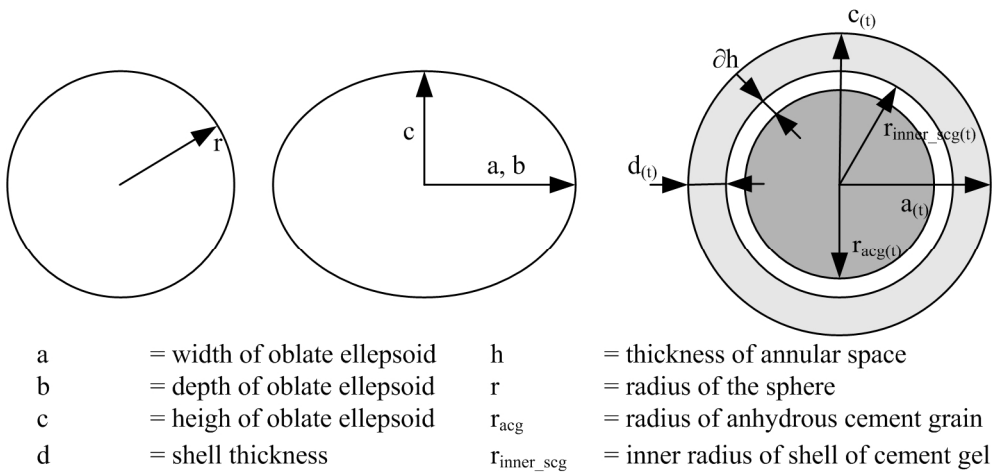


Figure 3.8 Parameters of a sphere (left) an oblate ellipsoid (middle) and a hollow shell particle (right)

Proposed model for time-dependent behaviour

with:

- r = radius of the sphere ($a = b = c = r$) [m]
 $a = b$ = elliptic radii of the oblate ellipsoid (a perpendicular to b) [m]
 c = elliptic radius (height) of the oblate ellipsoid [m]

The volume of the annular space ' $V_{\text{annular}(t)}$ ' is the volume inside the spherical shell of cement gel minus the volume of the spherical anhydrous cement grain:

$$V_{\text{annular}(t)} = \frac{4}{3} \cdot \pi \cdot r_{\text{inner_scg}(t)}^3 - \frac{4}{3} \cdot \pi \cdot r_{\text{acg}(t)}^3 \quad [3.20]$$

with:

- V_{annular} = volume of the annular space
 $r_{\text{inner_scg}}$ = inner radius of the spherical shell of cement gel
 r_{acg} = radius of the anhydrous cement grain

After the deformation of the shell of cement gel, the volume of the annular space becomes (as a function of time):

$$V_{\text{annular}(t)} = \frac{4}{3} \cdot \pi \cdot c_{(t)} \cdot a_{(t)}^2 - \frac{4}{3} \cdot \pi \cdot r_{\text{acg}(t)}^3 \quad [3.21]$$

with:

- $V_{\text{annular}(t)}$ = volume of the annular space
 t = age of the cement paste [s]
 $c_{(t)}$ = elliptic inner radius (high) of the shell of cement gel
 $a_{(t)}$ = elliptic inner radius (width) of the shell of cement gel
 $r_{\text{acg}(t)}$ = radius of the anhydrous cement grain

The volume change is determined from Δc and Δa (Figure 3.9).

$$\Delta V = \frac{4}{3} \cdot \pi \cdot (c_t + \Delta c - d_t) \cdot (a_t + \Delta a - d_t)^2 - \frac{4}{3} \cdot \pi \cdot (c_t - d_t) \cdot (a_t - d_t)^2 \quad [3.22]$$

with

$d_{(t)}$ = thickness of the shell of cement gel [m]

An expression for the elastic deformations of a uniformly loaded hollow sphere has been derived based on the theory of elastic plates and shells (Appendix B).

$$\Delta c = \left(0.7883 \cdot \left(\frac{r}{d} \right) + 0.0388 \right) \cdot \frac{\sqrt{3(1-\nu^2)}}{4} \cdot \frac{(q \cdot \pi \cdot r^2) \cdot r}{E_{gel} \cdot d^2} \quad [3.23]$$

$$\Delta a = 0.5069 \cdot \Delta c \quad [3.24]$$

In this equation, the constant ratio between Δc and Δa is defined as ‘ ρ ’, where $\rho = 0.5069$.

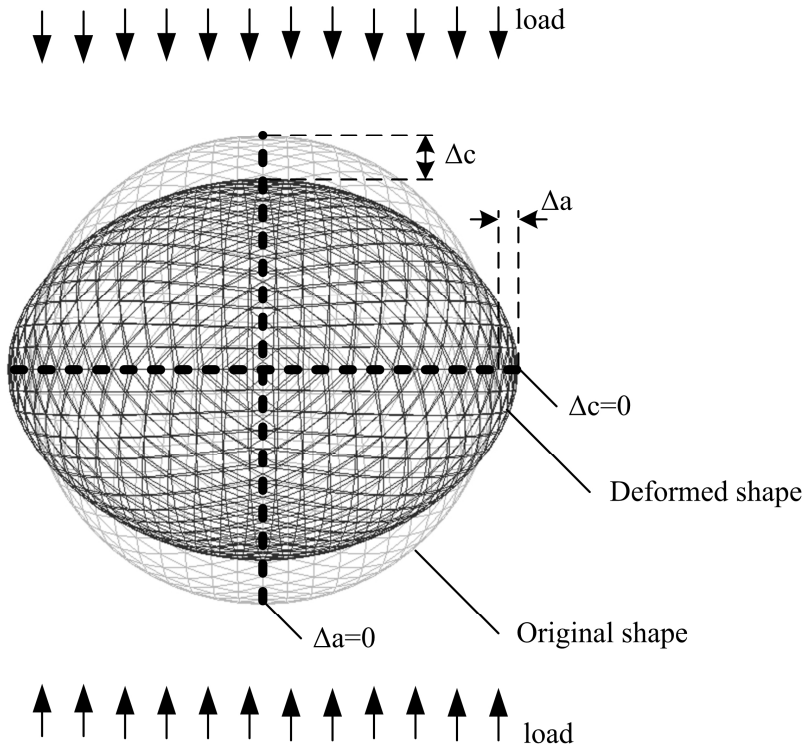


Figure 3.9 Simulated elastic deformations of a loaded hollow sphere

Proposed model for time-dependent behaviour

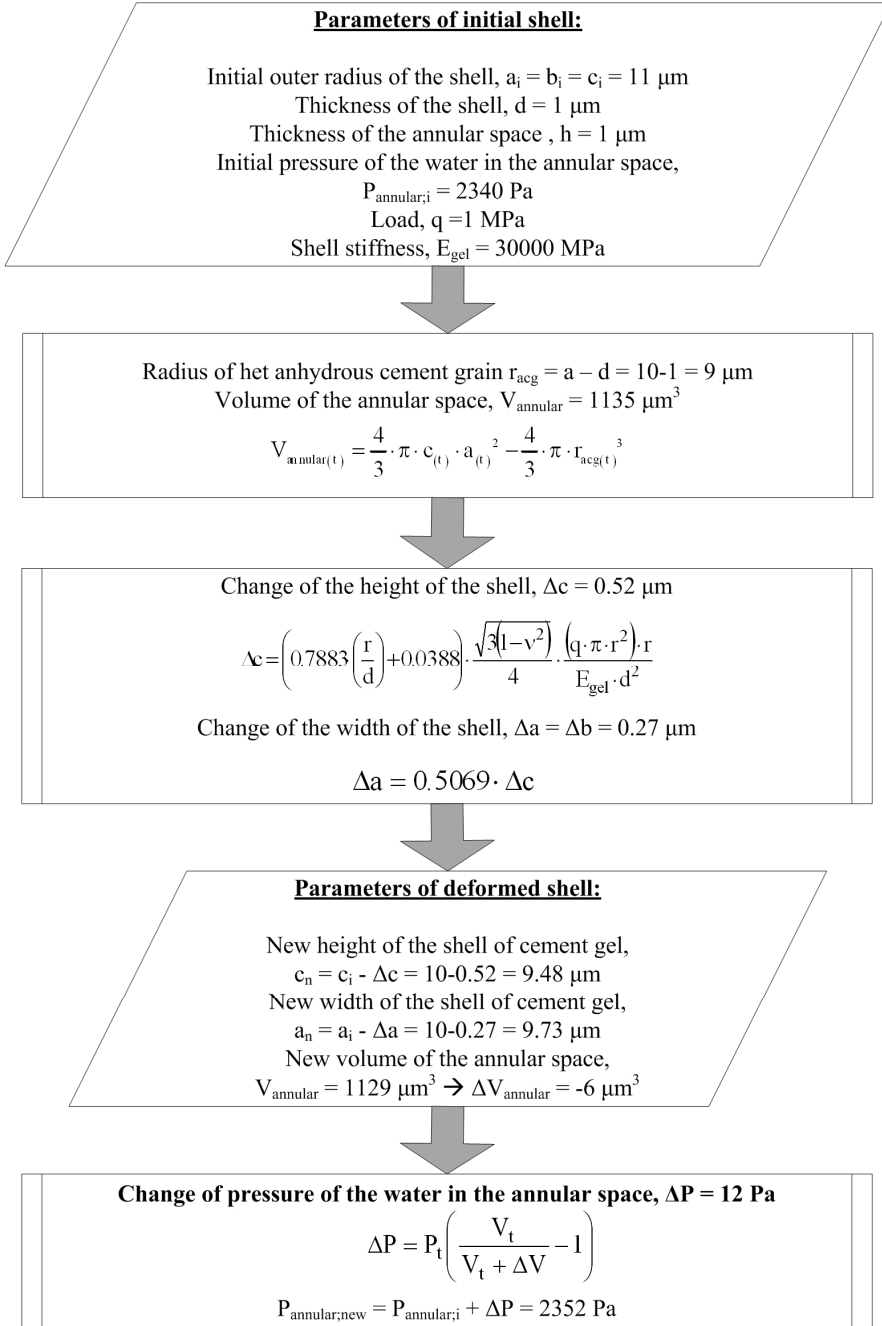


Figure 3.10 Flow chart of the procedure to calculate the pressure increment of the water in the annular space

E_{gel} is taken as 30 GPa (average of $E_{\text{gel};\text{inner}}$ and $E_{\text{gel};\text{outer}}$)[Manzano, 2009]. The pressure increment induced by a volume change can be calculated by Boyle's law:

$$\Delta P = P_t \left(\frac{V_t}{V_t + \Delta V} - 1 \right) \quad [3.25]$$

The influence of several parameters is presented in Figure 3.11 and Figure 3.12. A flowchart for the calculation procedure is presented in Figure 3.10. In this flowchart, one value of Figure 3.11 is calculated as an example. All graphs of Figure 3.11 and Figure 3.12 are calculated according to this procedure.

The calculated pressure due to a load is presented for different cement grain sizes (Figure 3.11, left) and for different shell thicknesses (Figure 3.12, right). In Figure 3.11 the influence of respectively the outer radius of a shell of cement gel on the initial pressure build-up inside the shell of cement gel directly after applying the load (left) and the ratio of radius and thickness of the shell of cement gel around a cement grain on the shell deformations (right) is presented. An increase of the radius of the cement grain results in an increase of the pressure build-up due to a load. An increase of the shell thickness results in a decrease of the pressure build-up in the annular space. This is the result of both the change of the ratio between radius of the sphere and the thickness of the shell. An increase of this ratio means a stiffer shell. The increase in stiffness results in a higher load bearing capacity of the shell and a lower pressure build-up in the water inside the shell. From Figure 3.12 it follows that increasing the load results in an expected increase of the pressure build-up inside the shell. An increase the shell thickness results in an expected decrease of the pressure build-up inside the shell.

Proposed model for time-dependent behaviour

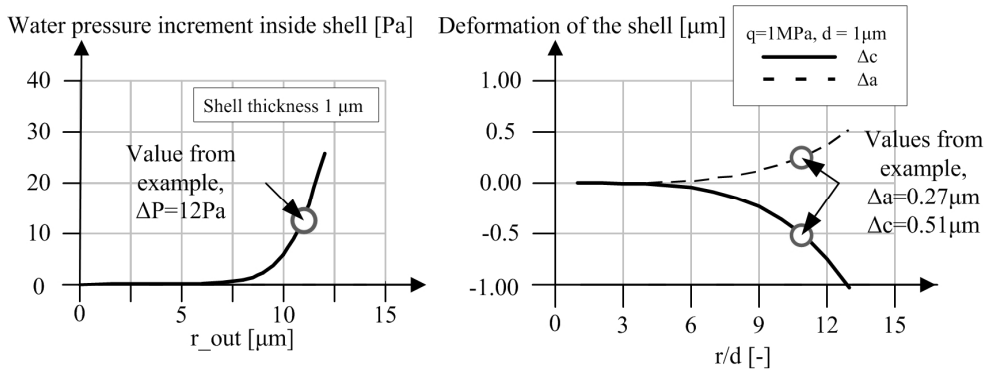


Figure 3.11 Influence of outer radius of cement grain on pressure build-up inside a hollow shell (left) and r/d ratio on shell deformations (right) for $q = 1$ MPa and shell thickness of $1\ \mu\text{m}$

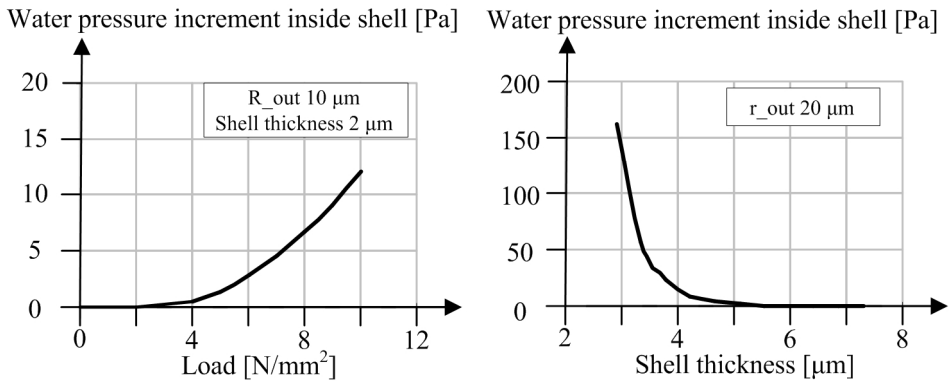


Figure 3.12 Pressure build-up inside a hollow shell as a function of a uniformly distributed load and as a function of shell thickness

3.4.2 Permeability of CSH-gel

Besides the pressure difference over the shell, the permeability of this shell is a very important parameter for the rate of moisture flow through the shell as well. A high permeability results in a higher rate of the moisture flow. The pressure difference decreases quickly and the final shape is obtained. This results in a high interaction factor. A low permeability on its turn, results in a low interaction factor.

Cement gel consist primarily of CSH gel and CH. The intrinsic permeability of CSH gel is approximately $\kappa = 7 \times 10^{-23} \text{ m}^2$ [Powers 1958]. The permeability is related with the intrinsic permeability by [Powers, 1958]:

$$k_w = \frac{\kappa \cdot \rho_w \cdot g}{\eta_e} = 3.16 \cdot 10^{-15} \text{ m/s} \quad [3.26]$$

with:

- k_w = permeability [m/s]
- κ = coefficient of permeability $7 \times 10^{-23} \text{ m}^2$
- ρ_w = density of water 1000 kg/m^3
- g = gravitational constant 10 m/s^2
- η_e = effective coefficient of viscous resistance [kg/m.s]

The effective coefficient of viscous resistance is also calculated by [Powers, 1979]:

$$\eta_e = \frac{h \cdot N}{V} \exp^{\Delta G/R \cdot T} = 2.218 \cdot 10^{-4} \quad [3.27]$$

with:

- h = Planck's constant $6.6256 \times 10^{-27} \text{ erg-sec}$
- N = avogadro's number $6.0225 \times 10^{23} \text{ molecules/mol}$
- V = molar volume of the fluid $18 \text{ cm}^3/\text{mol}$
- ΔG = Gibbs free energy of activation for flow 2.240 cal/mol [Powers, 1979]
- R = gas constant $1.8972 \text{ cal/deg/mol}$
- T = absolute temperature 293 K

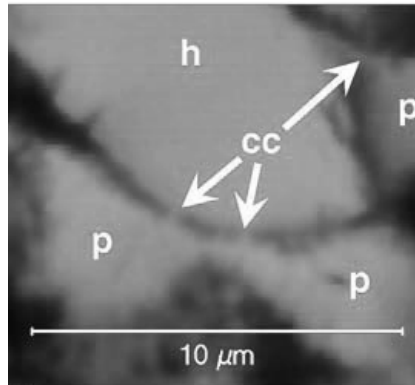


Figure 3.13 Fine connecting channels (cc) between hollow shell (h) and capillary pores (p), observed by Head [Head, 2006]

However, the permeability of the shell of CSH gel surrounding the anhydrous core of a cement particle does not consist of perfectly ordered CSH gel. Gel pores reside in CSH gel. Head observed fine connecting channels (cc) through the shell of CSH gel that connects the space inside the shell (h) with the capillary pores (p) (Figure 3.13) [Head, 2006]. Based on these connecting channels, the permeability of the gel can be determined from the permeability of cement paste. For cement pastes with an initial water/cement ratio lower than 0.35 the volume of the CSH gel is sufficient to fill all the space originally occupied by water in the hardening paste completely (at complete hydration) [Powers, 1954]. Therefore, the measured permeability of hardened cement paste for these water/cement ratios is assumed to be linearly dependent on the permeability of the gel itself. For cement pastes with an initial water/cement ratio below 0.35, the water permeability is below $1 \cdot 10^{-14}$ m/sec [Powers, 1954], which is in accordance with the calculated permeability of a pure CSH phase ($3.16 \cdot 10^{-15}$ m/s).

3.5 Time dependent deformation of the shell

With the volume change in time known from the transported water in time (equation 3.18), the deformation of the shell in loading direction and in the

direction perpendicular to the direction of the load, can be calculated from equation 3.22:

$$\frac{\partial V_{\text{annular}(t)}}{\partial t} = \frac{4}{3} \cdot \pi \cdot \left(c_t + \frac{\partial c}{\partial t} - d_t \right) \cdot \left(a_t + \frac{\partial a}{\partial t} - d_t \right)^2 - \frac{4}{3} \cdot \pi \cdot (c_t - d_t) \cdot (a_t - d_t)^2 \quad [3.28]$$

where the deformation of the sphere perpendicular to the load direction is described by (Figure 3.9):

$$\frac{\partial a}{\partial t} = \rho \cdot \frac{\partial c}{\partial t} \quad [3.29]$$

In paragraph 3.4.1 the ratio ‘ ρ ’ between Δc and Δa was determined at 0.5069. Substitution of equation 3.29 in 3.28 results in a third order equation:

$$\begin{aligned} \left(\frac{\partial c}{\partial t} \right)^3 + \frac{[(c_t - d_t) \cdot \rho^2 + 2 \cdot (a_t - d_t) \cdot \rho]}{\rho^2} \cdot \left(\frac{\partial c}{\partial t} \right)^2 + \\ + \frac{[(c_t - d_t) \cdot 2 \cdot (a_t - d_t) \cdot \rho + (a_t - d_t)^2]}{\rho^2} \cdot \left(\frac{\partial c}{\partial t} \right) + \\ \frac{\left(\frac{\partial V_{\text{annular}(t)}}{\partial t} + \frac{4}{3} \cdot \pi \cdot (c_t - d_t) \cdot (a_t - d_t)^2 \right)}{\frac{4}{3} \cdot \pi} - (c_t - d_t) \cdot (a_t - d_t)^2 \\ \hline \rho^2 = 0 \end{aligned} \quad [3.30]$$

assume:

$$f = \frac{[(c_t - d_t) \cdot \rho^2 + 2 \cdot (a_t - d_t) \cdot \rho]}{\rho^2} \quad [3.31]$$

$$g = \frac{[(c_t - d_t) \cdot 2 \cdot (a_t - d_t) \cdot \rho + (a_t - d_t)^2]}{\rho^2} \quad [3.32]$$

Proposed model for time-dependent behaviour

$$h = \frac{\left(\frac{\partial V_{\text{annular}(t)}}{\partial t} + \frac{4}{3} \cdot \pi \cdot (c_t - d_t) \cdot (a_t - d_t)^2 \right) - (c_t - d_t) \cdot (a_t - d_t)^2}{\frac{4}{3} \cdot \pi \rho^2} \quad [3.33]$$

then equation 3.30 becomes:

$$\left(\frac{\partial c}{\partial t} \right)^3 + f \cdot \left(\frac{\partial c}{\partial t} \right)^2 + g \cdot \left(\frac{\partial c}{\partial t} \right) + h = 0 \quad [3.34]$$

Equation 3.40 can be solved with the equation of Cardano [Kreyszig, 1988]:

$$\frac{\partial c}{\partial t} = -\frac{1}{3}f + \sqrt[3]{\frac{1}{2}q + \sqrt{\frac{q^2}{4} + \frac{p^3}{27}}} + \sqrt[3]{\frac{1}{2}q - \sqrt{\frac{q^2}{4} + \frac{p^3}{27}}} \quad [3.35]$$

where:

$$p = g - \frac{1}{3}f^2 \quad \text{and} \quad q = -\frac{2}{27}f^3 + \frac{1}{3}fg - h \quad [3.36]$$

In Figure 3.14 the simulated development of the pressure with time, inside the shell of cement gel with a shell thickness of 1 μm (left) and for a shell thickness of 2 μm (right) is presented for saturated samples. An increase of the shell thickness resulted in a decrease of the initial pressure build-up directly after loading. This was also presented in Figure 3.11 (right) for a particle with a larger radius.

A decrease of the permeability of the shell of cement gel results, as expected, in a decrease of the rate of pressure release (Figure 3.15). For this characteristic particle, the decrease of the permeability ($k_w/4$) results in a slower pressure release. For a permeability of ' k_w ' it took about 1 hour to release the pressure and for a permeability of ' $k_w/4$ ' it took about 3 hours to release the pressure.

Comparing Figure 3.14 (left) and Figure 3.15 (left), shows that smaller particle sizes result in an increase of the pressure release. All dependencies between the

rate of pressure release, deformation rate, radius of the cement grain, thickness of the shell of cement gel etc., show that for the behavior of a system of cement grains (i.e. cement paste), the deformational behavior of each single cement grain (e.g. Figure 3.16) has to be taken into account explicitly. The behavior of cement paste is presented in paragraph 3.6.

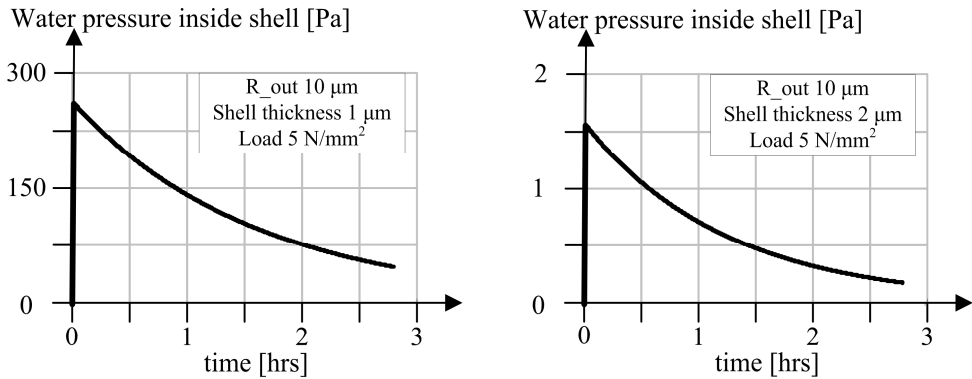


Figure 3.14 Pressure development of water in the annular space, for a saturated sample with a cement particle with shell thickness of $1 \mu m$ (left) and $2 \mu m$ (right)

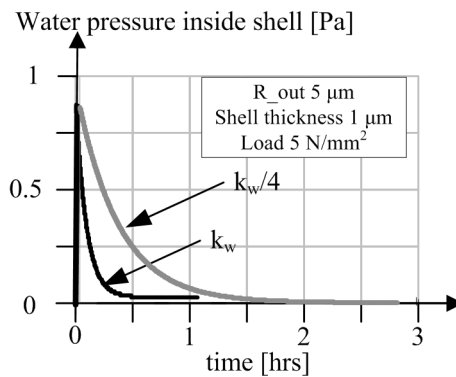


Figure 3.15 Pressure development for a cement particle with different permeabilities of the CSH gel

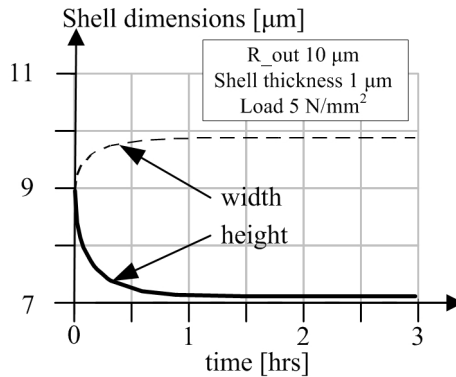


Figure 3.16 Development of the deformations (width and height) of a loaded cement particle

3.6 Cement paste

The proposed model describes the interaction between a shell of CSH gel and an anhydrous core, which are separated by a layer of water, for one single grain. However, concrete consists of aggregates and cement paste. The cement paste is located in between the aggregates and consists of cement grains with a certain grain size distribution (Figure 3.17). In this paragraph, the behaviour of cement paste will be described by a series of single cement grains. A Ribbon model [Koenders, 1997] is used to simulate the hydration of the tubular element, representing a paste situated in-between two aggregate particles (Figure 3.18).

In the Ribbon model, a tubular paste element is randomly filled with cement grains following a predefined grain size distribution. An overall interaction factor is determined, which describes the interaction between the shells of CSH gel and the anhydrous cement grains in a cement paste while the paste is under load.

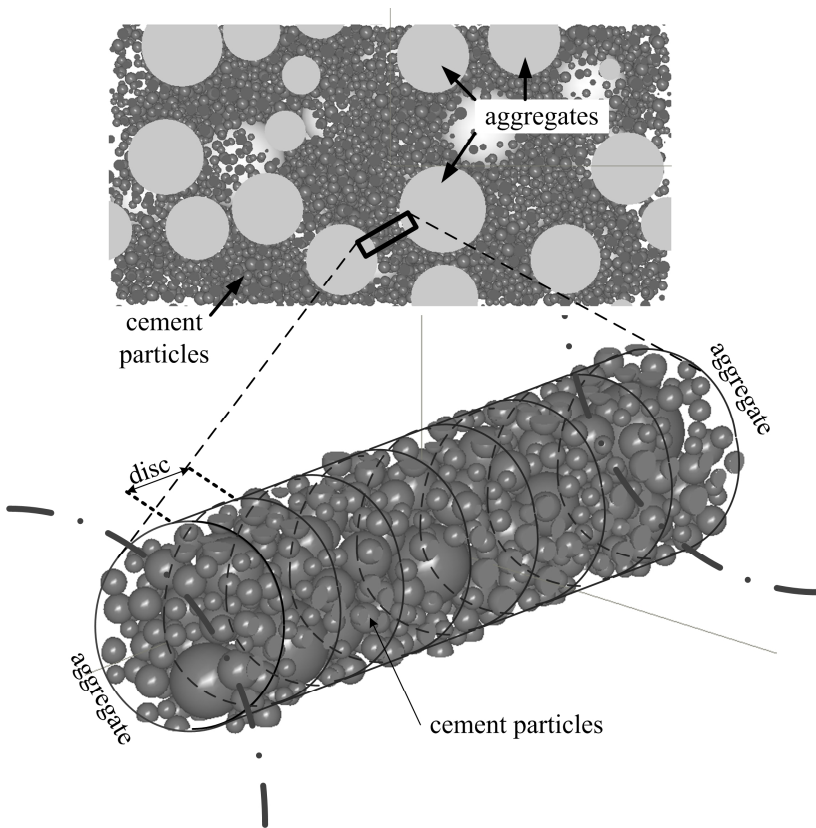


Figure 3.17 Cement paste between aggregate particles

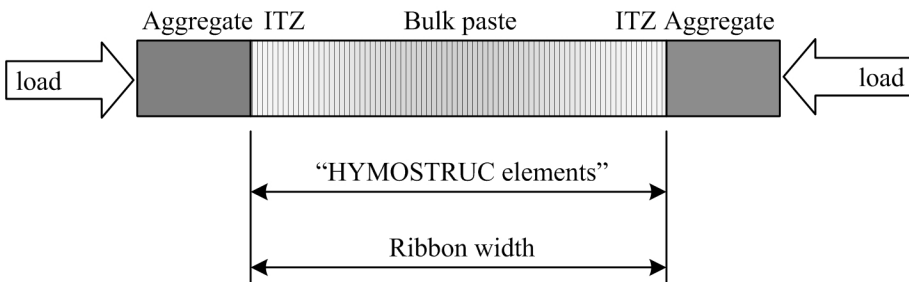


Figure 3.18 Loaded ribbon model (discs filled with cement particles) between two aggregate particles

Proposed model for time-dependent behaviour

The interaction factor relates the effective stiffness of hardening concrete to the visco-elastic behaviour of hardening concrete. The development of the interaction factor is determined by the proposed model for each particle in the ribbon model. All interaction factors for all individual particles in the Ribbon model are taken into account according to a parallel-series system in an overall interaction factor 'IF'. For this, the Ribbon is subdivided in a number of equal 'discs', where the parallel-series system is assumed to consist of (Figure 3.18). The grains inside one disc act as the parallel part, and the individual discs act as a serial part of the parallel-series system:

$$IF = \sum_{j=1}^m \left[\frac{\sum_{i=1}^n IF_i}{n} \right] \quad [3.37]$$

with:

- IF = overall interaction factor [-]
- m = total number of discs [-]
- j = disc number [-]
- n = total number of particles in one disc [-]
- i = particle number [-]
- IF_i = interaction factor of each individual particle [-]

From the parallel-series system, the visco-elastic behaviour of a microstructure can be determined while considering the overall interaction factor 'IF'. A parameter study with the proposed model is performed to study the effects of hydration on the visco-elastic behaviour of hardening concrete. The following parameters were studied:

- Age and degree of hydration at loading
- Water/cement ratio
- Fineness of the cement

3.6.1 Influence of age and degree of hydration at loading

In Figure 3.19 the simulated development of the interaction factor is presented for a cement paste with a Portland Cement and a Blaine value of $300 \text{ m}^2/\text{kg}$. The water/cement ratio of the paste was 0.50. From Figure 3.19, a significant increase of the interaction factor can be distinguished with elapse of time. This means that loading the system at later ages leads to an increased effective modulus (equation 3.13) which, on its turn, has the same result as a decrease of the creep coefficient. In Figure 3.20 the development of the interaction factor is plotted against the degree of hydration. For the very young concrete, the interaction factor starts to develop from one. This implies a full interaction between the shell of CSH gel (which is very thin at low degrees of hydration) and the core of anhydrous cement grains. This can be explained by the absence of a load bearing capacity of the very thin shells of CSH gel. With increasing thickness of the shell of CSH gel, i.e. with increasing degree of hydration, also the load bearing capacity of the shell of CSH gel will increase, which results in a lower interaction value. Besides the developing degree of hydration, the associated thickening of the shells of CSH gel and the increase of the load bearing capacity of the shell, there will be larger contact areas with the neighbouring particles. The latter will, on its turn, also reduce the area available for water movement (Figure 3.6). The reduction of the water transport between the annular space and the capillary pores dominates the interaction factor, which results in an increase of the interaction factor with an increasing degree of hydration.

Proposed model for time-dependent behaviour

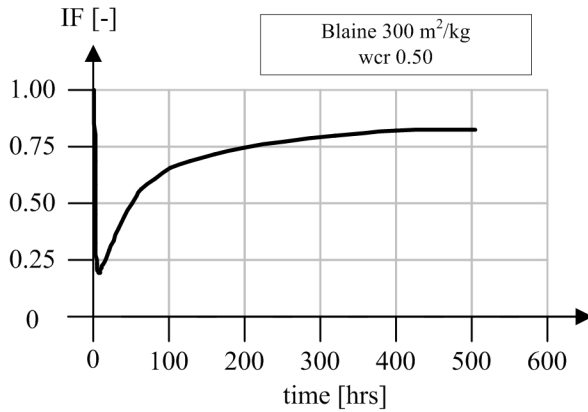


Figure 3.19 Interaction factor 'IF', which describes the interaction between the shells of CSH gel and the anhydrous cement grains, as a function of time (IF = 1, full interaction; IF = 0, no interaction)

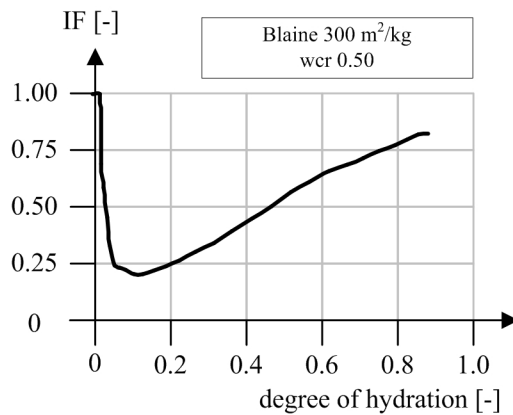


Figure 3.20 Interaction factor 'IF' of a simulated cement paste as a function of the degree of hydration

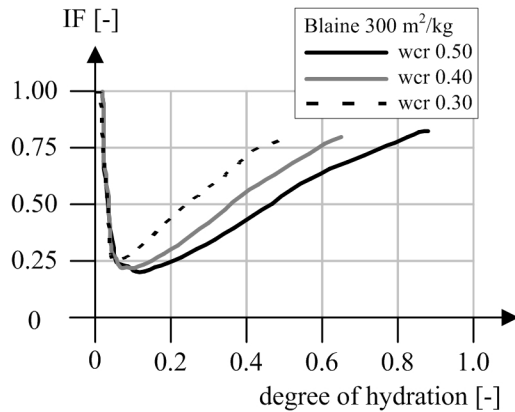


Figure 3.21 Influence of water/cement-ratio on interaction factor ‘IF’

3.6.2 Influence of the water/cement ratio

From literature it is known that an increase of the water/cement ratio will lead to a significant increase of the visco-elastic deformation of hardening concrete [Lorman, 1940]. A similar trend is found with the proposed model (Figure 3.21). Because of the smaller distances between the cement particles, a decrease of the water/cement ratio results in an increased density of the microstructure. The lower the water/cement ratio is, the higher is the contact area between the cement particles at equal degree of hydration. This results in a smaller area remaining for the water to be transported between the hollow shells and the capillary pores. Due to this reduced ability of water transport, the pressure inside the shell of cement gel will decrease slower. This slower rate results in a stiffer behaviour of the system (a higher interaction factor).

3.6.3 Influence of cement fineness

In literature, some authors report an increase of creep of hardening concrete with increasing cement fineness [Wischers, 1977] and [Neville, 1983], whereas others report a decrease of creep of hardening concrete with increasing fineness of the cement [Neville, 1983], [Nakamoto, 1997] and [Lokhorst, 2001].

Proposed model for time-dependent behaviour

The influence of cement fineness is studied with the proposed model. The cement fineness is characterized by the Blaine value of the cement. Since the diameter of the cement grains is a direct input parameter for the proposed model by means of the grain size distribution of the simulated cement, it is possible to analyze the influence of the cement fineness on the visco-elastic behaviour of hardening concrete. In Figure 3.22 the influence of the cement fineness on the interaction factor is presented in the degree of hydration domain (left). The development of the interaction factor 'IF' is presented for Portland cement-based pastes with Blaine values of 300 m²/kg, 420 m²/kg and 550 m²/kg and a water/cement ratio of 0.50. A slight decrease of the interaction factor 'IF' is calculated for an increasing cement fineness. The cement fineness itself has hardly any influence on the visco-elastic behaviour of hardening concrete. However, it must be said that increasing the cement fineness also results in an increase of the rate of hydration (Figure 3.22 (right) & Figure 3.23). In the time domain creep decreases with increase of the cement fineness (due to the different rate of hydration).

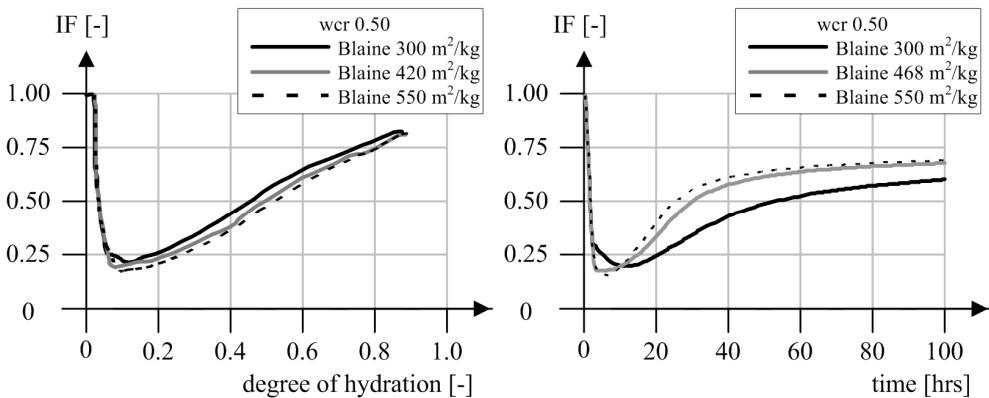


Figure 3.22 Influence of cement fineness on interaction factor 'IF' on degree of hydration domain (left) and time domain (right)

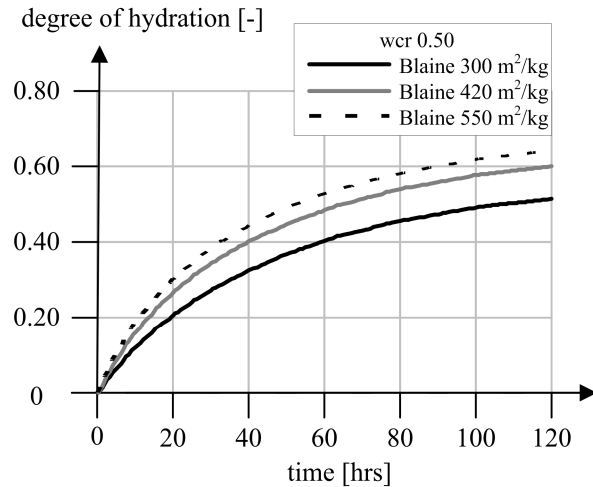


Figure 3.23 Development of degree of hydration in Portland cement based concretes with a water/cement factor of 0.5 and Blaine values from 300 – 550 m²/kg (simulated by HYMOSTRUC)

3.7 Validation grid

The validation grid, as presented in Figure 3.24, is adopted to validate the results of the theory proposed in this chapter. The grid covers relevant cement pastes with water/cement ratio's of 0.3, 0.4 and 0.5, while using cements with Blaine values of 300, 420 and 550 m²/kg. From the simulated results for the validation grid (Figure 3.25) it turns out that the water/cement ratio has a dominating influence on the interaction factor 'IF'. Lowering the water/cement ratio results with the same degree of hydration in a higher interaction factor, what results in less visco-elastic deformations of cement pastes with lower water/cement ratios. This is in agreement with the general accepted opinion about the influence of the water/cement ratio on the visco-elastic behaviour of hardening concrete.

	w/c-ratio 0.2	w/c-ratio 0.3	w/c-ratio 0.4	w/c-ratio 0.5	w/c-ratio 0.6
Blaine value 300 m ² /kg		○	○	○	
Blaine value 420 m ² /kg		○	○	○	
Blaine value 550 m ² /kg		○	○	○	

Figure 3.24 Validation grid, which indicates the studied combinations of Blaine value and w.c-ratio (indicated with dots) on the interaction factor

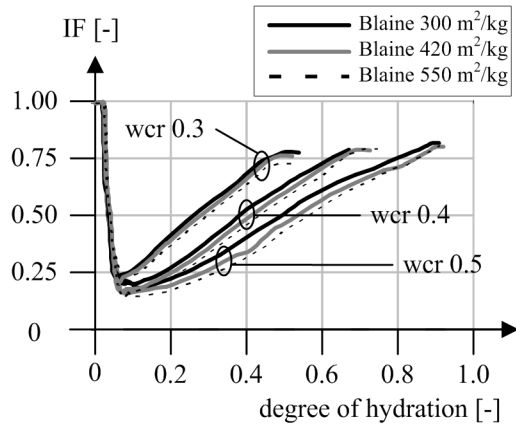


Figure 3.25 Interaction factors 'IF' for the validation grid

The influence of the Blaine value of the cement results in a negligible influence on the interaction factor 'IF' (Figure 3.25). In the literature, there is no agreement about the influence of the Blaine value of the cement. More experimental results are needed to determine the influence of the Blaine value on the visco-elastic behaviour of hardening concrete. This will be part of the experimental program to be discussed in the next chapter. The proposed model results in similar results for cement pastes loaded in compression and loaded in tension. Because also about the influence of this parameter (load sign) no agreement exists in literature, this will also be part of the experimental program.

3.8 Discussion

In this chapter, a model is presented which calculates an interaction factor between the shell of the CSH gel and the anhydrous cement grain. The procedure is based on the presence of hollow shells and the transport of water accumulated inside the hollow shells and water in the capillary pores. With the presented procedure, the visco-elastic behaviour is coupled to an explicit description of the micro-structural development as well as to moisture movements when the system is loaded. All parameters necessary for the determination of the interaction factor 'IF' are based on physical concepts. In this chapter, the proposed model is used to study the influence of several parameters on the visco-elastic behaviour. Based on the findings addressed in this chapter, the following remarks are drawn.

- The deformational behaviour of cement pastes with different water/cement ratios simulated by the proposed model, show lower interaction factors for lower water/cement ratios. A lower water/cement ratio results in more time dependent deformations.
- From the simulated results it turned out that the fineness of cement hardly influences the visco-elastic behaviour of the hardening concrete directly; however it does influence the rate of hydration. From the literature, no agreement was found about the influence of the fineness of the cement on the visco-elastic behaviour of hardening concrete.
- The proposed model assumes an equal time dependent behaviour for cement paste loaded in tension and compression.

Proposed model for time-dependent behaviour

The visco-elastic behaviour of a hardening concrete is related to microstructural developments and to the transport of water from the annular space inside the shell of cement gel to the capillary pores. The rate of transport of this water largely depends, among other aspects, on the moisture state in the capillary pores. Therefore, in order to obtain reliable and accurate results from the proposed model, it is accessory also to consider the moisture state in the capillary pores as accurately as possible. For this, it is needed to relate the moisture state in the system to the hydration of cement. This is described in next chapter.

4 Moisture movements at microlevel

4.1 Moisture state in microstructures

The proposed model as presented in Chapter 3 relates the visco-elastic behaviour of a hardening concrete to the transport of water between the annular space between the shell of cement gel and the core of anhydrous cement grain to the capillary pores. The rate of transport of this water depends, among other things (Chapter 3), on the moisture state in the capillary pores. Therefore, in order to obtain reliable and accurate results from the proposed model it is necessary to model the moisture state in the capillary pores as accurately as possible. For this, it is needed to relate the moisture state of the system to the hydration process of cement. If a cement paste would be completely homogenous, the progress of hydration is equal throughout the cement paste system. However, this will never be the case. Cement particles are not homogeneously distributed through the cement paste. Based on the packing of the cement particles in the paste and interfacial transition zone (ITZ), the paste density near aggregate surfaces differs substantially from the density in the bulk paste [Koenders, 1997]. The water/cement ratio for the paste in the ITZ is higher compared to the water/cement ratio in the bulk paste, resulting in much smaller pore diameters in the bulk paste relative to the pore diameters in the ITZ.

Due to the inhomogeneous distribution of the particles in the cement paste between the aggregates, pressure differences exist between water in the pores of cement paste located near the aggregates and water in the pores of cement paste in-between the aggregates. This pressure difference initiates a moisture flow through the cement paste from the water rich ITZ towards the water lacking regions in the bulk paste. This influences the development of properties of the hardening concrete, like degree of hydration, strength, stiffness, permeability, shell thickness. By taking these effects into account the reliability and accuracy of the micro structural

development and the prediction of concrete properties, including the visco-elastic properties, increases.

4.2 Modelling moisture state

In order to model the state of moisture in a cement paste system the inter-particle ribbon model is applied [Koenders, 1997]. The ribbon model is a three dimensional tubular envelop volume (Figure 4.1) for simulating the hardening behaviour of cement paste situated between two aggregate particles. The ribbon is divided into disc elements (Figure 4.2), and for each individual disc element the hydration process is simulated with the particle-based hydration model HYMOSTRUC [Breugel, 1997] [Koenders, 1997]. The degree of hydration depends on the local availability of water. The state of capillary water available in the evolved pore structure can be expressed in terms of the degree of saturation $s(\alpha)$. Whenever the volume of capillary water is consumed during hydration the degree of saturation will reduce. In addition, the degree of saturation is also influenced by the decrease of pore volume with increasing degree of hydration.

It is assumed that the tube of cement paste hardens under sealed conditions; there is only internal distribution of moisture possible. Addition of moisture from outside the simulated tube is not accounted for.

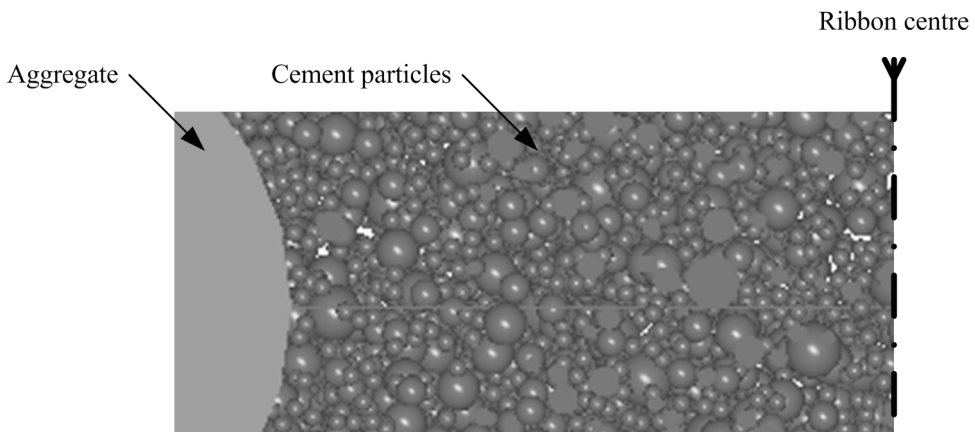


Figure 4.1 Hymostruc elements between two aggregate particles, tube filled with spherical cement particles

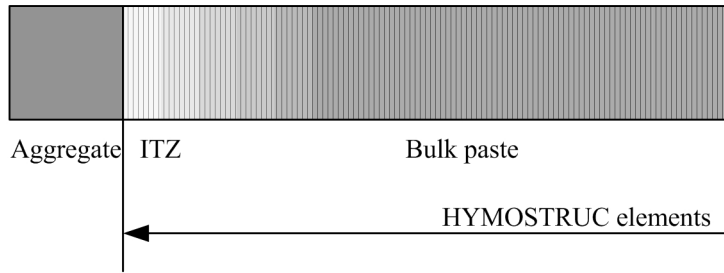


Figure 4.2 Tube divided into hymostruc elements

The degree of saturation is expressed as [Koenders, 1997]:

$$s(\alpha) = \frac{V_w(\alpha)}{V_{por}(\alpha)} \quad [4.38]$$

with:

$s(\alpha)$ = degree of saturation [-]

$V_w(\alpha)$ = actual volume of capillary water [m^3]

$V_{por}(\alpha)$ = actual pore volume [m^3]

α = degree of hydration [-]

If the volume of available water decreases (degree of saturation decreases), the rate of hydration will decrease. The hydration process (re)activates again if the amount of capillary water, V_w , increases (degree of saturation increases). With the degree of saturation, a direct relation between the amount of available capillary water and the degree of hydration is described.

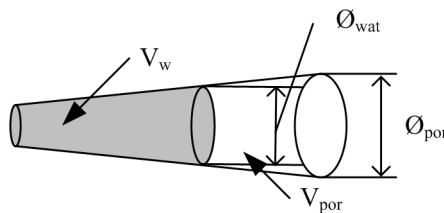
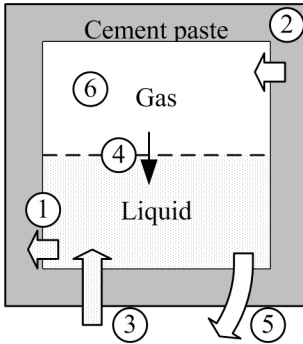


Figure 4.3 Visualisation of capillary water in the pore volume [Breugel, 1997]



Components involved in the Law of conservation of volume

- 1 = consumption of water
- 2 = production of gasses
- 3 = transport of water
- 4 = exchange between gas and water
- 5 = transport of gasses
- 6 = compression of gasses

Figure 4.4 Moisture movement based on law of conservation of volume

4.3 Conservation of volume

The differential equation which describes the flow of fluid and gas in the capillary pore system of a cement paste system is described by a law of conservation and is build up by constitutive equations. The conservation of volume requires that the change rate of a property defined inside a control volume must be equal to what is lost through the boundaries of the volume plus what is produced or consumed, also called source and sink, inside the control volume. For a hydrating cement paste element, this law of conservation results in an element that is visualized in Figure 4.4. In that figure the different components involved in the law of conservation of volume are listed.

4.3.1 Source and sink

The consumption of water and increase of volume of vapour are respectively the source and sink within the law of conservation. With respect to the moisture balance of the system, hydration of cement results in a consumption of water and an increase of volume of vapour (empty pores are vapour filled). The consumption of capillary water (sink) due to hydration of cement as described by van Breugel [Breugel, 1997], and differentiated with respect to time, gives:

$$\frac{1}{V} \cdot \frac{\partial V_w}{\partial t} = - \frac{0.4 \cdot \rho_{ce}}{\rho_w + \rho_{ce} \cdot \omega_0} \cdot \frac{\partial \alpha}{\partial t} \quad [4.39]$$

with:

- V = volume [m³]
- V_w = capillary water volume [m³]
- t = time [s]
- ρ_{ce} = specific mass of cement [kg/m³]
- ρ_w = specific mass of water [kg/m³]
- ω₀ = water/cement ratio [-]
- α = degree of hydration [-]

The increase of volume of vapour is correlated with chemical shrinkage. Since chemical shrinkage does not (or hardly), result in an external volume change, the chemical shrinkage as a function of the degree of hydration as described by van Breugel should be equal to the increased vapour volume due to hydration of the cement. In van Breugel's description, it is assumed that the volume of chemical shrinkage corresponds to about 25% of the chemically bound water and that the chemical bound water is estimated at 25% of the weight of the reacted cement. Differentiating the gas contribution (source) by van Breugel's model [Breugel, 1997] to the time results in:

$$\frac{1}{V} \cdot \frac{\partial V_v}{\partial t} = \frac{0.0625 \cdot \rho_{ce}}{\rho_w + \rho_{ce} \cdot \omega_0} \cdot \frac{\partial \alpha}{\partial t} \quad [4.40]$$

with:

- V = volume [m³]
- V_v = vapour volume [m³]
- t = time [s]
- ρ_{ce} = specific mass of cement [kg/m³]
- ρ_w = specific mass of water [kg/m³]
- ω₀ = water/cement ratio [-]
- α = degree of hydration [-]

By use of the formulas which describe the source and sink contributions, the water consumption and the increase of volume of vapour, the driving forces for transport of capillary water can be calculated as a function of the degree of hydration. The

Moisture movements at microlevel

pressure of the capillary water after 1000 hours of hydration (arbitrary) is presented in Figure 4.5. The procedure to calculate the moisture transport due to the capillary pressure difference is presented in next paragraph.

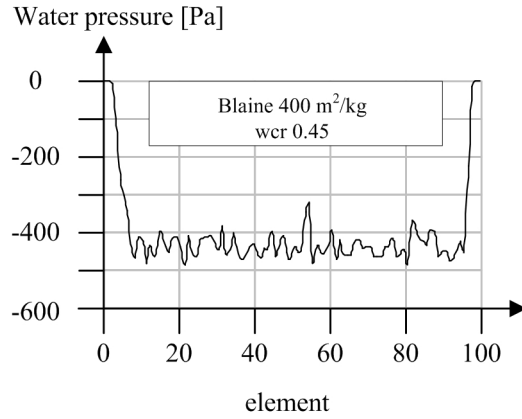


Figure 4.5 Water pressure in the capillary pores of a cement paste with w/c-ratio of 0.45 and cement with a Blaine value of 400m²/kg after 1000 hours of hydration (1 element = 1μm)

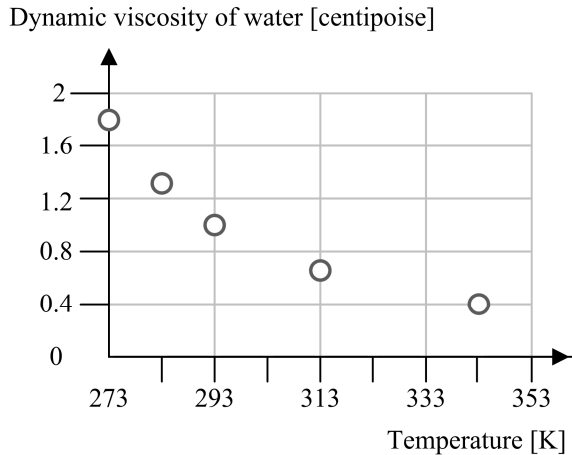


Figure 4.6 Relation between dynamic viscosity of water and temperature [Bear, 1972] (1 centipoise = 0.01 poise = 0.01 g/cm/sec)

4.3.2 Transport components

Capillary water will move through the pore system depending on the driving force that is associated to the pressure difference between the capillary water in the ITZ (high pressure) and in the bulk paste (low pressure). This moisture movement is described by Darcy's law that covers the flow of a liquid through a porous medium:

$$\frac{1}{V} \cdot \frac{\partial V_w}{\partial t} = \frac{\partial}{\partial x} \left(\frac{k_w}{\gamma_w} \cdot \frac{\partial p_w}{\partial x} \right) \quad [4.41]$$

with:

- V = volume [m³]
- V_w = capillary water volume [m³]
- t = time [s]
- x = thickness of the medium (one element) [m]
- k_w = permeability of the medium for water [m/s]
- γ_w = specific density of water [N/m³]
- p_w = applied water pressure difference [Pa]

The water permeability can be deduced from the developing pore structure by applying the actual border limits of the capillary pores which can be deduced from the pore size distribution [Koenders, 1997]:

$$k_w = \frac{(\phi_0^2 + \phi_{\text{wat}}^2) \cdot g}{64 \cdot \nu_w} \quad [4.42]$$

where:

$$\nu_w = \frac{\eta}{\gamma_w} \quad [4.43]$$

- k_w = permeability of the medium for water [m/s]
- ϕ₀ = minimum diameter of capillary pores [m]
- ϕ_{wat} = maximum pore diameter of filled pores [m]
- g = gravity constant of the earth [m/s²]

Moisture movements at microlevel

- ν_w = kinematic viscosity [m^2/s]
 η = dynamic viscosity [$kg/m \cdot s = Pa \cdot s$] (Figure 4.6)
 γ_w = specific density of water [kg/m^3]

By the transport of capillary water, also in the capillary water dissolved gas is transported. This influences the equilibrium of dissolved gasses in the system. The amount of gas dissolved in the pore water can be calculated by Henry's law. Henry's law states that the gas pressure is equal to the number of molecules that touches the surface of the capillary water. For a given temperature, the amount of a given gas dissolved in a given type and volume of liquid is directly proportional to the partial pressure of that gas in equilibrium with that liquid. In mathematical formulation, it states that:

$$e^p = e^{k_\theta \cdot c} \quad \Leftrightarrow \quad p = \lim_{c \rightarrow 0} \left(\frac{\partial p}{\partial c} \right) \cdot c \quad \Leftrightarrow \quad p = k \cdot c \quad [4.44]$$

- p = partial pressure of the solute above the solution [Pa]
 k = Henry's law constant, [L.atm/mol, atm/(mol fraction) or Pa.m³/mol]
 c = concentration of the solute in the solution [mol/m³]

If the temperature increases and the concentration of dissolved gasses is constant, the partial pressure of the solute above the solution increases. If the partial pressure is constant, the concentration of the solute in the solution decreases if the temperature increases, in formula form:

$$k = k_\theta \cdot e^{-C \left(\frac{1}{T} - \frac{1}{T_\theta} \right)} \quad [4.45]$$

with:

- k = Henry's law constant, [L.atm/mol, atm/(mol fraction) or Pa.m³/mol]
 k_θ = Henry's law reference constant 29.41L.atm/mol
 C = constant 2400 [K]
 T = temperature [K]
 T_θ = reference temperature 298.15K (25.15°C)

If Henry's law is differentiated to time, to make it applicable for calculation, we get:

$$\frac{\partial c}{\partial t} = c \left(\frac{1}{p} + \frac{\partial p}{\partial t} \cdot \frac{k_t}{k_{t+1}} - 1 \right) \quad [4.46]$$

In equation 4.46, p is the partial pressure of the solute above the solution, and not the general pressure above the solution (p_g) or the water pressure (p_w) and c is the concentration of the solute in the solution. The partial pressure can be calculated by Dalton's law. Dalton's law is an empirical law that states that the total pressure exerted by a gaseous mixture is equal to the sum of the partial pressures of each individual component in a gas mixture. In formula form:

$$p_g = \sum_{i=1}^n p_i \quad \text{or} \quad p_i = \frac{p_g \cdot c_i}{1.000.000} \quad [4.47]$$

with:

p_g = total gas pressure [Pa]

p_i = partial pressure of component i [Pa]

n = total number of different components

c_i = concentration of the solute i in the solution [mol/m^3]

The change of concentration of components in the gas and in the pore water (mol/m^3) will result in a change of volume of the gas and the pore water. Assuming that water vapour and the dry air components in the gaseous phase behave as ideal gases, the volume change can be calculated by the ideal gas law:

$$p_w \cdot V_w = n \cdot R \cdot T \quad \Leftrightarrow \quad V_w = \frac{n \cdot R \cdot T}{p_w} \quad [4.48]$$

$$p_g \cdot V_g = n \cdot R \cdot T \quad \Leftrightarrow \quad V_g = \frac{n \cdot R \cdot T}{p_g} \quad [4.49]$$

with:

Moisture movements at microlevel

- p_w = pressure of the pore water [Pa]
 V_w = volume of the pore water [m³]
 p_g = pressure of the gas [Pa]
 V_g = volume of the gas [m³]
 n = amount of substance of gas [mol]
 R = gas constant 8.314472 [m³.Pa/K.mol]
 T = temperature [K]

Now the relative volume changes due to the interaction of molecules between a fluid and a gas during a single time step can be calculated by replacing the change of amount of solute (n) in the solution into the change of concentration of solute, Δc , in the solution, c :

$$\frac{\Delta V_g}{V} = \frac{R \cdot T}{p_g} \cdot \Delta c \quad \text{and} \quad \frac{\Delta V_w}{V} = \frac{R \cdot T}{p_w} \cdot \Delta c \quad [4.50]$$

Substitution of formula 4.46 into formula 4.50 leads to the following relation:

$$\frac{1}{V} \cdot \frac{\partial V_g}{\partial t} = \frac{R \cdot T}{p_g} \cdot c_t \left(\frac{p_t + \frac{\partial p}{\partial t} \cdot \frac{k_t}{k_{t+1}}}{p_t} - 1 \right) \quad [4.51]$$

$$\frac{1}{V} \cdot \frac{\partial V_w}{\partial t} = \frac{R \cdot T}{p_w} \cdot c_t \left(\frac{p_t + \frac{\partial p}{\partial t} \cdot \frac{k_t}{k_{t+1}}}{p_t} - 1 \right)$$

By the above formula, the change of volume of gas and water in the pore system driven by the partial pressure difference between water and gas is calculated. Due to this change of volume of gas and water in the pore system, a gradient of diffused gas particles exist in the system. Fick's second law of diffusion is applied to describe the diffusion flow of gas particles in a non-steady or continually changing state diffusion:

$$\frac{\partial c}{\partial t} = D \cdot \frac{\partial^2 c}{\partial x^2} \quad [4.52]$$

with:

- c = concentration dissolved gasses in water [mol/m³]
- D = diffusion coefficient of dissolved gasses in water 0.0016·10⁻⁶ [m²/s]
- x = length [m]

Due to the transport of capillary water in the cement paste system, the pressure of the water and gas in the system changes. Boyle's law states that at a constant temperature the volume of a gas increases when the pressure decreases. In mathematical formulation and differentiated to time, this can be described by:

$$\frac{1}{V} \cdot \frac{\partial V_g}{\partial t} = - \frac{(1-s) \cdot n}{p_g} \cdot \frac{\partial p_g}{\partial t} \quad [4.53]$$

with:

- V = volume [m³]
- V_g = volume of gasses [m³]
- t = time [s]
- s = degree of saturation [-]
- n = porosity [-]
- p_g = gas pressure [Pa]

All presented components involved in the law of conservation of volume are summarized by a Balance equation as presented in the next section.

4.4 Balance equation

Since the microstructure contains three phases (solids, water and gas) the total volume change can be calculated from the volume change of each individual component:

Moisture movements at microlevel

$$\frac{\partial V}{\partial t} = \frac{\partial V_s}{\partial t} + \frac{\partial V_w}{\partial t} + \frac{\partial V_{fg}}{\partial t} \quad [4.54]$$

During a time step, the volume of solids is assumed to be constant:

$$\frac{\partial V_s}{\partial t} = 0 \quad [4.55]$$

The volume change of the total body “e” is equal to the external volume change and is assumed to be zero in a time step:

$$\frac{1}{V} \cdot \frac{\partial V}{\partial t} = \frac{\partial e}{\partial t} = 0 \quad [4.56]$$

The gas volume in the pores will change by the contribution of gas due to hydration, compression of gas and exchange between pore air and pore water:

$$\frac{\partial V_g}{\partial t} = V \cdot \left[\frac{0.0625 \cdot \rho_{ce}}{\rho_w + \rho_{ce} \cdot \omega_0} \cdot \frac{\partial \alpha}{\partial t} - \frac{(1-s) \cdot n}{p_g} \cdot \frac{\partial p_g}{\partial t} - \frac{R \cdot T}{p_g} \cdot c_t \left(\left(1 + \frac{1}{p_g} \frac{\partial p_g}{\partial t} \right) \cdot \frac{k_t}{k_{t+1}} - 1 \right) \right] \quad [4.57]$$

The water transport in a time step is calculated by the summation of water transport, the exchange between gas and water, transport of dissolved gasses and water consumption:

$$\frac{\partial V_w}{\partial t} = V \cdot \left[\frac{k_w \cdot \partial^2 p_w}{\gamma_w \cdot \partial x^2} + \frac{R \cdot T}{p_w} \cdot c_t \left(\left(1 + \frac{1}{p_g} \frac{\partial p_g}{\partial t} \right) \cdot \frac{k_t}{k_{t+1}} - 1 \right) + \frac{R \cdot T}{p_w} \cdot D_{gw} \cdot \frac{\partial^2 c_{gw}}{\partial x^2} - \frac{0.4 \cdot \rho_{ce}}{\rho_w + \rho_{ce} \cdot \omega_0} \cdot \frac{\partial \alpha}{\partial t} \right] \quad [4.58]$$

The moisture movement during cement hydration is solved by Galerkin’s Finite Element approach, where the element vector and mass matrix are obtained by applying the Newton-Cotes rule (Appendix A). The influences of moisture

movements during cement hydration on several properties are studied. Focus is on properties which are used in Chapter 3 (degree of hydration, moisture content, degree of saturation and modulus of elasticity). The influence of moisture movements on the visco-elastic behaviour is presented by the change of concrete properties.

4.5 Calculated effects of moisture movements on concrete properties

Differences between properties of the hardened cement paste with and without moisture movement are presented after 1000 hrs of hydration. A tube of cement paste (ribbon) inbetween two aggregate particles, as presented in Figure 4.1 and Figure 4.2, is divided into a mesh of 100 elements, where each element represents $1\mu\text{m}$ of a ribbon thickness of $100\mu\text{m}$, which is assumed to be representative for ordinary concrete [Koenders, 1997]. Roughly, a tube cement paste (ribbon) represents an interfacial transition zone of $10\mu\text{m}$ (10 elements) around the aggregates and $80\mu\text{m}$ bulkpaste (80 elements). Results are presented for an element in the interfacial transition zone (ITZ) and for an element in the bulk paste (Figure 4.2).

4.5.1 Influence of moisture transport

During hydration of the cement in the ribbon, a capillary pressure or distribution differential in the water, accumulated in the capillary pores of the bulk paste, will develop (Figure 4.7, left). Due to this pressure, moisture will move from the water rich zones around the aggregates (ITZ) towards the water lacking zone in the bulk cement. After transport of moisture as induced by the pressure difference between the elements, the pressure is equal over the whole ribbon (Figure 4.7, left). By the transport of moisture from the ITZ into the bulk paste, the amount of capillary water in the ITZ decreases (Figure 4.7, right) what results in a lower degree of saturation for the elements in the ITZ (Figure 4.8, left). This water is transported from the ITZ to the bulk paste. This does not directly result in a higher degree of saturation for the elements in the bulk paste, because the hydration process for the bulk paste elements is reactivated again due to the supply of extra (ITZ) water (equation 3.2). The movement of extra capillary water into the bulk paste results in a higher degree of hydration for the bulk paste elements (Figure 4.8, right).

Moisture movements at microlevel

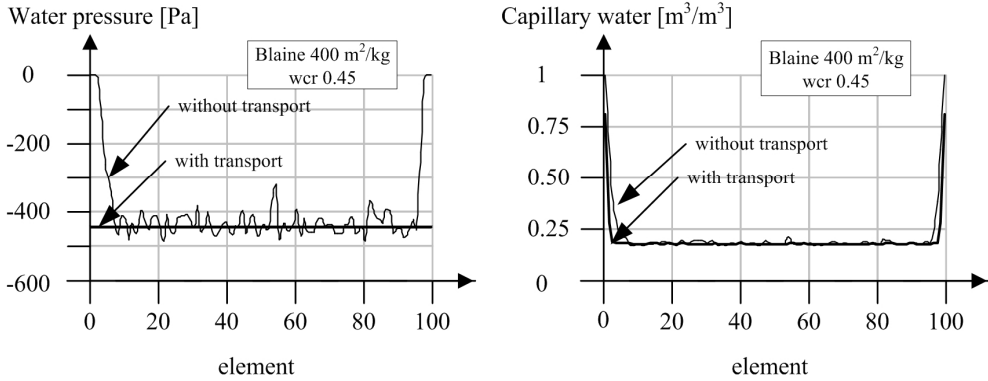


Figure 4.7 Water pressure (left) and capillary water after 1000 hrs (right) (1 element = 1 μ m)

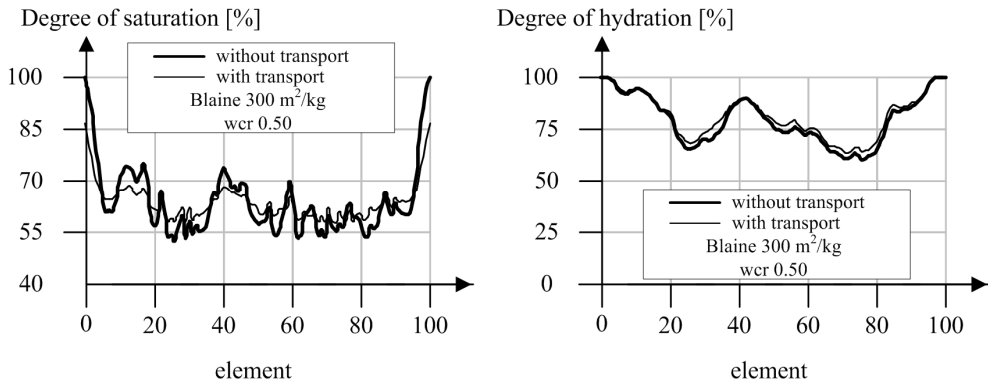


Figure 4.8 Degree of saturation and degree of hydration after 1000 hrs (1 element = 1 μ m)

4.5.2 Transport from ITZ into the bulk paste

As mentioned before, to get a better insight into the moisture movements, results are provided for two typical elements out of the 100 elements where the tube of cement paste consists of, located in between two aggregate particles (Figure 4.1). The first element is located in the interfacial transition zone, near an aggregate particle. Another element in the centre of the bulk paste.

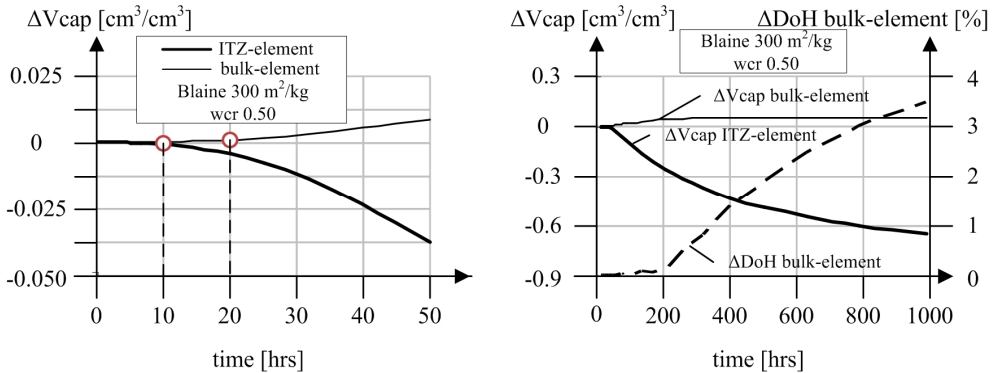


Figure 4.9 Moisture movement for ITZ and bulk paste (left) and effect of moisture transport for ITZ and bulk paste element (right)

From Figure 4.9 (left) it can be seen that water is transported from the element in the ITZ towards the element in the centre of the bulk paste. This results in a higher degree of hydration in the bulk paste (Figure 4.9, right). It takes some time until the moisture movement affects the centre of the bulk paste. For an element in the ITZ, the volume of capillary water starts to decrease after 10 hours due to the transport phenomena. For an element in the centre of the bulk paste, the amount of capillary water starts to increase after 20 hrs (Figure 4.9, left). It takes about 10 hrs until the water out of an ITZ element reaches an element in the centre of the bulk paste (a distance of about 50 μm).

4.5.3 Influence of water/cement-ratio

The influence of the water/cement ratio on moisture transport is studied by the simulation of moisture transport for three cement pastes with a water/cement-ratio of, respectively, 0.5, 0.4 and 0.3. In Figure 4.10 (left) the simulated degree of hydration is presented for the cement pastes after 1000 hours of hydration, with and without moisture transport from the ITZ to the bulk paste. All pastes show an increase of the degree of hydration. The mean increase of the degree of hydration over the whole ribbon of the three pastes is presented in Figure 4.11. The same influence of moisture transport is observed for the elastic modulus of the pastes (Figure 4.11). The modulus of elasticity is calculated by the Bar-model [Lokhorst, 2001]. The influence of supply of additional water to the bulk paste appears to have

Moisture movements at microlevel

almost negligible influence on the development of the elastic modulus ($< 0.5\%$). That this influence is only 0.5% results from the nonlinear relation between degree of hydration and modulus of elasticity (Figure 4.12). Especially for higher degrees of hydration, this relation becomes non-linear.

From Figure 4.11 it appears that the influence of moisture transport on the degree of hydration and modulus of elasticity is the biggest for higher water/cement ratios. For the paste with a water/cement-ratio of 0.3 the influence of moisture transport on the development of the degree of hydration and elastic modulus is negligible. This can be explained by the amount of water in the ITZ that is available for moisture transport. From the distribution of the capillary water with and without moisture transport (Figure 4.13, left) it follows that for the paste with water/cement ratio of 0.3 the volume of capillary water in the ITZ is lower compared the other pastes (Figure 4.13, right). Comparing Figure 4.11 and Figure 4.13 (right) shows a direct relation between the amount of capillary water in the ITZ available for transport and the influence on the degree of hydration and elastic modulus.

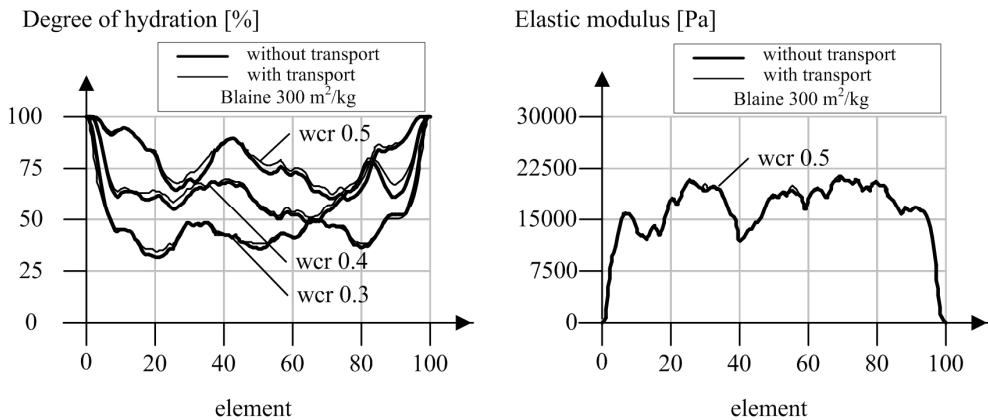


Figure 4.10 Influence on degree of hydration (left) and elastic modulus (right) after 1000 hrs (1 element = $1\mu\text{m}$)

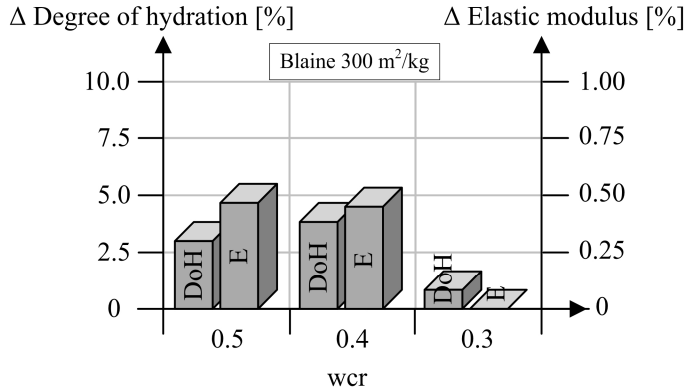


Figure 4.11 Mean influence of moisture transport on Degree of Hydration (DoH) and Elastic modulus (E) after 1000 hrs for water/cement-ratio between 0.3 and 0.5

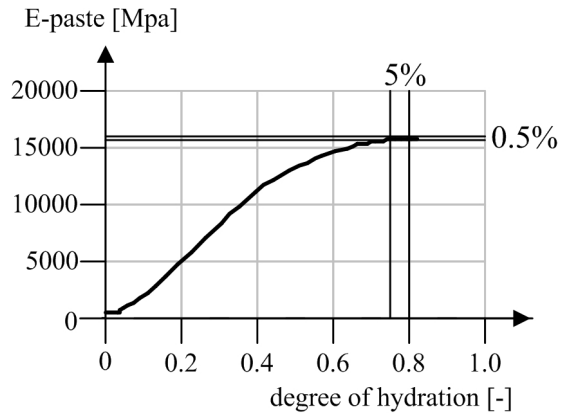


Figure 4.12 Non-linear relation between degree of hydration and simulated modulus of elasticity of a hardening cement paste (water/cement ratio = 0.5 and Blaine value = 300 m²/kg) (simulated by HYMOSTRUC)

Moisture movements at microlevel

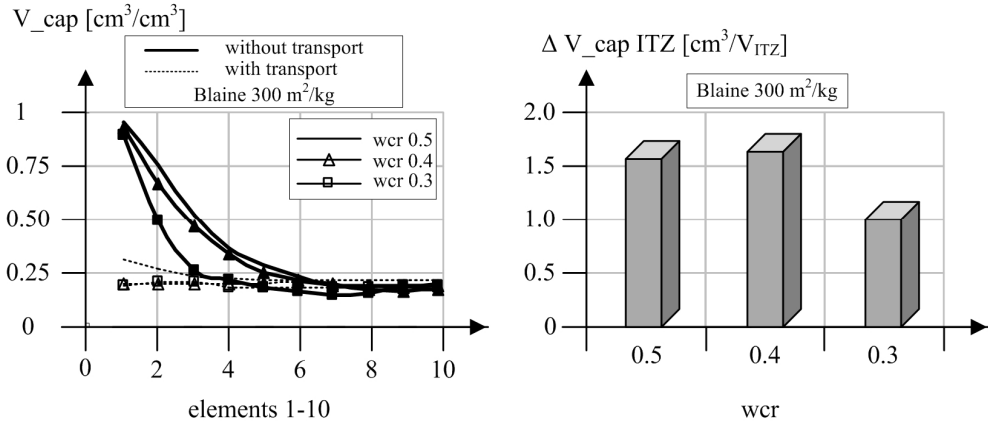


Figure 4.13 Volume of capillary water after 1000 hrs of hydration for ITZ elements (1 element = 1 μ m) (left) and changed volume of capillary water summarized for the ITZ due to moisture transport after 1000 hrs (right)

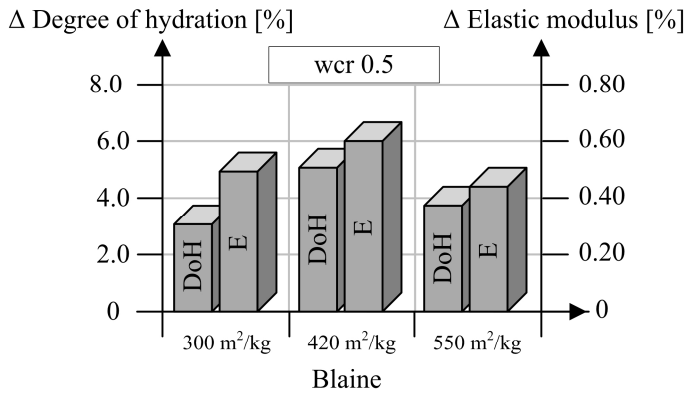


Figure 4.14 Influence of moisture transport on Degree of Hydration (DoH) and Elastic modulus (E) for cement with Blaine values between 300 and 550 m^2/kg

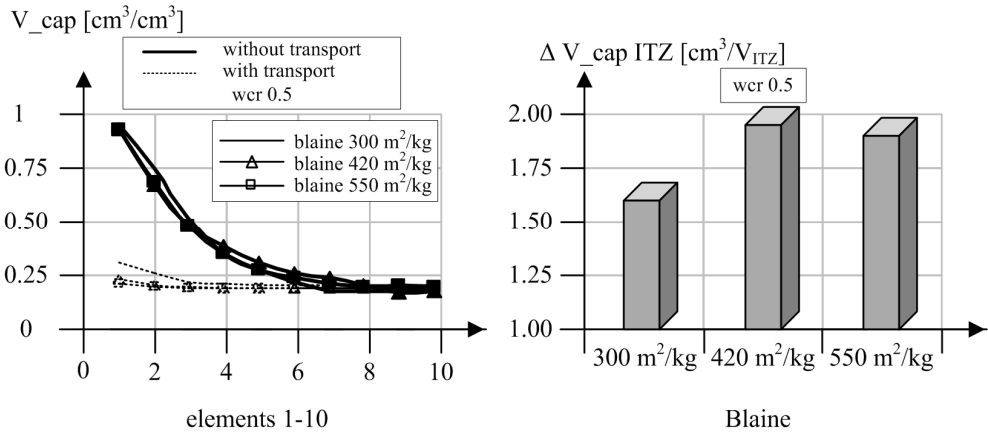


Figure 4.15 Volume of capillary water after 1000 hrs of hydration for ITZ elements (1 element = 1 μ m) (left) and changed volume of capillary water in ITZ after 1000 hrs (right)

4.5.4 Influence of cement fineness

Besides the influence of the water/cement-ratio, also the influence of the fineness of cement is investigated. The Blaine values of the investigated cements are 300 m²/kg, 420 m²/kg and 550 m²/kg respectively. For all cement finenesses, a positive influence of moisture transport on the simulated degree of hydration and elastic modulus is found (Figure 4.14). Again the influence of moisture transport for different cement finenesses is related to the amount of capillary water in the ITZ available for transport (Figure 4.15).

4.6 Validation grid

To cover a complete field of relevant water/cement ratio's and cement finenesses, a validation grid has been developed. The validation grid is presented in Figure 4.16. It covers a range of Blaine values between 300 m²/kg and 550 m²/kg and water/cement ratios between 0.3 and 0.5.

	w/c ratio 0.2	w/c ratio 0.3	w/c ratio 0.4	w/c ratio 0.5	w/c ratio 0.6
Blaine value 300 m ² /kg		○	○	○	
Blaine value 420 m ² /kg		○	○	○	
Blaine value 550 m ² /kg		○	○	○	

Figure 4.16 Validation grid (simulated combinations indicated with dots)

The influence of the water/cement ratio and the Blaine value of the used cement on the degree of hydration is shown in Figure 4.17. From this figure, it becomes clear that the Blaine value of the used cement has no influence on moisture transport from ITZ to the bulk paste. However, the water/cement ratio does have influence on the moisture transport. The lower the water/cement ratio, the lower the influence of moisture transport on the overall degree of hydration. The effect of the water/cement ratio on moisture transport (Figure 4.17) can be increased, because for the 0.5 water/cement ratio, there is still some water in the ITZ available for moisture transport (Figure 4.15). What is observed for the influence of moisture transport on the degree of hydration can also be observed for the influence of moisture transport on the modulus of elasticity (Figure 4.18), the Blaine value of the cement has no influence on the moisture transport, while the water/cement ratio does have influence on the moisture transport. Also here, a lower water/cement ratio results in less influence of moisture transport on the modulus of elasticity.

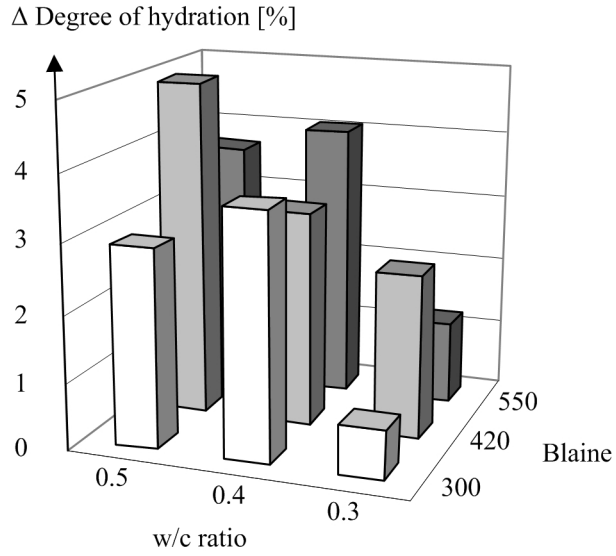


Figure 4.17 Validation grid for influence of moisture transport on overall degree of hydration

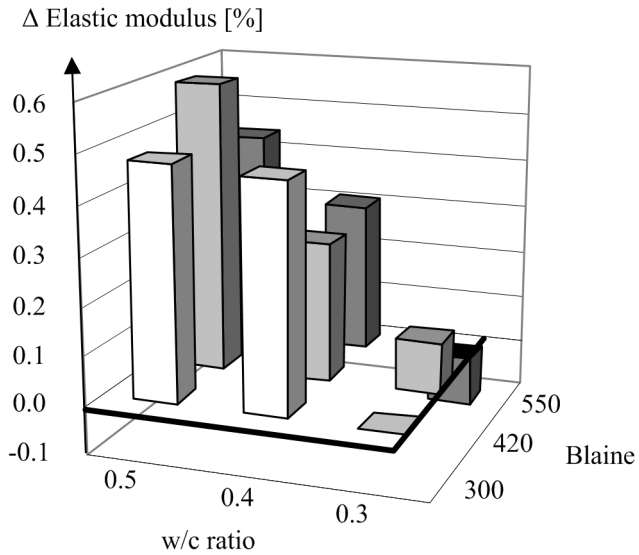


Figure 4.18 Validation grid for influence of moisture transport on overall elastic modulus

4.7 Influence of capillary water transport on visco-elastic behaviour

The influence of moisture transport from the ITZ to the bulk paste, results in changes of the moisture state in the pore system. On its turn, this changed moisture state influences the development of the degree of hydration and concrete properties, like the modulus of elasticity. The changed moisture state also influences the visco-elastic properties of the hydrating cement paste. Since the degree of hydration increased up to 5% as an influence of moisture transport (Figure 4.17), moisture transport parameters, which describe the transport of water from the annular space between the shell of cement gel and the anhydrous cement grain to the capillary pores are changed as well (shell thickness, water pressure). The influence of moisture transport on the visco-elastic behaviour is described as a change of the calculated interaction factor 'IF' (chapter 3.3), which describes the interaction between the shell of cement gel and the core of anhydrous cement grain. The change of this interaction factor by the transport of capillary water is presented in Figure 4.19. Since the degree of hydration develops at a higher rate for the lower water/cement ratios, the interaction factor changes earlier for lower water/cement ratios. The first significant change is observed after 40 hours, where for a cement paste with water/cement ratio of 0.3 and cement with a Blaine value of 300 m²/kg the interaction factor increased with 2%, followed by a paste with water/cement ratio of 0.3 with a Blaine value of 300 m²/kg, where the interaction factor increased about 4%. The changes become bigger for an increasing water/cement ratio.

Overall, all studied combinations of water/cement ratios and Blaine values as presented in the validation grid (Figure 4.16) show an increase of the interaction factor (up to 8%), what results in a stiffer behaviour of the system and less time dependent deformations.

A reliable description of the microstructure and the state of moisture distribution is indispensable for the analysis of visco-elastic behaviour of hardening concrete. Transport of capillary water through the pore system influences the visco-elastic behaviour, especially at later ages (after 50 hours of hydration). This can also be concluded from Figure 4.9, where the amount of capillary water started to increase in the bulk paste after 20 hours of hydration. When in stress simulations, the visco-elastic behaviour is taken into account by the Shell Deformation Model (interaction

factor 'IF'), determined from the transport of water from the annular space between the shell of cement gel and the core of anhydrous cement grain to the capillary pores, the influence of transport of capillary water should be taken into account (influence on the interaction factor up to 8% in the first 1000 hours of hydration).

The way how the microstructural development and moisture movements are taken into account by the modelling of the visco-elastic behaviour of hardening concrete will be elucidated in detail in the next chapter.

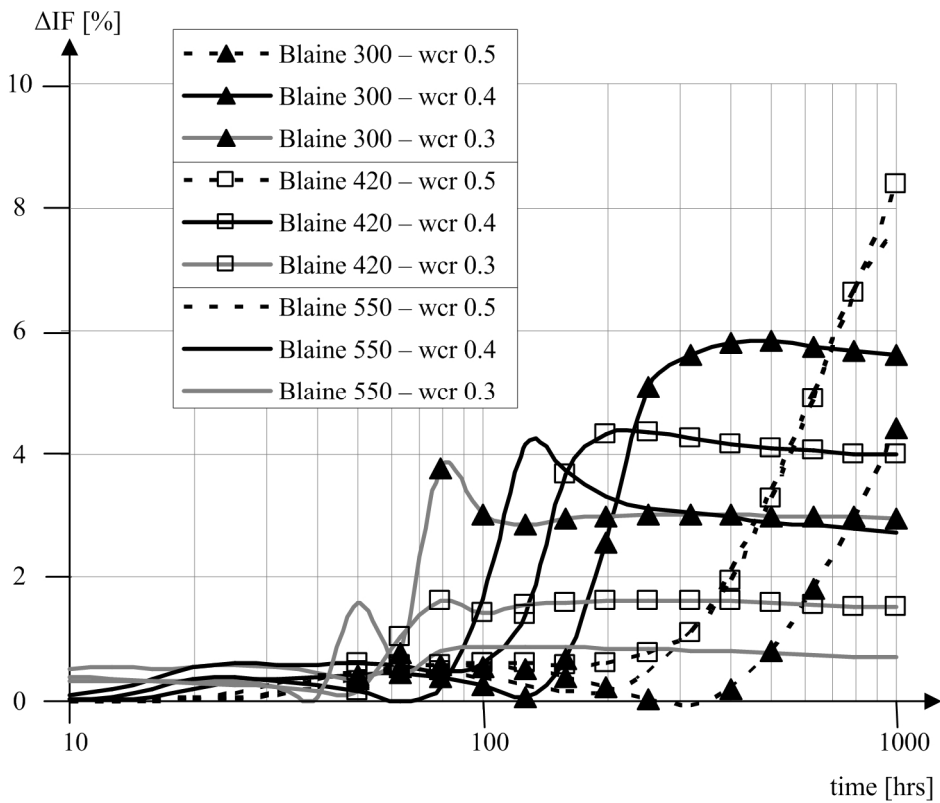


Figure 4.19 Influence of moisture transport on the interaction factor 'IF'

5 Experiments and validation of the proposed model

5.1 Aim of the experimental research

The main aim of the experiments performed in this study is to validate the performance of the Shell Deformation Model ‘SDM’ or the interaction factor ‘IF’, which describes the interaction between the shells of cement gel and the cores of anhydrous cement grains. The interaction factor is calculated with the models as presented in chapter 3 and 4. Second aim is to determine the influence of the interaction factor on the reliability of stress predictions. The interaction factor is based on the behaviour of cement paste. By a parallel series system, the behaviour of cement paste is translated to the behaviour of concrete. Validation of the model is based on the experimental results on concrete specimen.

Besides the main aim, the experimental program is also used to check the reliability of the SDM. The calculated results of the model are compared with general accepted trends (Figure 2.5). However, about some parameters, no agreement exists in literature about their influence. Those parameters are the cement fineness and the load sign (tension or compression). In Figure 5.1 an overview is provided of the results of research on the influence of those parameters found in literature. Since the proposed model shows almost equal visco-elastic behaviour for different Blaine values (Figure 3.25), there is need for an experimental prove. Also for the load sign, the Shell Deformation Model does not show any different behaviour which has to be proven by experiments.

Experiments and validation of the proposed model

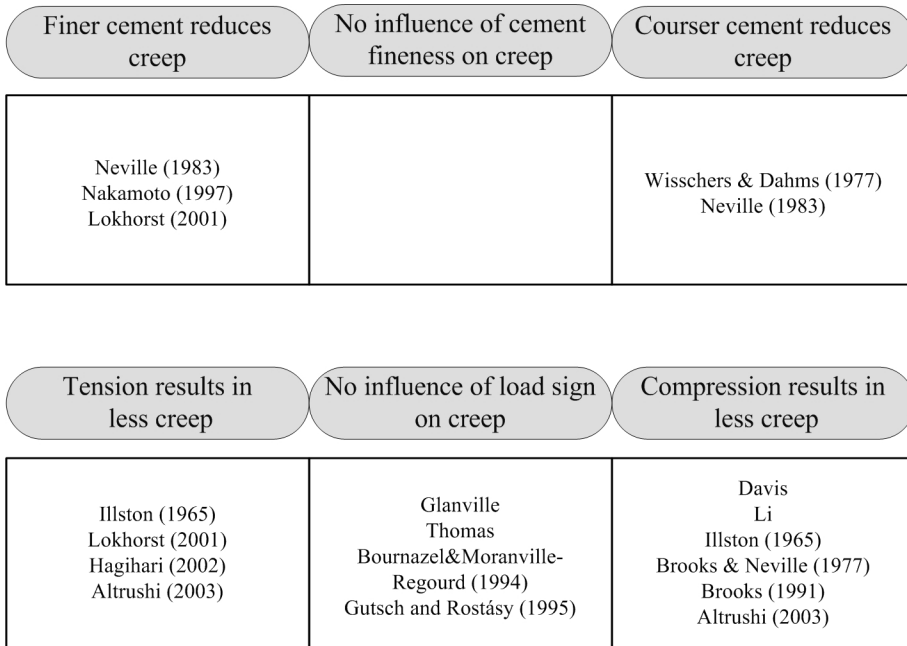


Figure 5.1 Disagreement in literature about influencing parameters (cement fineness (top) and load sign (bottom)) on visco-elastic behaviour of hardening concrete

Aims of the experimental research are now:

- To investigate the influence of cement fineness and load sign on the visco-elastic behaviour of hardening concrete;
- To provide experimental data that can be used to validate the proposed model by simulation of stresses.
- To determine whether the reliability of stress predictions is increased if the Shell Deformation Model is used to take time dependent deformations into account in stress simulations.

5.2 Cement properties, concrete mix composition and mixing procedure

In this research, a normal strength concrete (NSC) has been investigated as a reference concrete. This mixture (Tabel 5.1) is chosen from earlier research projects [Lokhorst, 2001] & [Sule, 2003].

Experiments are performed on three types of Portland cement. Major difference is the Blaine value of the cements (300, 468 and 550 m²/kg). All mixtures contained 350 kg/m³ cement. The characteristics of the cements used in this study are presented in Tabel 5.2.

Table 5.1 Concrete compositions [kg/m³] of the mixtures used in the experimental program

	Mixture 1	Mixture 2	Mixture 3
Water	175.0	175.0	175.0
CEM I 42.5 N	350.0	-	-
CEM I 52.5 N	-	350.0	-
CEM I 52.5 R	-	-	350.0
Gravel 4-8 mm	827.6	827.6	827.6
Sand 0-4 mm	1011.5	1011.5	1011.5
Compressive cube strength at 28 days [MPa]	39.3	54.3	57.4

Table 5.2 Characteristics of the cement types based on data provided by the cement producer (ENCI)

	CEM I 42.5 N	CEM I 52.5 N	CEM I 52.5 R
Blaine value [m ² /kg]	300	468	550
Potential heat [kJ/kg]	495	496	513
C ₃ S [%]	68.13	68.4	75.1
C ₂ S [%]	12.42	12.18	5.1
C ₃ A [%]	8.82	8.81	8.98
C ₄ AF [%]	10.63	10.62	10.82

5.3 Experimental set-up

The experimental set-up is presented schematically in Figure 5.2. The load dependent deformations and stress development of restrained deformations are measured in the Temperature Stress Testing Machine (TSTM). Load independent deformations are measured in the Autogenous Deformation Testing Machine (ADTM). The concrete strength is tested in (compressive strength and tensile splitting strength) from cubes hardened under identical circumstances as the specimen in the ADTM and the TSTM equipment.

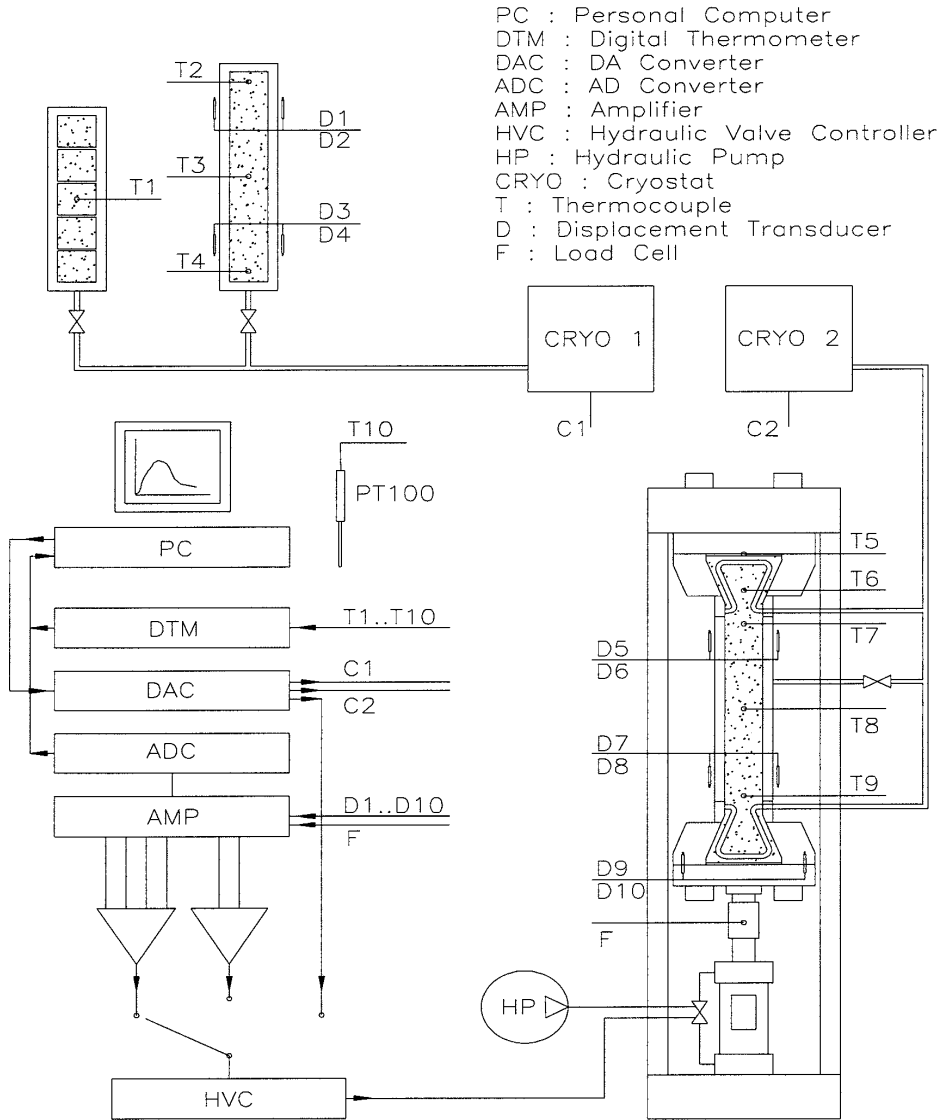


Figure 5.2 Schematic representation of the experimental set-up [Lokhorst, 2001]

5.3.1 Autogenous Deformation Testing Machine

The Autogenous Deformation Testing Machine (ADTM) is used to carry out early-age shrinkage tests. The ADTM measures the deformation of a hardening specimen that is free to deform and hardens at a prescribed temperature regime. An insulated mould is used of 1000 mm long, 150 mm wide and 100 mm high. The walls of the mould contain plastic tubes that are connected to cryostats units. The temperature of the specimen is measured by means of three thermocouples, one in the middle and two in the ends of the specimen. The cryostats control the water flow through the tubes to maintain the required temperature regime in the specimen. Directly after casting, the specimen is covered with plastic foil and an insulated plate. Two small steel bars were embedded in the specimen, 750 mm apart from each other. These bars protrude through two holes in the long side faces of the mould, while not making contact with the mould itself. Thus, the ends of the steel bars could move freely over a certain deformation range. As soon as the fresh concrete starts to develop some strength and stiffness, the LVDT's (linear voltage displacement transducers) positioned along the long side faces of the mould were activated and attached to the small steel bars that protrude through the mould (Figure 5.3).

5.3.2 Temperature Stress Testing Machine

The Temperature Stress Testing Machine (TSTM) is shown in Figure 5.4. The specimen has a total length of 1450 mm and consists of two wedge-shaped ends (300 mm long and at their end 300 mm wide and 150 mm high) and a mid section 850 mm in length, 150 mm wide and 100 mm high. The side-faces and bottom of the mould at the wedge-shaped ends are curved to obtain a 'smooth' transition of the specimen's cross-section. Just as for the specimen in the Autogenous Deformation Testing Machine (paragraph 5.3.1), the mid part of the TSTM-specimen is provided with two small steel bars spaced at 750 mm, protruding through the mould. LVDT's at both sides measure the deformation (Figure 5.3).

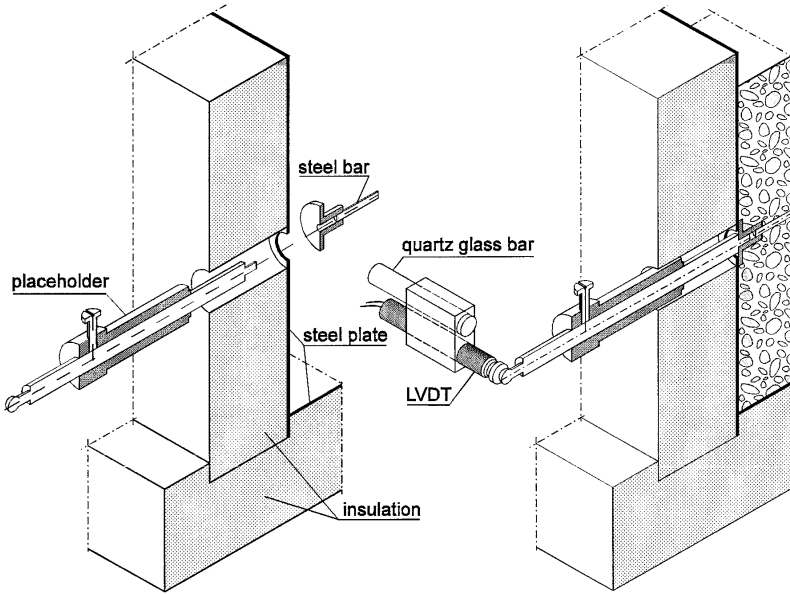


Figure 5.3 Installation of measuring bars and placeholders before casting (left) and installation of LVDT's after casting (right) [Lokhorst, 2001]

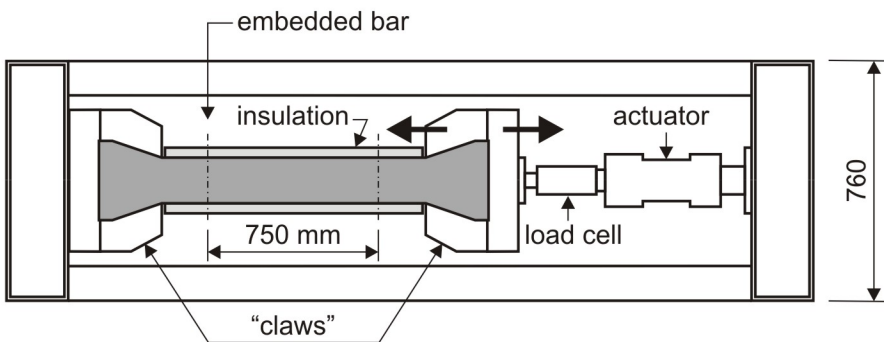


Figure 5.4 The Temperature Stress Testing Machine (top view - schematic) [Lokhorst, 2001]

Both wedge-shaped ends can introduce a longitudinal compressive or tensile force; one end acting as a passive support, the other one active since it is connected to a hydraulic jack and a load cell. The force is controlled by the mean displacement measured by the LVDT's at the front and rear of the specimen. The TSTM-specimen is cast in an insulated mould that is provided with plastic tubes which are connected with cryostats to control the temperature of the specimen. Thermocouples are put in the specimen. Two possibilities are available to operate the TSTM; force controlled and deformation controlled.

- Force controlled mode. The force controlled mode is used for the sustained loading experiments. During the experiment, the force on the specimen is kept at a constant level and the deformations of the specimen are registered.
- Deformation controlled mode. The deformation controlled mode is used for the relaxation experiments, where the deformation is kept constant and the stress development is registered.

The percentage of restraint of the free deformation of the specimen can vary between 0 and 100%. For no restraint, the specimen is free to deform and then reacts as the ADTM. If a certain percentage of restraint is imposed, the free deformation of the specimen hardening in the ADTM is input. The hydraulic jack of the TSTM is then controlled such that the LVDT's of the TSTM specimen register a deformation that is a percentage of the deformation registered for the ADTM specimen. For $R=100\%$ the deformation of the TSTM specimen is fully restrained and the TSTM could function stand-alone without receiving output from the ADTM: The load cell is then controlled such that the LVDT's of the TSTM specimen register a zero deformation. The degree of restraint tests described here were carried out under fully restrained conditions; $R=100\%$.

5.4 Sustained loading experiments

Sustained loading experiments (creep experiments) are performed to study the influence of two parameters. These are the cement fineness (Blaine value) and the

load sign (tension or compression). To study the influence of the cement fineness, three mixtures are tested where only the cement type is varied (Table 5.1 and Table 5.2). To study the influence of the load sign, experiments are performed in compression as well as in tension.

Since the mixtures with different Blaine values of the used cements will hydrate at different rates (higher rate of hydration for higher Blaine values), the creep experiments will all start at equal degree of hydration instead of equal time after start of the hydration process (adding water to the mixture). The degree of hydration at the start of the sustained loading experiments are set at respectively 16 hours, 24 hours and 48 hours after start of the hydration process of the reference mixture (CEM I 42.5 N). To calculate the equivalent time, the degree of hydration of each mixture is simulated by HYMOSTRUC. The equivalent times for the different mixtures are calculated from Figure 5.5 and provided in Table 5.3.

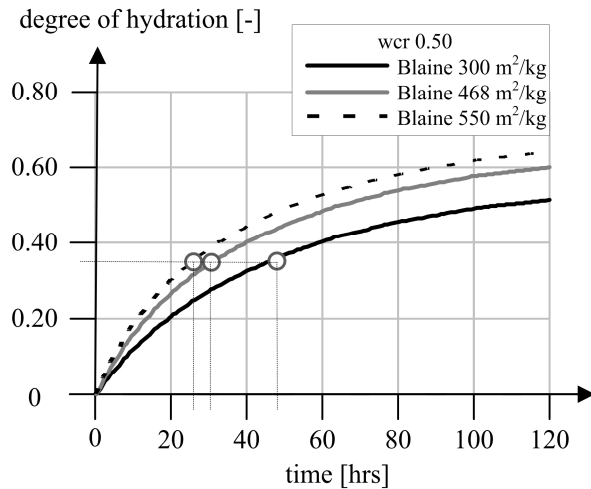


Figure 5.5 Equivalent times for degree of hydration of 0.35 for concrete specimen, w/c-ratio of 0.5 and Blaine values between 300 and 550 m²/kg

Table 5.3 Equivalent times for equal degree of hydration for concrete specimen, w/c-ratio of 0.5 and Blaine values between 300 and 550 m²/kg

Degree of hydration	Loading	Time after adding water to the mixture [hrs]		
		CEM I 42.5 N	CEM I 52.5 N	CEM I 52.5 R
0.17	Compression	16h	10h 22'	9h 25'
0.23	Compression	24h	15h 16'	13h 50'
	Tension	24h	15h 16'	13h 50'
0.35	Compression	48h	29h 48'	26h 45'
	Tension	48h	29h 48'	26h 45'

All experiments are performed with compressive load as well as a tensile load, except the experiments at a degree of hydration of 0.17 which are only loaded in compression. Reason for this is the sensitivity of the testing equipment. At very early ages, the tensile strength is so low that already a small variation of the controlled force will crack the specimen.

The load path used for the sustained loading experiments is shown in Figure 5.6. This load path is used for the tests in compression and in tension. The strength of the specimen was determined from cubes, hardened under circumstances identical to the ADTM and TSTM specimen. To identify the instantaneous deformations, which are necessary to determine the creep factor, the specimens were first loaded and immediately unloaded. The loading rate was 1 kN/s (0.067N/mm²/s) for the compression tests and 0.1 kN/s (0.0067N/mm²/s) for the tension tests. The sustained loading experiments took place in the TSTM-equipment. To correct for the free deformations (autogenous deformations) every loaded specimen was accompanied by a dummy specimen in the ADTM-equipment to measure the autogenous shrinkage strains. All sustained loading experiments are performed under isothermal conditions at 20 °C and specimens are sealed to avoid drying.

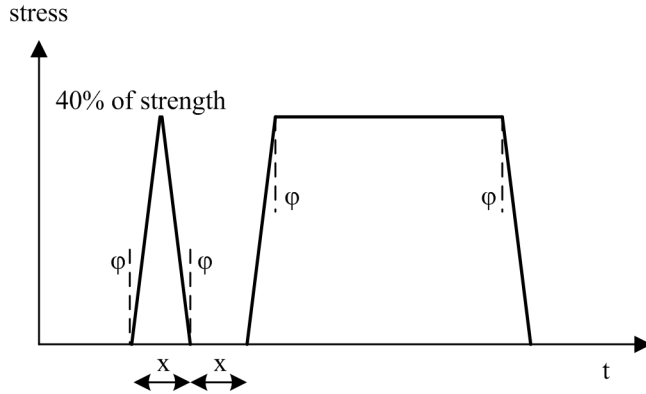


Figure 5.6 Load path used for the sustained loading tests

The creep experiments show the development of extra deformations in time after loading, which is dependent of the applied force on the specimen. This force is not of the same magnitude for all specimens, because it is a ratio of the strength at the moment of loading (40%). To compare the creep experiments, it is elegant to compare the creep factors instead of comparison of the time dependent strains. The creep factor is the result of the absolute ratio between the extra deformations during sustained loading and the elastic deformations:

$$\varphi(t) = \frac{\varepsilon_c(t)}{\varepsilon_e} \quad [5.59]$$

with $\varepsilon_c(t)$ the deformations after 't' hrs sustained loading and ε_e the elastic deformations.

5.4.1 Influence of cement fineness

The results of the specimen loaded in compression show a consistent behaviour of equal visco-elastic deformations of the specimens with different cement fineness (Figure 5.7). The observed differences are not significant and can be ascribed to variation in the test results. Based on the theories of the Shell Deformation Model, for the specimen loaded in tension, the same behaviour was expected as for

Experiments and validation of the proposed model

specimen loaded in compression; however no consistent view is obtained from the results. As presented in Figure 5.8, for the specimen loaded at a degree of hydration of 0.23, the specimen with a Blaine value of 468 m²/kg shows the largest visco-elastic deformations, however, for the specimen of the same cement loaded at a degree of hydration of 0.35 this resulted in the smallest visco-elastic deformations. This inconsistency is subscribed to the difficulty of the test if a specimen is loaded in tension. The bond between the embedded steel bars (Figure 5.3) might be less if loaded in tension compared to the bond if a specimen is loaded in compression. Also the bond between the specimen and the steel claws at both ends of the specimen (Figure 5.4) might be less if a specimen is loaded in tension. The presented results are results without repetition. The number of tests is too small to draw decisive conclusions. The quality of the results of these experiments will increase if the number of experiments increases.

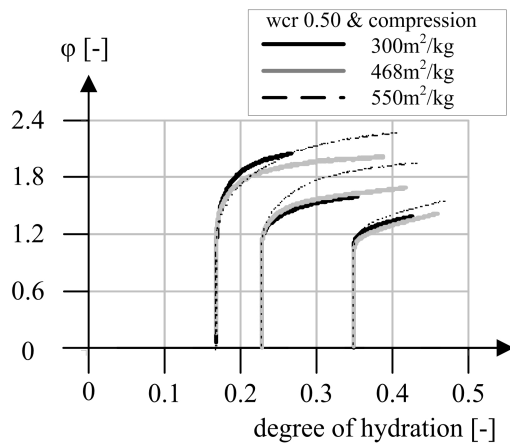


Figure 5.7 Influence of cement fineness on compressive creep of concrete specimen, w/c-ratio of 0.5 and Blaine values from 300 - 550 m²/kg

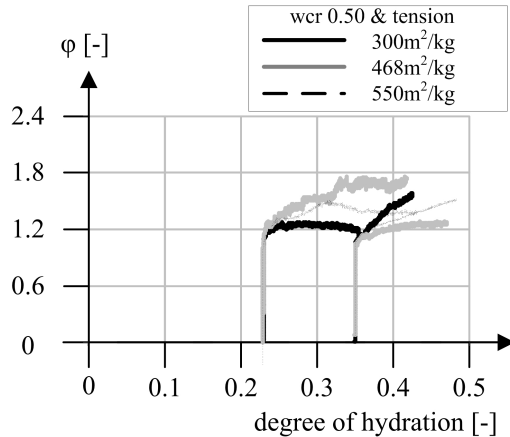


Figure 5.8 Influence of cement fineness on tensile creep of concrete specimen, w/c-ratio of 0.5 and Blaine values from 300 - 550 m²/kg

5.4.2 Influence of load sign

A series of twelve experiments are performed to study the influence of the load sign on the visco-elastic behaviour of hardening concrete. Mixtures containing different cements with Blaine values of 300m²/kg, 468 m²/kg and 550 m²/kg are loaded in tension and compression at a degree of hydration of 0.23 and 0.35. Out of the six double experiments, four sets show a more or less equal behaviour when loaded in tension and compression. Two sets show a different behaviour. Both diverging sets are loaded at a degree of hydration of 0.23 and it has to be mentioned that the results of the experiments loaded in tension at this degree of hydration are non-systematic, like a decrease of the creep factor for the sustained loading at a degree of hydration of about 0.23 (Figure 5.11). This effect might be ascribed to the lack of contact between the measuring device and the concrete if loaded in tension, which is no material behaviour. For the experiments that started at a degree of hydration of 0.35 the behaviour of the specimen loaded in tension is equal to the behaviour of a specimen loaded in compression.

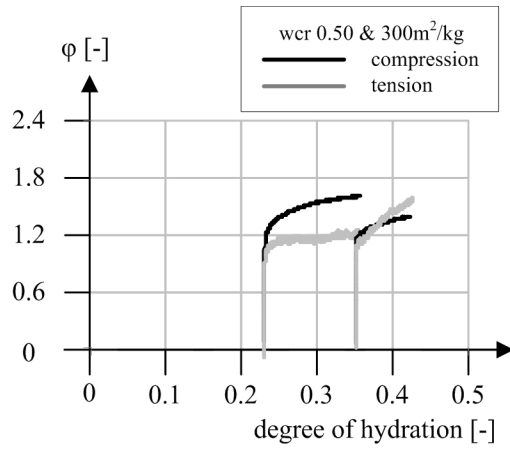


Figure 5.9 Influence of load sign on creep of concrete specimen, w/c-ratio of 0.5 and cement with a Blaine value of 300m²/kg

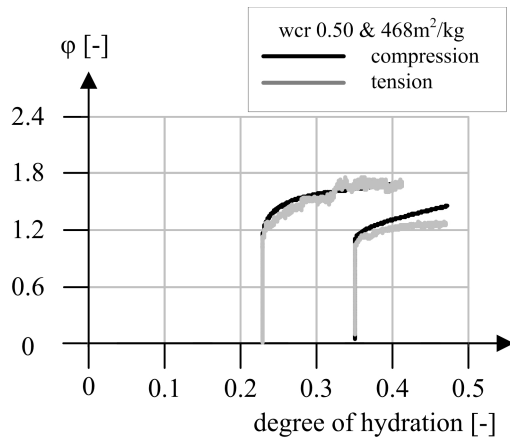


Figure 5.10 Influence of load sign on creep of concrete specimen, w/c-ratio of 0.5 and cement with a Blaine value of 468m²/kg

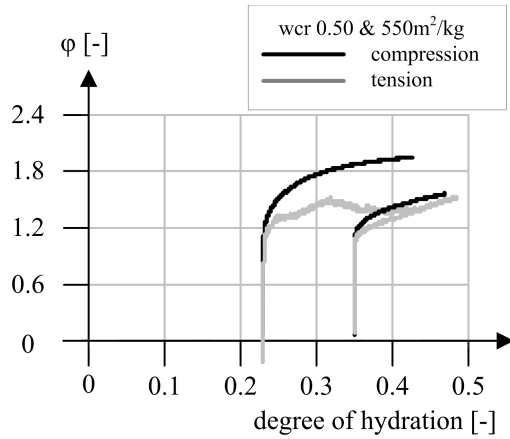


Figure 5.11 Influence of load sign on creep of concrete specimens, w/c-ratio 0.5 and cement with a Blaine value of $550 \text{ m}^2/\text{kg}$

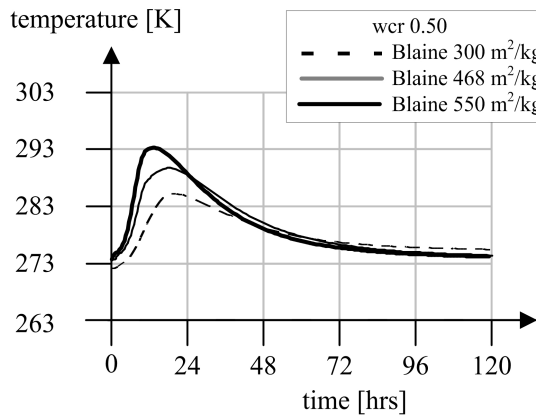


Figure 5.12 Measured temperatures of concrete specimens, w/c-ratio 0.5 and cement with a Blaine value of $550 \text{ m}^2/\text{kg}$

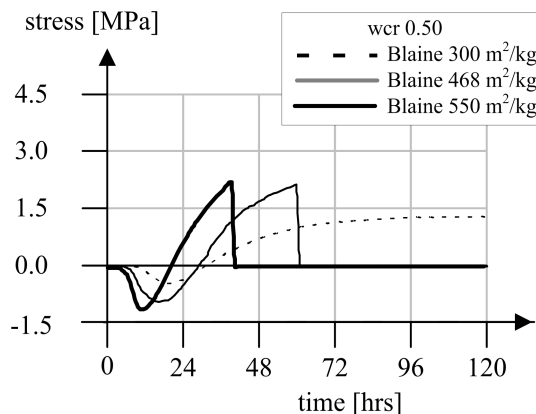


Figure 5.13 Measured stress development during hardening of 100% restrained concrete specimens, w/c-ratio 0.5, Blaine value between 300 and 550 m²/kg

5.5 Relaxation experiments

Fresh concrete is casted in the TSTM-equipment. The specimen in the TSTM-equipment hardens at a temperature regime, which is measured from a simultaneously semi-adiabatic hardening specimen in the ADTM-equipment (Figure 5.12). The deformations of the TSTM-specimen are completely restrained. This results in stress development in the hardening specimen. The free deformations of the specimen hardening in the ADTM-equipment are registered as well. For the three mixtures with different cement fineness, the measured stress development is presented in Figure 5.13. The cement with the highest Blaine value results in a fast stress build-up, which can be explained by the higher rate of hydration of that hardening specimen which results in higher rate of temperature rise (Figure 5.12). Furthermore, the specimen made with cement with a higher Blaine value also results in higher stresses. For the highest Blaine value, the specimen broke after about 40 hrs of hardening. The specimen with cement of moderate Blaine value cracked after about 60 hours of hardening. The specimen with cement of lowest Blaine value did not crack.

5.6 Simulation of experimental results

The procedure used to simulate the measured stress developments in restrained hardening specimen is presented in Figure 5.14. Numerical simulations of the experimental results are performed with the so called UCON-system [van Beek, 1995]. UCON stands for Universal concrete curing CONTROL system. The system determines the degree of hydration of a hardening specimen or structure if the temperature of the specimen and the adiabatic degree of hydration are known. The temperature can be measured directly from the hardening specimen. The adiabatic degree of hydration can be simulated by simulation software (e.g. HYMOSTRUC) or can be determined from adiabatic temperature measurements. The rate of hydration at semi-adiabatic process temperature $T_p(t)$ (Figure 5.12) is related to the rate of hydration at adiabatic temperature $T_a(t)$ (Figure 5.15) by the Arrhenius-like temperature function:

$$f(\alpha, T_p, T_a) = \exp\left(\frac{E_A(\alpha, T)}{R} \cdot \frac{T_a - T_p}{T_a \cdot T_p}\right) \quad [5.60]$$

with:

α = degree of hydration [-]

E_A = activation energy [Laube, 1991]

$T < 293 \text{ K}$, $E_A = 33.5 + 1.47 (20 - T) \text{ kJ/mol}$

$T > 293 \text{ K}$, $E_A = 33.5 \text{ kJ/mol}$

R = universal gas constant (8.31 J/mol.K)

The development of the degree of hydration for the specimen cured under simulated semi-adiabatic conditions is presented in Figure 5.16.

The development of the free deformations of the hardening specimen measured by the ADTM is presented in Figure 5.17. These deformations (thermal deformations and autogenous deformations) are used as input to simulate the stress development in the restrained specimen as measured by the TSTM.

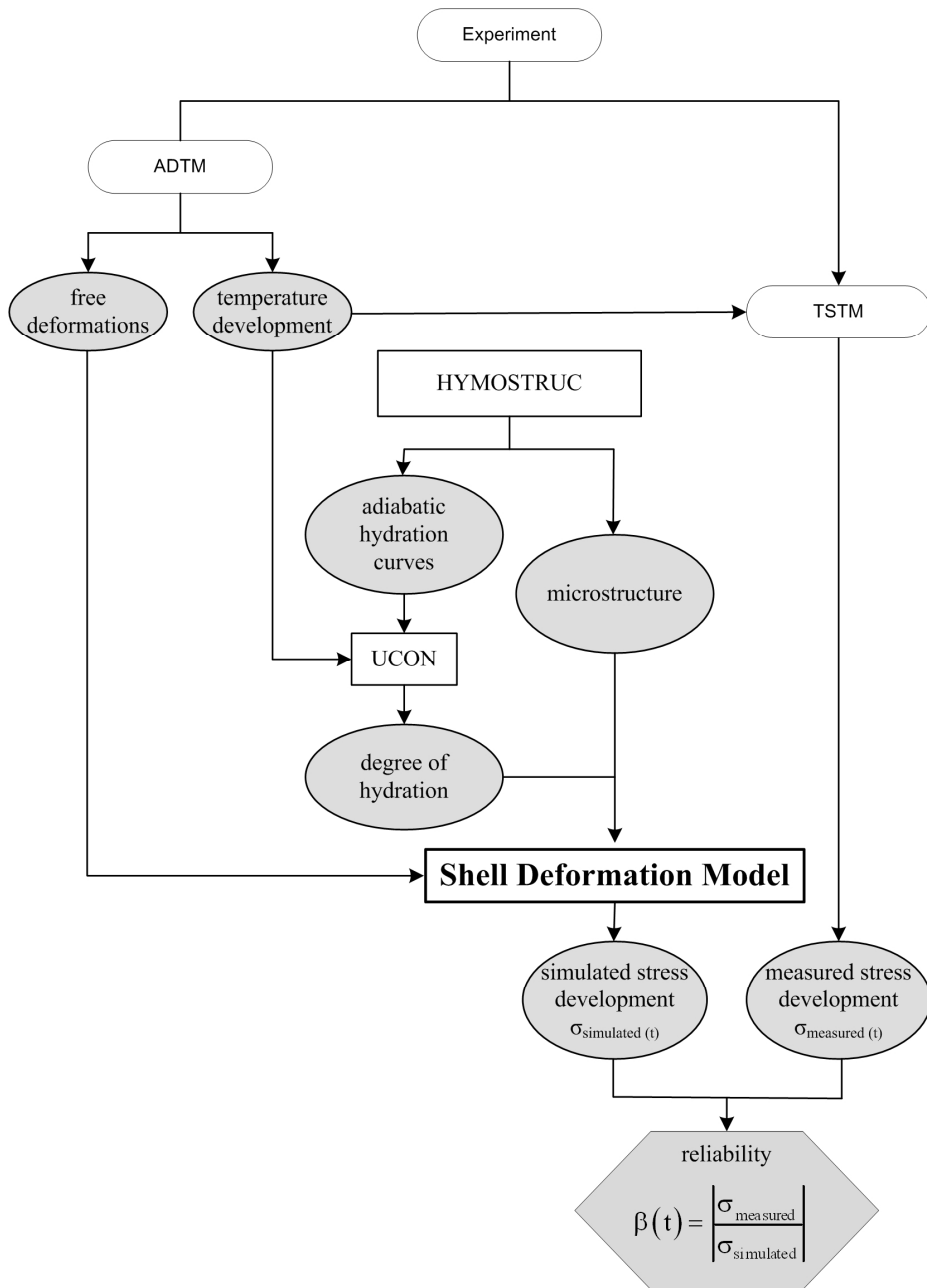


Figure 5.14 Procedure to simulate experimental results and to determine the reliability of stress predictions in hardening concrete elements

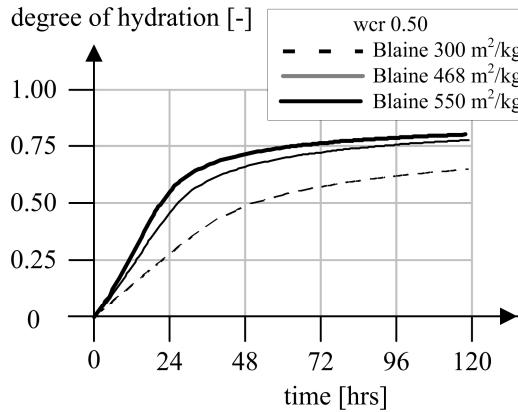


Figure 5.15 Development of adiabatic degree of hydration of concrete specimens simulated by HYMOSTRUC, w/c-ratio 0.5, Blaine value between 300 and 550 m²/kg

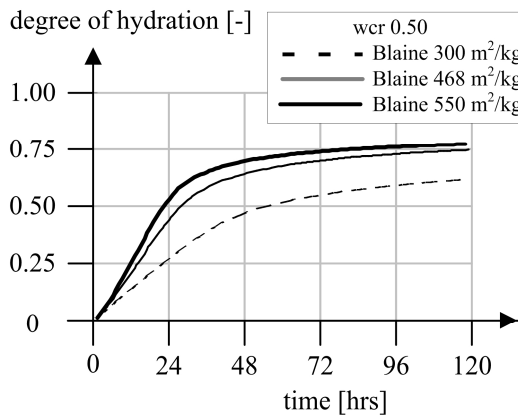


Figure 5.16 Development of semi-adiabatic degree of hydration of concrete specimens simulated by HYMOSTRUC, w/c-ratio 0.5, Blaine value between 300 and 550 m²/kg

Experiments and validation of the proposed model

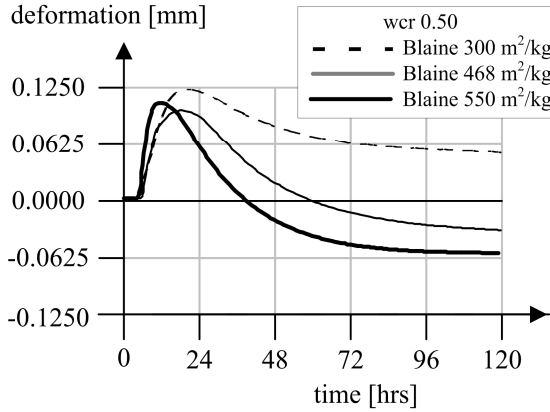


Figure 5.17 Measured free deformations of concrete specimens, w/c-ratio 0.5, Blaine value between 300 and 550 m²/kg

The Shell Deformation Model (SDM) is used to quantify the visco-elastic behaviour of the hardening concrete specimen. The simulated interaction factor ‘IF’ is presented in Figure 5.18 for the three cements as a function of the degree of hydration. Application of this interaction factor results in an effective stiffness of the specimen. The development of the effective stiffness is also presented in the degree of hydration domain in Figure 5.19.

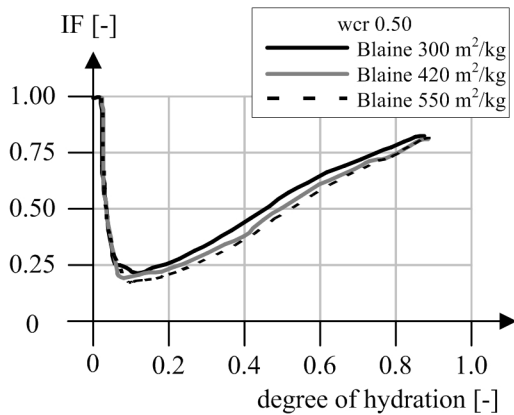


Figure 5.18 Interaction factors simulated by the Shell Deformation Model for Blaine values between 300 and 550 m²/kg

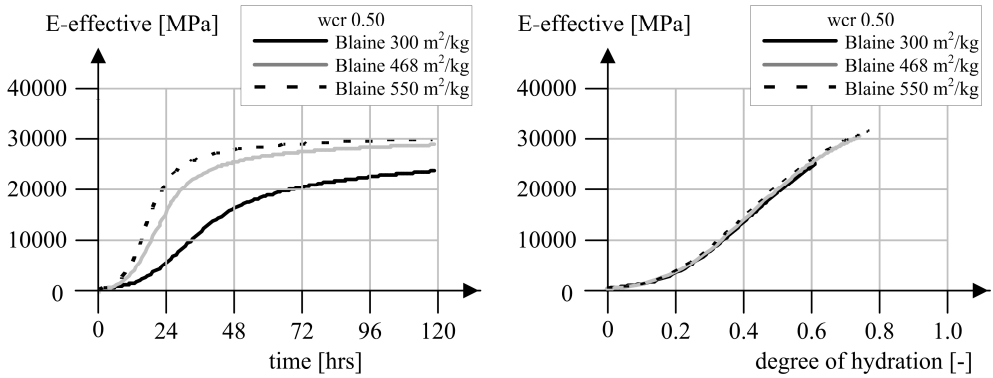


Figure 5.19 Simulated Effective stiffness in the time domain (left) and in the degree of hydration domain (right)

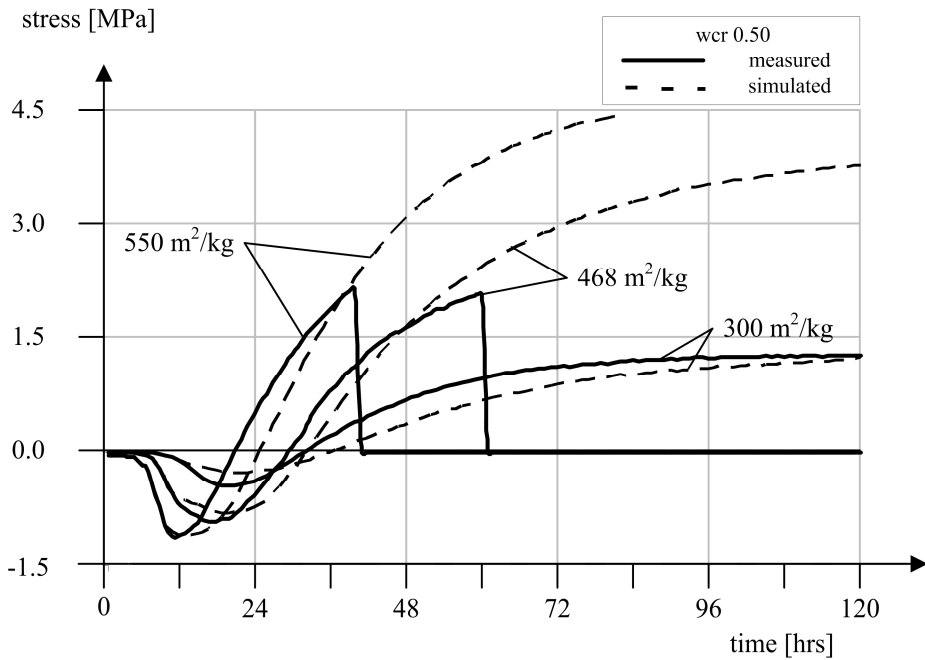


Figure 5.20 Measured versus simulated stress development of concrete specimens, w/c-ratio 0.5, Blaine value between 300 and 550 m²/kg

The simulated stress development and the measured stress development are presented in Figure 5.20. Using the Shell Deformation Model, good agreement is found between measured and calculated stresses. However, for both cracked specimens the simulated stresses just before cracking turned out to be too high compared to the measured stresses. Reason for the lower measured stresses can be micro cracking. Micro cracking is not considered in the SDM while cracking lowers the stiffness of the specimen and, therefore, results in lower stresses in the hardening concrete.

5.7 Reliability of stress predictions

To calculate the probability of cracking, the stress predictions have to be as reliable as possible. The reliability of a stress prediction is defined as the absolute ratio between the measured and the simulated stresses. In this case it is a measure for the gap between measured and simulated stresses:

$$\beta(t) = \left| \frac{\sigma_{\text{measured}}}{\sigma_{\text{simulated}}} \right| \quad [5.61]$$

The reliabilities of the simulated stress predictions in this chapter are presented in Figure 5.21. From the beginning of the hardening period until cracking, the average reliability of the stress predictions are 76% (Blaine value of 300 m²/kg), 82% (Blaine value of 468 m²/kg) and 77% (Blaine value of 550 m²/kg). For the cracked specimen, the reliability of the stress prediction at the moment of cracking was 83% (Blaine value of 468 m²/kg) and 94% (Blaine value of 550 m²/kg). Compared to the results obtained by the old fixed interaction factor (Table 2.1), the average reliability increased by application of the calculated variable interaction factor (Figure 5.22).

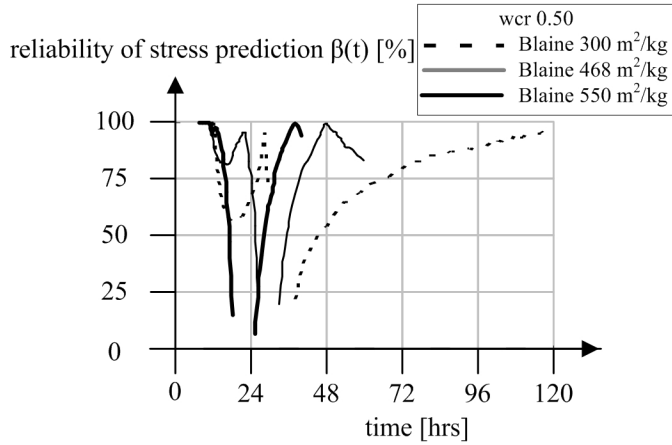


Figure 5.21 Reliability of stress predictions of concrete specimens, w/c-ratio 0.5, Blaine value between 300 and 550 m²/kg

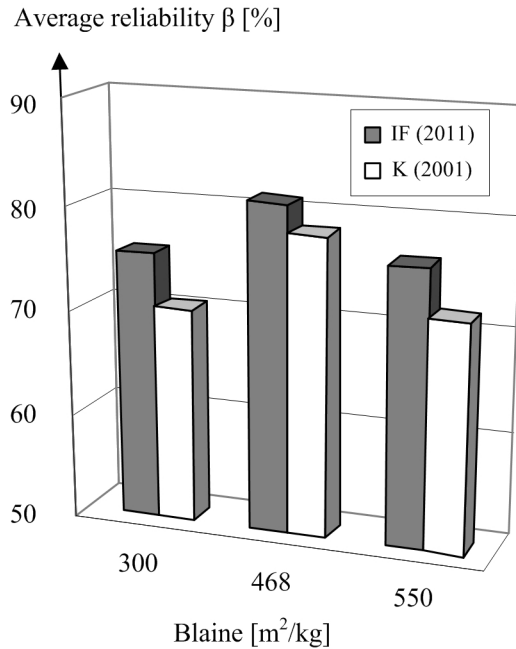


Figure 5.22 Average reliability of stress prediction by 'IF' (Shell Deformation Model) and 'K' (Bar model) [Lokhorst, 2001]

5.8 Discussion

In literature, no agreement exists about the influence of the cement fineness and the load sign on the visco-elastic behaviour of hardening concrete. By the experimental program as presented in this chapter, the influence of those parameters is studied.

In chapter 3, it was already concluded from the results simulated by the Shell Deformation Model that the fineness of cement hardly influences the visco-elastic behaviour. This conclusion is confirmed by the experimental results, where the fineness of cement did not influence the time dependent deformations, if the results are presented in the degree of hydration domain. The results should be presented in the degree of hydration domain, because the fineness of cement does influence the rate of hydration.

One of the assumptions of the Shell Deformation Model is that the model assumes an equal time dependent behaviour for cement paste loaded in tension and compression (Chapter 3). This assumption is confirmed by experiments as described in this chapter, where it turned out that the load sign has no influence on the visco-elastic behaviour of hardening concrete. Result of the experiments is that no significant influence can be ascribed to both parameters (fineness of cement and load sign).

The change of the interaction factor with time can be described by the moisture state in the hardening cement paste and to the microstructural changes. The influence of the presented interaction factor 'IF', which relates the visco-elastic behaviour of hardening concrete to the moisture state and hollow shell mode of the hydrating cement paste (chapter 3) is studied by experiments where the deformations were 100% restrained.

Measured stresses are compared with simulated stresses, making use of the presented interaction factor. As a first validation, it turned out that the reliability of stress predictions is increased by using this new interaction factor 'IF', compared to the previously proposed interaction factor 'K' [Lokhorst, 2001].

6 Conclusions

6.1 Evaluation

After many years of research by many researchers, models and calculation procedures have been developed to calculate the stresses during hardening of a concrete structure. However, there still exists a gap between stresses during hardening predicted by simulation models and stresses measured in experiments. This gap showed the need for new research in this field. The main research question to be examined in this thesis was therefore:

How can the accuracy of stress prediction in hardening concrete be improved by a more detailed description of microstructure and transport phenomena?

Models developed in the past and experiments reveal a trend that leading parameters for the visco-elastic behaviour of hardening concrete should be microstructural development and moisture movements (from seepage theory [Lynam, 1934] to the influence of capillary water, gel water and interlayer water in Mabrouks model [Mabrouk, 2004]). Continuing hydration of a hardening cement paste causes a continuously changing microstructure and moisture state. A description of the visco-elastic behaviour is obtained in this thesis by relating the visco-elastic behaviour of hardening concrete to both the microstructural development of the hardening concrete and physical phenomena, like moisture movements in the system. A model based on microstructural developments by the hollow shell mode of cement hydration and moisture movements is proposed which has the potential to simulate the time-dependent behaviour of hardening concrete under a sustained load and to predict stresses due to restrained deformations in hardening concrete accurately.

Conclusions

The visco-elastic behaviour of hardening concrete is directly coupled to the micro-structural development of hardening cement paste and the state of moisture in the pore space. A model based on physical concepts is presented that takes into account the visco-elastic behaviour of hardening concrete based upon the presence of hollow shells and the transport of water accumulated inside the hollow shells and water in the capillary pores. With the presented procedure, the visco-elastic behaviour is coupled to the development of the micro-structural development as well as to moisture movements.

The state of capillary water, which is a key parameter for cement hydration and visco-elastic behaviour, is determined. Capillary moisture movements, initiated by capillary pressure gradients, are modelled and it is investigated that those moisture movements, from water rich zones in the ITZ to zones with a lack of water in the bulk paste, have a positive influence on the overall development of the degree of hydration and concrete properties. The reliability and accuracy of the microstructural development and the prediction of concrete properties should be increased, which is important for the analysis of visco-elastic behaviour of hardening concrete.

A parameter study revealed that with the proposed model less time dependent deformations are predicted with increasing age at loading. A decrease of the water/cement ratio results in a decrease of creep deformations. The results obtained with the model also revealed that the fineness of cement hardly influences the visco-elastic behaviour of the hardening concrete directly. However, it does influence the rate of hydration. In the model the load sign has no influence on the visco-elastic behaviour of hardening cement paste. Since there is no general agreement about these parameters in literature, these results of the model (influence of cement fineness and load sign) are validated and approved by experiments.

As a first validation of the proposed model two test series are performed. First test series contains sustained loading experiments. The results are used to study the influence of the cement fineness and to study the influence of the load sign. Result of this program is that no influence on the visco-elastic behaviour can be ascribed to both parameters. Second test series are the degree of restraint experiments to validate

the Shell Deformation Model. For three mixtures with different cement finenesses, it turned out that stress developments are predicted more accurate by using the proposed model compared to a model previously proposed [Lokhorst 2001]. For a more extended validation, more experimental research is recommended.

6.2 Conclusions

With the presented shell deformation model, the time-dependent behaviour is now related to microstructural changes and the moisture state in the system, as recommended in literature [Carol, 1993], [Lokhorst, 2001], [Bazant, 2004], [Mabrouk, 2004]. The model is able to predict the visco-elastic behaviour of hardening cement paste accurate for the simulated cases and can be used in stress prediction simulation software easily.

The following specific conclusions and remarks can be listed from the modelling approach as presented in this thesis:

- 1 The visco-elastic behaviour of hardening cement paste can be described by the microstructural development of the hardening cement paste and moisture transport between water inside a shell of cement gel and the capillary pores.
- 2 The proposed model is able to predict stress development in hardening concrete for the studied cases. It decreased the gap between simulated and measured stress developments.
- 3 From the proposed model and the experimental program, it can be concluded that the cement fineness (range from $300\text{m}^2/\text{kg}$ to $550\text{m}^2/\text{kg}$) has no influence on the visco-elastic behaviour of hardening concrete.
- 4 In the model, it is assumed that, as long as micro-cracking does not occur, visco-elastic behaviour of hardening concrete is independent of the load sign. Experimental results did not reveal an effect of the load sign either.
- 5 The contribution of moisture transport through the capillary pore system on the development of the degree of hydration, visco-elastic behaviour and other properties (e.g. modulus of elasticity) is modelled explicitly.

Conclusions

- 6 Capillary moisture transport has a bigger influence on the degree of hydration (up to 5%), visco-elastic behaviour (up to 8%) and other properties for higher water/cement-ratios (based on results with and without moisture transport).
- 7 The visco-elastic behaviour is predicted more accurate if capillary moisture transport is taken into account. Property predictions will become more reliable.

6.3 Recommendations and outlook

The model to predict stresses in hardening concrete based on microstructural changes and moisture state as presented in this thesis shows good results and describes the general trends as well (influence water/cement ratio, cement fineness etc). However, the presented model is based on the hollow shell mode of hydrating Portland cement particles. More study is needed on the hollow shell mode of hydrating cement grains and the research should be extended to blast furnace slag cements as well.

The interior space between the shell of cement gel and the anhydrous cement grain is bridged by hydration products (“rods”) [Dalglish, 1982]. Those rods might influence the interaction between the shell of cement gel and the anhydrous cement grain, when the shell is loaded.

In this thesis, the main assumption for capillary water transport was the boundary condition. Sealed conditions were assumed for the pore system of the cement paste, without interaction with the environment. In a real structure, the moisture balance of the outer layer of the structure is influenced by, for instance, relative humidity of the environment, which on its turn influences the degree of hydration, and visco-elastic behaviour. This interaction might be taken into account as well.

The model to predict the visco-elastic behaviour of hardening concrete as presented in chapter three of this thesis can be a helpful research tool and can be used to analyse the visco-elastic behaviour of mix designs and to optimize new mix designs to get a concrete with higher or lower creep or relaxation behaviour.

An additional application of the capillary moisture transport model, as presented in Chapter 4 of this thesis, is the possibility to model internal curing. Internal curing is a method to offset self-desiccation and helps avoiding self-desiccation shrinkage by adding internal water-reservoirs, providing a source of curing water to the paste volume in their vicinity. This internal water storage can be water-saturated lightweight aggregates [Hammer, 1992] or water-saturated Super Absorbent Polymers (SAP) [Jensen, 2001]. By changing the boundary conditions of the capillary moisture transport model as presented in this thesis, it is possible to add lightweight particles at one or both sides of the ribbon (Figure 6.1, top). It is also possible to add SAP-particles to the ribbon-model (Figure 6.1, bottom).

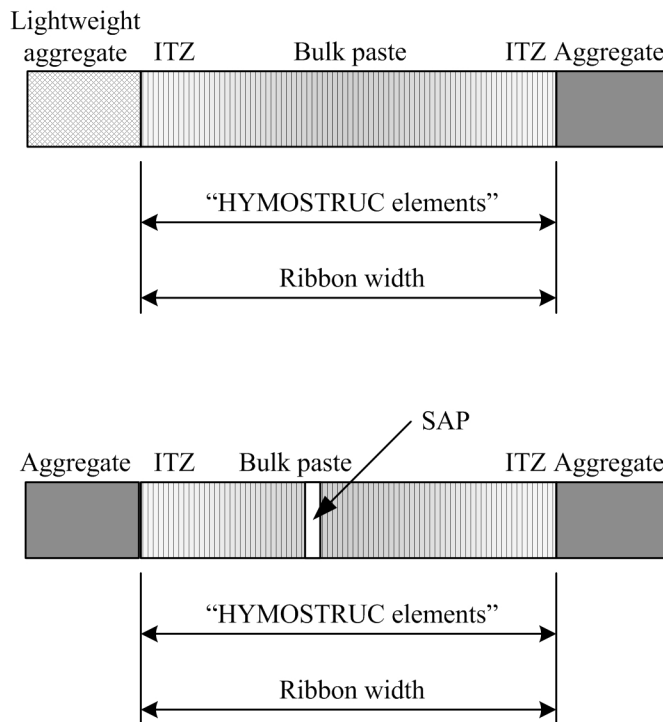


Figure 6.1 Lightweight aggregate (top) or Super Absorbent Polymer (bottom) added to ribbon model

References

Acker, P. (2001): "Micromechanical analysis of creep and shrinkage mechanisms", in: F.J. Ulm, Z.P. Bazant, F.H. Wittmann (Eds.), Creep, Shrinkage, and Durability Mechanics of Concrete and other Quasi-Brittle Materials, Elsevier Science Ltd., New York, 2001, pp. 15–25

Ali, I., and Kesler, C.E. (1963): "Creep in concrete with and without exchange of moisture with the environment", University of Illinois, Urbana, Dept. Theor. Appl. Mech., Report No. 641

Altoubat, S. A. and Lange, D. A., (2001): "The Pickett Effect in Early Age Concrete Under Restrained Conditions". RILIM International Conference on Early Age Cracking in Cementitious Systems (EAC'01), Haifa, pp. 133-144

Altrushi, D. S., (2003): "Tensile and Compressive Creep of Early Age Concrete: Testing and Modelling". Ph.D. Thesis, Department of Civil Engineering The Norwegian University of Science and Technology, Trondheim, Norway

Bamforth, P. B., (1982): "Advantages from Temperature Studies". C&C Ass. Train. Centre, THD 7346

*Bazant, Z.P. and Osman, E. (1976): "Double power law for basic creep of concrete". *Materiaux et Construction*, Vol. 9, No. 49, pp. 3-11*

*Bazant, Z. P., Cusatis, G. and Cedolin, L., (2004): "Temperature Effect on Concrete Creep Modeled by Microprestress-Solidification Theory". *Journal of Engineering Mechanics*, ASCE, pp. 691-699*

References

Bear, J., (1972): “Dynamics of fluids in Porous media”. American Elsevier, New York

Beek, A. van, (1995): “Determination of strength of young concrete”. Master thesis, Delft University of Technology, The Netherlands

Bentz, D. P., Garboczi, E. J. and Martys, N. S., (1996): “Application of Digital-Image Based Models to Microstructure, Transport Properties, and Degradation of Cement-Based Materials”. The Modelling of Microstructure and Its Potential for Studying Transport Properties and Durability. Kluwer Academic Publishers, The Netherlands, pp. 167-185

Bentz, D. P., (1997): “Computer Simulation of Portland Cement Hydration and Microstructure Development”. Journal of the American Ceramic Society, Vol. 80, No. 1, pp. 3-21.

Bernander, S., (1973): “Cooling of hardening concrete with cooling pipes”. Nordisk Betong, No. 2, pp. 21-30.

Bernander, S., (1982): “Temperature stresses in early-age concrete due to hydration”. Proc. Int. Conf. on Concrete at Early Ages, RILEM, Paris, Vol. II, pp. 218-221

Bernander, S. and Emborg, M., (1994): “Risk of Cracking in Massiv Concrete Structures – New Development and Experiences”. Thermal Cracking in Concrete at Early ages, Proc. of the RILEM International Symposium, London, pp. 385-392

Bjøntegaard, Ø., (1999): “Thermal dilation and autogenous deformations as driving forces to self-induced stresses in high performance concrete”. Ph. D. thesis, Norwegian University of Science and Technology, Trondheim, Norway

Breugel, K. van, (1980): “Relaxation of Young concrete”. Report 5-80-D8, Delft University of Technology, The Netherlands

- Breugel, K. van, (1997):* “Simulation of hydration and formation of structure in hardening cement-based materials (second edition)”. Ph.D. thesis, Delft University of Technology, The Netherlands
- Breugel, K. van, (2007):* “Integral service life technology”. International Seminar on Durability and Lifecycle Evaluation of Concrete Structures, Hiroshima, pp. 3-18
- Byfors, J., (1980):* “Plain concrete at early age”. Swedish cement and concrete research institute.
- Carol, I. and Bazant, Z. P., (1993):* “Viscoelasticity with aging caused by solidification of nonaging constituent”. Journal of Engineering Mechanics, Vol. 119, No 11, pp. 2252-2269
- Czerny, F., (2004):* “Reliability of crack predictions in hardening concrete structures”. Master thesis, Delft University of Technology, The Netherlands, Universität Karlsruhe (TH), Germany, 65 p.
- Dalgleish B. J., Pratt, P. L. and Toulon, E., (1982):* “Fractographic studies of microstructure development in hydrated Portland cement”. Journal of materials science, No. 17, pp. 2199-2207
- Diamond, S., (2004):* “The microstructure of cement paste and concrete – a visual primer”. Journal of Cement and Concrete Composites, No. 26, pp. 919-933
- Ditlevsen, O. and Madsen, H. O., (2005):* “Structural Reliability Methods”. Coastal, maritime and structural engineering department of mechanical engineering, Technical University of Denmark
- Emborg, M., Bernarder, S., (1994):* “Avoidance of Early age thermal Cracking in Concrete Structures – Predesign, Measures, Follow-up”. Thermal Cracking in Concrete at Early ages, Proc. Of the RILEM International Symposium, London, pp. 409-416

References

- Fib*, (1999): "Structural concrete, the textbook on behaviour, design and performance". Three volumes, Lausanne
- Gosh, R. S.*, (1973): "A hypothesis on mechanisms of maturing creep of concrete". *Materiaux et Construction*, Vol. 6, No. 31, pp. 23-26
- Hagihara, S., Masuda, Y. and Nakamura, S.*, (2002): "Creep Behaviour of High-Strength Concrete in Early Age". 6th International Symposium on High Strength / High Performance concrete
- Hamfler, H.*, (1988): "Berechnung von Temperatur-, Feuchte- und Verschiebungsfeldern in erhärtenden Betonbauteilen nach der Methode der finiten Elemente". *Deutscher Ausschuss für Stahlbeton*, H. 395
- Hammer, T. A.*, (1992): "High strength LWA concrete with silica fume – Effect of water content in the LWA on mechanical properties". *ACI Int. Conf. On Fly Ash, Silica Fume and natural Pozzolans in Concrete*, Turkey, pp. 314-330
- Hansen, T.C.*, (1958): "Creep of concrete". *Swedish Cement and Concrete Research Institute, Stockholm, Bulletin No. 33*, 48pp.
- Head, M. K., Wong, H. S. and Buenfeld, N. R.*, (2006): "Characterisation of 'Hadley' grains by confocal microscopy". *Cement and Concrete Research*, Vol. 36, pp. 1483-1489
- Igarashi, S. I., Bentur, A. and Kovler, K.*, (1999): "Stress and Creep Relaxation Induced in Restrained Autogenous Shrinkage of High-Strength Pastes and Concretes". *Advances in Cement Research*, No 4, pp. 169-177
- Igarashi, S. I., Mawamura, M.* (2002): "Effect of microstructure on Restrained Autogenous Shrinkage behaviour in High Strength Concrete at Early Ages". *Material and Structures*, Vol 35, pp. 80-84

Ishai, O., (1968): “The time-dependent deformational behaviour of cement paste, mortar and concrete”. Proceedings of International Conference On the Structure of Concrete, Cement and Concrete Association, England, pp. 345-364

Jensen, O. M. and Hansen, P. F., (2001): “Water-entrained cement-based materials 1. Principles and theoretical background”. Cement and Concrete Research, Vol. 31, pp. 647-654

Kjellsen, K. O., Lagerblad, B. and Jennings, H. M., (1997): “Hollow-shell formation – an important mode in the hydration of Portland cement”. Journal of Materials Science, No 32, pp. 2921-2927

Kjellsen, K. O. and Lagerblad, B., (2007): “Microstructure of tricalcium silicate and Portland cement systems at middle periods of hydration-development of Hadley grains”. Cement and Concrete Research, No 37, pp. 13-20

Koenders, E. A. B., (1997): “Simulation of Volume Changes in Hardening Cement-Based Materials”. Ph.D. Thesis, Delft University of Technology, The Netherlands

Koenders, E. A. B. and Rooij, M. de, (2006): “Moisture flow by micro structural contraction”. Materials and Structures, No 39, pp. 869-876

Kovler, K., Igarashi, S. and Bentur, A., (1999): “Tensile creep behaviour of high strength concretes at early ages”. Materials and Structures, No 32, pp. 383-387

Kreyszig, E., (1988): “Advanced Engineering mathematics”. Sixth edition, Wiley, ISBN 0-471-62787-9

Laube, M., (1991): “Werkstoffmodell zur Berechnung von Temperaturspannungen in massigen Betonbauteilen im jungen alter“. Ph.D. thesis, Technischen Universität Carolo-Wilhelmina, Braunschweig, Germany

Lea, F. M. and Lee, C. R., (1946): “Shrinkage and creep in concrete”. The Society of Chemical Industry, London, Symp. On the Shrinkage and Cracking of Cementive Materials, pp. 7-17

References

Locher, F. W., Richtz, W. and Sprung, S. (1976): "Erstarren von Zement". Zement Kalk Gips 29(10), pp. 435-442

Lokhorst, S. J., (2001): "Deformational behaviour of concrete influenced by hydration related changes of the microstructure". Stevin Report 25.5-99-05, Delft University of Technology, The Netherlands

Lorman, W. R., (1940): "The theory of concrete creep". ASTM proc. 40, pp. 1082-1102

Lura, P. and Breugel, K. van (2001): „Numerical evaluation of cracking risk in massive cellar walls cast on slab“. IPACS report No. 2001:63-X, IS 91-89580-63-X, 28 p.

Lynam, C. G., (1934): "Growth and movement in Portland Cement Concrete". Oxford University Press, London, 139 p.

Mabrouk, R., Ishida, T. and Maekawa, K., (2004): "A unified solidification model of hardening concrete composite for predicting the young age behaviour of concrete". Cement and Concrete Composites, Vol. 26, Issue 5, pp. 453-461

Manzano, H., Dolado, J. S. and Ayuela, A., (2009): "Elastic properties of the main species present in Portland cement pastes". Acta Materialia, Vol. 57, pp. 1666-1674

Nakamoto, J., Togawa, K., Miyagawa, T. and Fujii, M., (1997): "Creep, Drying Shrinkage and Autogenous Shrinkage of High Slag Content Concrete". Proc. International Conference on Engineering Materials. CSCE/JSCE. Ottawa, Canada, pp. 357-372

Neville, A. M., (1973): "Properties of Concrete". Pitman publ., 687 p.

Neville, A. M., Dilger, W. H. and Brooks, J. J., (1983): "Creep of Plain and Structural Concrete". Construction Press, 361p.

Nilson, M., (2003): “Restraint Factors and Partial Coefficients for Crack Risk Analyses of Early Age Concrete Structures”. Ph. D. Thesis, Lulea University of Technology, Sweden

Noakowski, P., (1978): “Die Bewehrung von Stahlbetonbauteilen bei Zwangsbeanspruchung infolge Temperatur”. Deutscher Ausschuss für Stahlbeton, Heft 296

Nolting, E. H., (1989): “Zur Frage der Entwicklung lastunabhängiger Verformungen und Wärmedehnzahlen junger Betone”. Mitteilungen aus dem Institut für Baustoffkunde und Materialprüfung, Heft 56, University of Hannover

Nowak, A. S., Collins, K. R., (2000): “Reliability of Structures”. McGraw-Hill Higher Education, ISBN 0-07-048163-6

Onken, P. and Rostasy, F., (1995): “Wirzame Betongzugfestighur im Bauwerk bei fruh einsetzendem Temperaturzwang”. Deutscher Ausschuss für Suklbeton, Heft 449, Berlin

Østergaard, L., Lange, D. A. and Stang, H., (2001): “Tensile Basic Creep of Early-age Concrete Under Constant Load”. Cement and Concrete Research, No 31, pp. 1895-1899

Picket, G., (1942): “The effect of change in moisture-content of the creep of concrete under a sustained load”. Proceedings for the American Concrete Institute, 38(4), pp. 333-355

Pommersheim, J. M. and Clifton, J. R., (1980): “Conceptual and mathematical models for tri-calcium silicate hydration”. 7th International Conference on Chemistry of Cements

Powers, T. C., Copeland, L. E., Hayes, J. C. and Mann, H. M., (1954): “Permeability of Portland cement pastes”. Proceedings of American Concrete Institute, Vol 51, PCA Research Bulletin 53, pp. 285-298

References

Powers, T.C., (1958): “Structure and physical properties of hardened Portland cement paste”. *Journal Am. Cer. Society*, Vol. 41, No. 1, pp. 1-6

Powers, T. C., Mann, H. M. and Copeland, L. E., (1958): “The flow of water in hardened Portland cement paste”. *Highway Research Board Special Report*, No 40, *PCA Research Bulletin* 106

Powers, T. C., (1979): “The specific surface area of hydrated cement obtained from permeability data”. *Materiaux et Constructions*, Vol. 12, No 69

Rilem, (1982): “General Report, Session 1: Mechanical Properties”. *International Conference on Concrete at Early ages*, Volume II, Paris

Sule, M. S., (2003): “Effect of Reinforcement on Early-Age Cracking in High Strength Concrete”. *Ph.D. Thesis*, Delft University of Technology, The Netherlands

Thomas, F. G., (1937): “Creep of concrete under load”. *International Association of Testing Materials*, London Congress, pp. 292-294

Westman, G., (1999): “Concrete Creep and Thermal Stresses”. *Ph.D. Thesis*, Lulea University of Technology, Sweden

Wischers, G. and Dahms, J. (1977): “Kriechen von Frühbelastetem Beton mit hoher Anfangsfestigkeit”. *Beton*, Vol. 2, 3: 69-74, 104-108.

Wittmann, F. H., (1974): “Bestimmung physikalischer Eigenschaften des Zementsteins”. *Deutscher Ausschuss für Stahlbeton*, Heft 232

Wittmann, F. H., (1977): “Grundlagen eines Modells zur Beschreibung charakteristischer Eigenschaften des Betons. *Deutscher Ausschuss für Stahlbeton*. Heft 290

Appendix A Finite Element approach

A.1 Galerkin's Finite Element method

In this section, it will be outlined how the differential equations (equation 4.57 & 4.58) are solved numerically. Several numerical techniques can be applied to solve a differential equation. In this thesis, it is chosen to solve it by using Galerkin's Finite Element method. To illustrate the solution procedure, the method is shown for the differential equation that describes Darcy's law.

$$\frac{\partial V_w}{\partial t} = V \cdot \left(\frac{k_w}{\gamma_w} \cdot \nabla^2 P_w \right) \quad [A.1]$$

Solving this differential equation by a Finite Element Method needs to multiply the differential equation by an arbitrary test function "f" which is a continuous function on [0,1], f is piecewise continuous and bounded on [0,1] and f(0) = f(1) = 0, followed by integration over the calculation domain. Assume a test function f:

$$\iint f \cdot \frac{\partial V_w}{\partial t} dx dy = \iint f \cdot \left[V \cdot \left(\frac{k_w}{\gamma_w} \cdot \nabla^2 P_w \right) \right] dx dy \quad [A.2]$$

$$\iint f \cdot \frac{\partial V_w}{\partial t} dx dy = \iint f \cdot \left[V \cdot \left(\frac{k_{w;x}}{\gamma_w} \cdot \frac{\partial^2 P_w}{\partial x^2} \right) + V \cdot \left(\frac{k_{w;y}}{\gamma_w} \cdot \frac{\partial^2 P_w}{\partial y^2} \right) \right] dx dy \quad [A.3]$$

Due to the arbitrary test function, this integral-formulation is equal to the original differential equation. Partial integration of this formulation results in an integral which only includes first order derivatives:

$$\int f(x) \cdot g'(x) dx = f(x) \cdot g(x) - \int g(x) \cdot f'(x) dx \quad [A.4]$$

Appendix A

$$\iint_{\Omega} f \cdot \frac{\partial V_w}{\partial t} dx dy = \int_{\Gamma} f \cdot \left(V \cdot \frac{k_{w;x}}{\gamma_w} \cdot \frac{\partial P_w}{\partial x} \right) dx + \int_{\Gamma} f \cdot \left(V \cdot \frac{k_{w;y}}{\gamma_w} \cdot \frac{\partial P_w}{\partial y} \right) dy -$$

[A.5]

$$\iint_{\Omega} \left[\left(\frac{\partial f}{\partial x} \cdot V \cdot \frac{k_{w;x}}{\gamma_w} \cdot \frac{\partial P_w}{\partial x} \right) + \left(\frac{\partial f}{\partial y} \cdot V \cdot \frac{k_{w;y}}{\gamma_w} \cdot \frac{\partial P_w}{\partial y} \right) \right] dx dy$$

The boundary integrals vanishes since $f = 0$ on the boundary (Γ) (Figure A.1), $f(0) = f(1) = 0$, thus the line integrals equals 0. Now the integral only includes first order partial differences. Dividing this integral (and the calculation domain (Ω)) into separate elements E (Ω^e) results in the following weak form, from which we have to find V_w :

$$\iint_{\Omega} f \cdot \frac{\partial V_w}{\partial t} dx dy = - \sum_E \iint_{\Omega^e} \left[\left(\frac{\partial f}{\partial x} \cdot V \cdot \frac{k_{w;x}}{\gamma_w} \cdot \frac{\partial P_w}{\partial x} \right) + \left(\frac{\partial f}{\partial y} \cdot V \cdot \frac{k_{w;y}}{\gamma_w} \cdot \frac{\partial P_w}{\partial y} \right) \right] dx dy \quad [A.6]$$

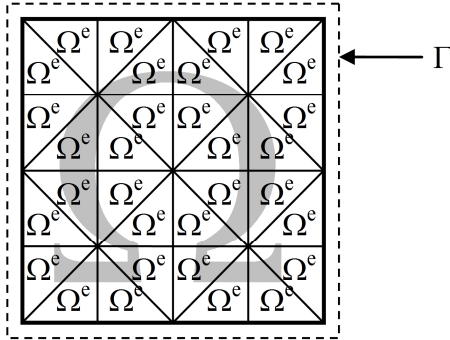


Figure A.1 Visualisation of a calculation domain (Ω) the elements (Ω^e) and the boundary (Γ)

Back to the one dimensional problem and back to the general calculation domain (the calculation domain Ω is from now one dimensional as well and the boundary Γ are points now):

$$\int_{\Omega} f \cdot \frac{\partial V_w}{\partial t} dx = - \int_{\Omega} \frac{\partial f}{\partial x} \cdot V \cdot \frac{k_{w;x}}{\gamma_w} \cdot \frac{\partial P_w}{\partial x} dx \quad [A.7]$$

The weak form can be solved by use of the Galerkin FEM. Piecewise linear basis-functions $\{\Psi_i(x)\}_{i=0}^n$ are used on the n grid nodes, with:

$$\Psi_i(x_j) = \begin{cases} 1, & j = i, \\ 0, & j \neq i. \end{cases} \quad [A.8]$$

$V_w(x,t)$ is approximated by:

$$V_{w_n}(x,t) = \sum_{i=0}^n V_{wi}(t) \cdot \Psi_i(x) = \Psi_0(x) + \sum_{i=1}^n \Psi_i(x) \cdot V_{wi}(t) \quad [A.9]$$

Note that $\{V_{wi}\}$ should be functions of x and t since $V_w(x,t)$ is a function of t and $\Psi_i(x)$ is a function of x only. Substitution gives:

$$\left. \begin{array}{l} \text{Find } \{V_{wi}(t)\}_{i=1}^n \text{ such that} \\ \int_0^1 \sum_{i=1}^n V_{wi}'(t) \Psi_i(x) \Psi_j(x) dx = - \int_0^1 \left\{ \Psi_0'(x) + \sum_{i=1}^n \Psi_i'(x) \cdot V_{wi}(t) \right\} \Psi_j'(x) dx \\ \forall j \in (1, \dots, n) \end{array} \right\} [A.10]$$

This problem represents a system of linear equations. Note that:

$$V_{wi}'(t) \approx \frac{V_{wi}(t + \Delta t) - V_{wi}(t)}{\Delta t} \quad [A.11]$$

Appendix A

A.2 Time integration

Taking the weak form of the one dimensional simplified problem:

$$\int_{\Omega} f \cdot \frac{\partial V_w}{\partial t} dx = - \int_{\Omega} \frac{\partial f}{\partial x} \cdot V \cdot \frac{k_{w;x}}{\gamma_w} \cdot \frac{\partial P_w}{\partial x} dx \quad [A.12]$$

Take $f|_{\Gamma}=0$ then we want to find V_w , subject to $V_w(0) = V_w 0$, $V_w(1) = V_w 1$, such that:

$$\int_0^1 f \cdot \frac{\partial V_w}{\partial t} dx = - \int_0^1 \frac{\partial f}{\partial x} \cdot V \cdot \frac{k_{w;x}}{\gamma_w} \cdot \frac{\partial P_w}{\partial x} dx \quad \forall f(0)=0=f(1) \quad [A.13]$$

Provided that the integral exists and taking basis-functions (piece-wise linear):

$$\psi_i(0) = 0 = \psi_i(1) \text{ for } i \in \{1, \dots, m-1\} \quad [A.14]$$

$$V_w(x, t) = \sum_{i=1}^{m-1} [c_i(t) \cdot \psi_i(x)] + u_0 \cdot \psi_0(x) + u_1 \cdot \psi_m(x) \quad [A.15]$$

take $u_0 = 0 = u_1$ then

$$\sum_{i=1}^{m-1} V_w'(t) \int_0^1 \psi_i(x) \cdot \psi_j(x) dx = - \sum_{i=1}^{m-1} \left[V \cdot \frac{k_{w;x}}{\gamma_w} \cdot P_w \right]_i(t) \cdot \int_0^1 \psi_i'(x) \cdot \psi_j'(x) dx$$

$$j \in \{1, \dots, m-1\} \quad [A.16]$$

For forward Euler, we obtain:

$$\sum_{i=1}^{m-1} \frac{V_{wi}^{n+1} - V_{wi}^n}{\Delta t} \cdot \int_0^1 \psi_i(x) \cdot \psi_j(x) dx = - \sum_{i=1}^{m-1} \left[V \cdot \frac{k_{w;x}}{\gamma_w} \cdot P_w \right]_i^t \cdot \int_0^1 \psi_i'(x) \cdot \psi_j'(x) dx$$

$$j \in \{1, \dots, m-1\} \quad [A.17]$$

Where the mass-matrix M_{ij} can be substituted:

$$\int_0^1 \psi_i(x) \cdot \psi_j(x) dx = M_{ij} \quad [\text{A.18}]$$

and the stiffness-matrix S_{ij} can be substituted:

$$\int_0^1 \psi_i'(x) \cdot \psi_j'(x) dx = S_{ij} \quad [\text{A.19}]$$

Which results in:

$$\sum_{i=1}^{m-1} \frac{V_{wi}^{n+1} - V_{wi}^n}{\Delta t} \cdot M_{ij} = - \sum_{i=1}^{m-1} \left[V \cdot \frac{k_{w;x}}{\gamma_w} \cdot P_w \right]_i^t \cdot S_{ij} \quad j \in \{1, \dots, m-1\} \quad [\text{A.20}]$$

The computation of S_{ij} is simple, since $\{\Psi_i\}$ are piecewise linear functions:

$$S_{ij} = \int_0^1 \psi_i'(x) \psi_j'(x) dx \quad [\text{A.21}]$$

$$\int_0^1 \psi_{i-1}'(x) \psi_i'(x) dx = \int_{x_{i-1}}^{x_i} \frac{1}{x_{i-1} - x_i} \cdot \frac{1}{x_i - x_{i-1}} dx = - \frac{1}{x_i - x_{i-1}} \quad [\text{A.22}]$$

$$\int_0^1 \psi_i'(x) \psi_i'(x) dx = \frac{1}{x_i - x_{i-1}} + \frac{1}{x_{i+1} - x_i} \quad [\text{A.23}]$$

$$\int_0^1 \psi_i'(x) \psi_{i+1}'(x) dx = \int_{x_i}^{x_{i+1}} \frac{1}{x_i - x_{i-1}} \cdot \frac{1}{x_{i+1} - x_i} dx = - \frac{1}{x_{i+1} - x_i} \quad [\text{A.24}]$$

$$\int_0^1 \psi_i'(x) \psi_{i+2}'(x) dx = 0 \quad [\text{A.25}]$$

Appendix A

Element wise it is obtained that:

$$\begin{aligned}
 & \frac{V_{w,j-1}^{n+1} - V_{w,j-1}^n}{\Delta t} \int_{e_j} \psi_j \cdot \psi_{j-1} dx + \frac{V_{w,j}^{n+1} - V_{w,j}^n}{\Delta t} \int_{e_j \cup e_{j+1}} (\psi_j \cdot \psi_j) dx + \frac{V_{w,j+1}^{n+1} - V_{w,j+1}^n}{\Delta t} \int_{j+1} \psi_j \cdot \psi_{j+1} dx \\
 &= - \left[V \cdot \frac{k_{w;x}}{\gamma_w} \cdot P_w \right]_{j-1}^n \int_{e_j} \psi_j' \cdot \psi_{j-1}' dx - \left[V \cdot \frac{k_{w;x}}{\gamma_w} \cdot P_w \right]_j^n \int_{e_j \cup e_{j+1}} \psi_j' \cdot \psi_j' dx - \left[V \cdot \frac{k_{w;x}}{\gamma_w} \cdot P_w \right]_{j+1}^n \int_{j+1} \psi_j' \cdot \psi_{j+1}' dx \\
 & \hspace{15em} \text{for } j \in \{1, \dots, m-1\} \\
 &= - \left[V \cdot \frac{k_{w;x}}{\gamma_w} \cdot P_w \right]_{j-1}^n \cdot \left(-\frac{1}{x_j - x_{j-1}} \right) - \left[V \cdot \frac{k_{w;x}}{\gamma_w} \cdot P_w \right]_j^n \cdot \left(\frac{1}{x_j - x_{j-1}} + \frac{1}{x_{j+1} - x_j} \right) - \left[V \cdot \frac{k_{w;x}}{\gamma_w} \cdot P_w \right]_{j+1}^n \cdot \left(-\frac{1}{x_{j+1} - x_j} \right) \\
 & \hspace{15em} \text{for } j \in \{1, \dots, m-1\}
 \end{aligned}$$

[A.26]

where $V_{w,i}^n$ denotes $V_w(x_i, t_n)$. Since $\psi_i(x)$ is defined element wise, the natural way to compute the stiffness matrix is to do this element-wise too. We store the four integrals in the element matrix:

$$S_j^e = \begin{bmatrix} \int_{e_j} \frac{d\psi_{j-1}}{dx} \cdot \frac{d\psi_{j-1}}{dx} dx & \int_{e_j} \frac{d\psi_{j-1}}{dx} \cdot \frac{d\psi_j}{dx} dx \\ \int_{e_j} \frac{d\psi_j}{dx} \cdot \frac{d\psi_{j-1}}{dx} dx & \int_{e_j} \frac{d\psi_j}{dx} \cdot \frac{d\psi_j}{dx} dx \end{bmatrix} \quad [A.27]$$

the element matrix for an arbitrary element e_j has now shape:

$$S_j^e = \frac{1}{x_j - x_{j-1}} \begin{bmatrix} 1 & -1 \\ -1 & 1 \end{bmatrix} \quad [A.28]$$

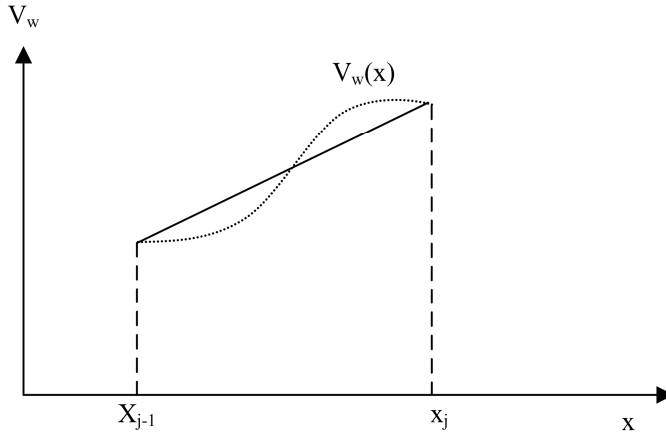


Figure A.2 Trapezium rule for linearization of $V_w(x)$

The large stiffness matrix can be assembled from all element matrices. The element vector and mass matrix can be obtained by applying the Newton-Cotes rule. In this case, the trapezium rule is applied (Figure A.2). Linear interpolation results in a tri-diagonal matrix, which is easy to solve, while application of quadratic elements results in a smaller approximation error. For linear interpolation, more elements are needed for the same accuracy of the results compared to quadratical elements.

$$V_w^e{}_j = (x_j - x_{j-1}) \cdot \frac{V_w(x_{j-1}) + V_w(x_j)}{2} \quad [\text{A.29}]$$

$$V_w^e{}_j = \frac{x_j - x_{j-1}}{2} \begin{bmatrix} V_w(x_{j-1}) \\ V_w(x_j) \end{bmatrix} \quad [\text{A.30}]$$

For the left boundary element, this becomes:

$$V_w^e{}_j = \frac{x_j - x_{j-1}}{2} \begin{bmatrix} 0 \\ V_w(x_j) \end{bmatrix} \quad [\text{A.31}]$$

and for the right boundary element:

Appendix A

$$V_w^e_j = \frac{x_j - x_{j-1}}{2} \begin{bmatrix} V_w(x_{j-1}) \\ 0 \end{bmatrix} \quad [\text{A.32}]$$

From substitution we got:

$$\sum_{i=1}^{m-1} M_{ij} \frac{V_{wi}^{n+1} - V_{wi}^n}{\Delta t} = - \sum_{i=1}^{m-1} S_{ij} \left[V \cdot \frac{k_{w;x}}{\gamma_w} \cdot P_w \right]_i^t \quad j \in \{1, \dots, m-1\} \quad [\text{A.33}]$$

$$\sum_{i=1}^{m-1} M_{ij} \frac{V_{wi}^{n+1}}{\Delta t} - \sum_{i=1}^{m-1} M_{ij} \frac{V_{wi}^n}{\Delta t} = - \sum_{i=1}^{m-1} S_{ij} \left[V \cdot \frac{k_{w;x}}{\gamma_w} \cdot P_w \right]_i^t \quad [\text{A.34}]$$

$$\sum_{i=1}^{m-1} M_{ij} \frac{V_{wi}^{n+1}}{\Delta t} = \sum_{i=1}^{m-1} M_{ij} \frac{V_{wi}^n}{\Delta t} - \sum_{i=1}^{m-1} S_{ij} \left[V \cdot \frac{k_{w;x}}{\gamma_w} \cdot P_w \right]_i^t \quad [\text{A.35}]$$

$$\sum_{i=1}^{m-1} M_{ij} \cdot V_{wi}^{n+1} = \sum_{i=1}^{m-1} M_{ij} \cdot V_{wi}^n - \Delta t \cdot \sum_{i=1}^{m-1} S_{ij} \left[V \cdot \frac{k_{w;x}}{\gamma_w} \cdot P_w \right]_i^t \quad [\text{A.36}]$$

So the Euler-forward time integration method can be written in matrix notation by:

$$M \underline{V_w}^{n+1} = M \underline{V_w}^n - \Delta t \cdot S \left[\underline{V \cdot \frac{k_{w;x}}{\gamma_w} \cdot P_w} \right]^n \quad [\text{A.37}]$$

Or in terms of concentration of the pore water:

$$M \frac{V_w^{n+1}}{V} = M \frac{V_w^n}{V} - \Delta t \cdot S \left[\frac{k_{w;x}}{\gamma_w} \cdot P_w \right]^n \quad [\text{A.38}]$$

$$M \left(\frac{V_w^{n+1}}{V} - \frac{V_w^n}{V} \right) = - \Delta t \cdot S \left[\frac{k_{w;x}}{\gamma_w} \cdot P_w \right]^n \quad [\text{A.39}]$$

The new water pressure, gas pressure and the water movement can now be calculated.

A.3 Stability

The solution of the numerical solution of the differential equation is unconditionally stable if for real values of the Eigenvalues:

$$\Delta t < \frac{c}{|\lambda_{\max}|} \quad [\text{A.40}]$$

with for an Euler solution $c = 2$.

The maximum Eigen value (λ_{\max}) can be determined by:

$$\det(S - \lambda I) = 0 \quad [\text{A.41}]$$

Appendix B Deformations of a hollow shell

According to the theory of plates and shells (Theory of plates and shells, second edition, Timoshenko, page 561), the deformation of a spherical shell loaded by a concentrated load (Figure B.1) can be described by:

$$\delta_c = \frac{\sqrt{3(1-\nu^2)}}{2} \cdot \frac{P \cdot r}{E \cdot h^2} \psi_3(x) \quad [\text{B.1}]$$

$\psi_3(x)$ can be found in Figure B.2 where:

$$x = \sin^2 \varphi \quad [\text{B.2}]$$

At the location of the load, ψ_3 has to be taken as 0.5.

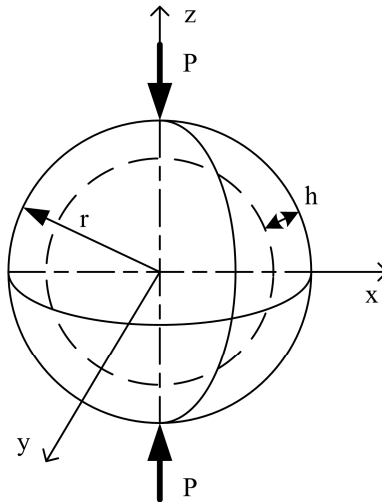


Figure B.1 Hollow sphere loaded by concentrated forces

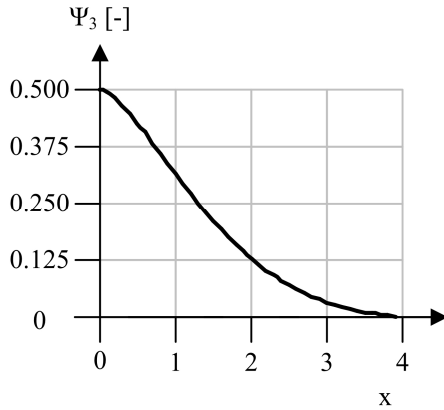


Figure B.2 Graph of the ψ_3 function

However, the sphere is not loaded by a concentrated force, but by a distributed load. To correct equation B.1 for this, a correction factor is determined by use of the finite element software DIANA. By use of DIANA the deformations of hollow spheres under distributed loads are studied. Spheres are studied with a radius (r) from 5, 10, 15 and 20 μm and the thickness of the shell (d) were varied between 0.1, 0.5, 1, 2, 3, 4, 5 and 10 μm . The used element type is a T15SH element, what is a three-node triangular isoperimetric curved shell element. For the case of a sphere with a radius of 20 μm and a shell thickness of 1 μm , loaded by a uniformly distributed load, the original and deformed shape are presented in Figure B.3.

The simulations resulted in a relation between the results of the Finite Element simulation and the results of the theory of plates and shells. This relation is described by the slenderness (λ) as the (radius (r) divided by shell thickness (h)).

The relation between the finite element simulations and the theory of plates and slabs turned out to be (with $R^2=1.00$) (Figure B.4):

$$\text{ratio} = 0.7883 \cdot \left(\frac{r}{h}\right) + 0.0388 \quad [\text{B.3}]$$

The deformation of the top of a hollow sphere loaded by an equally distributed force can now be described by the following analytical relation:

$$\partial c = \left(0.7883 \cdot \left(\frac{r}{h} \right) + 0.0388 \right) \cdot \frac{\sqrt{3(1-\nu^2)}}{4} \cdot \frac{(q \cdot \pi \cdot r^2) \cdot r}{E \cdot h^2} \quad [\text{B.4}]$$

By use of the finite element program DIANA, a linear relation is found between the deformations in the direction parallel to the load (∂c) and the deformations in the direction perpendicular to the load (∂a) of the loaded hollow sphere. The results for the studied spheres are plotted in Figure B.5. From the relation as presented in Figure B.5, it follows that (with $R^2=0.989$):

$$\partial a = 0.5069 \cdot \partial c \quad [\text{B.5}]$$

The effect of deformations perpendicular to the load direction can be explained by the effect of lateral creep (creep Poisson's ratio) of a uniaxial loaded specimen. There is no agreement on the magnitude of the creep Poisson's ratio. Values are reported up to 0.5 for cement paste [Neville (1970)].

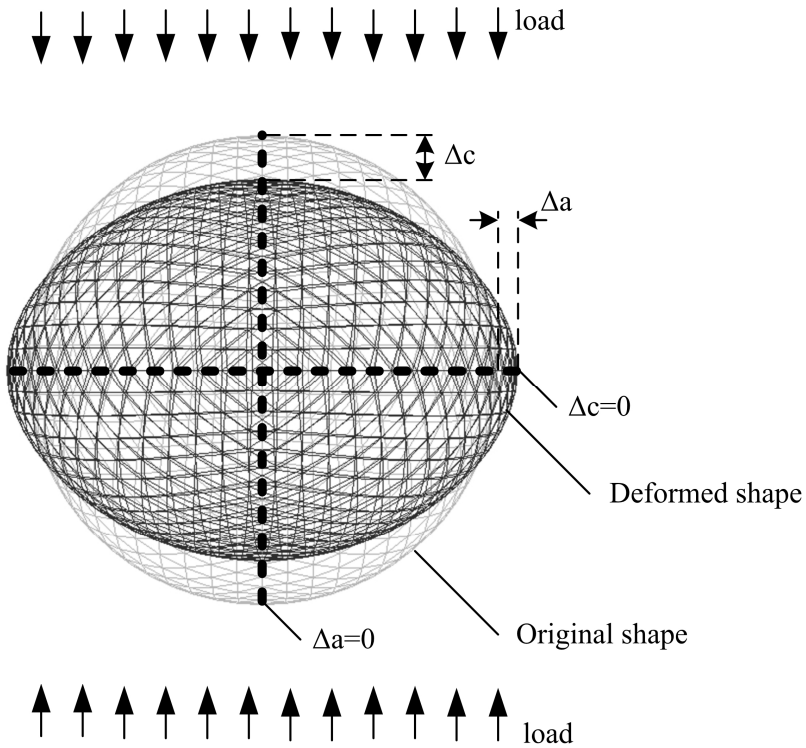


Figure B.3 Original and deformed shape of the Finite Element Model by DIANA

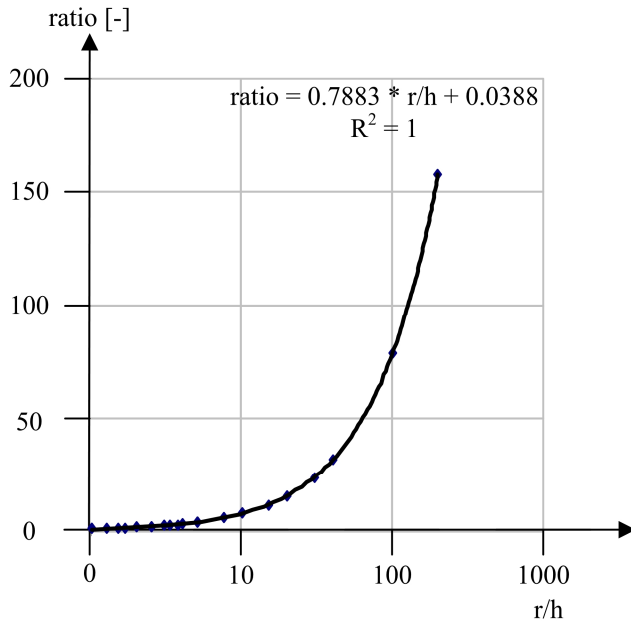


Figure B.4 Relation between FEM DIANA and Plates and shell theory

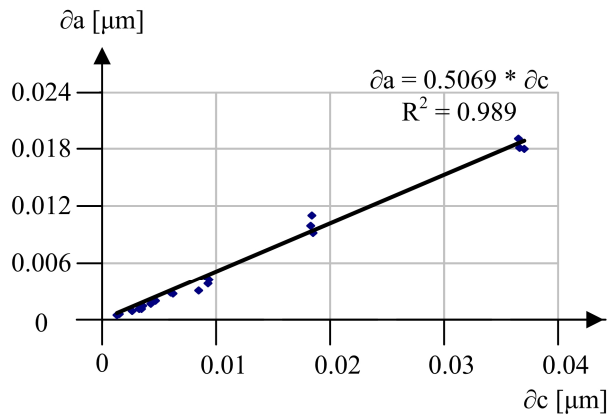


Figure B.5 Relation between ∂c and ∂a

Appendix C Hollow shells and microstructural development

The current version of Hymostruc is based upon the concept of inner hydration products and outer hydration products [Breugel, 1997]. The hollow shell will be situated in between the anhydrous cement grain and the inner product (Figure C.1). The diameter of the hydrated cement grain with hollow shell is slightly bigger than the diameter of the cement grain without hollow shell. The thickness of the annular space (δh) is approximately 1 μm [Dalglish, 1982] [Diamond, 2004] [Kjellsen, 2007]. Due to the addition of the hollow shell, the thickness of the hydration product will be reduced by the bigger radius of the shell:

$$\delta_{\text{in};x,j} = \left(\frac{x}{2} + \delta_h \right) \cdot \left[1 - \{1 - \alpha_{x,j}\}^{1/3} \right] \quad [\text{C.1}]$$

The volume of hydration products will be spread out over a larger diameter, what results in a smaller thickness of the layer of hydration products, so the increase of the diameter with hollow shell will be less than 2 μm .

The calculation of the volume of the outer product $v_{\text{ou};x,j}$ that corresponds to the degree of hydration $\alpha_{x,j}$ is independent of the thickness of the hollow shell:

$$v_{\text{ou};x,j} = (v - 1) \cdot \alpha_{x,j} \cdot v_x \quad [\text{C.2}]$$

As a result of the addition of the hollow shell, the outer radius $R_{\text{ou};x,j}$ yields into:

$$R_{\text{ou};x,j} = \left[\frac{v_{\text{ou};x,j}}{\frac{4\pi}{3}} + \left(\frac{x}{2} + \delta_h \right)^3 \right]^{1/3} \quad [\text{C.3}]$$

Appendix C

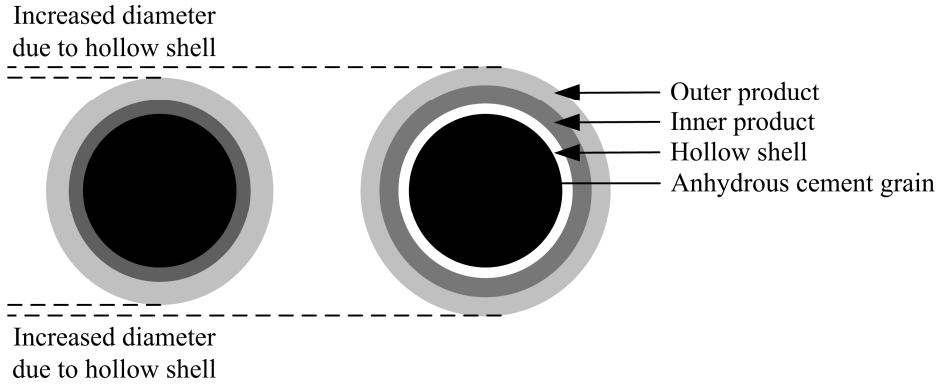


Figure C.1 Original HYMOSTRUC hydrating cement grain (left) hollow shell hydrating cement grain (right)

The thickness $\delta_{ou;x,j}$ of the outer shell automatically changes by the increase of the outer radius:

$$\delta_{ou;x,j} = R_{ou;x,j} - \left(\frac{x}{2} + \delta_h \right) \quad [C.4]$$

After applying the embedded and partly hydrated cement volume $v_{em;x,j}$ that accounts for an additional expansion of the outer shell of particle x , the outer radius $R_{ou;x,j}$ becomes:

$$R'_{ou;x,j} = \left[\frac{v_{ou;x,j} + v_{em;x,j}}{\frac{4\pi}{3}} + \left(\frac{x}{2} + \delta_h \right)^3 \right]^{1/3} \quad [C.5]$$

The new thickness of the outer shell becomes:

$$\delta'_{ou;x,j} = R'_{ou;x,j} - \left(\frac{x}{2} + \delta_h \right) \quad [C.6]$$

Since the production of the volume of hydration product is described by chemical reactions, which are prescribed by the diffusion rate of ions through the shell of cement gel, the volume of hydration products will change slightly as well due to the introduction of the hollow shell. This is taken into account by Hymostruc by a change of the ingress of ions through the shell of hydration products (cement gel).

Appendix D Practical application

D.1 General

In order to get more insight in the influence of stress development on the probability of cracking, a full scale structure is analysed in detail. The analysis starts with the description of the full scale structure, followed by a temperature analysis which is considered to be the imposed deformation together with the autogenous deformations. This results in a simulated stress development. Reinforcement is analysed which is necessary to control the crack widths and finally three possibilities are analysed to calculate the probability of cracking.

D.2 Description of the structure

The investigation of simulation of stresses will be conducted by means of considering a full-scale predefined arbitrary concrete element. This element has chosen to be a concrete wall with a thickness of 1m and a height of 3m on an existing base of concrete with a height of 1m and 3m wide (Figure D.1). The length deformations of the wall are assumed to be 100% restraint. Ambient conditions (formwork, wind, solar radiation) are taken into account, as well as the concrete mix parameters. Observation point for these analyses is the decisive point [Nilson, 2003], which is located slightly above the connecting surface between the old and new part. The decisive point is defined as the point in a structure which is most likely to crack.

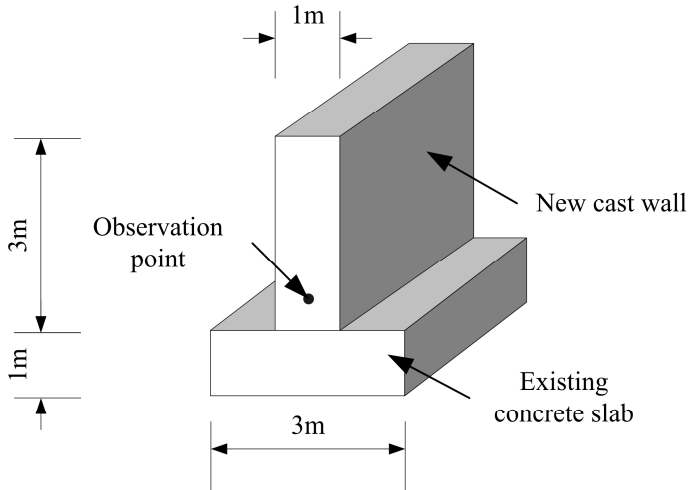


Figure D.1 Geometry of case used for simulations

D.3 Temperature development

Due to the hydration reaction of cement with water, the temperature field in the structure will change, resulting in thermal gradients. The development of hydration heat depends on the mixture design, cement type, amount of cement, dimensions of the structure and environmental conditions (wind, solar radiation, formwork etc.). The temperature field in a hardening concrete structure can be simulated by using the partial differential equation of Fourier which determines the temperature field in time and space:

$$\frac{\delta T}{\delta t} = \frac{\lambda_c}{c_c \cdot \rho_c} \cdot \left[\frac{\delta^2 T}{\delta x^2} + \frac{\delta^2 T}{\delta y^2} + \frac{\delta^2 T}{\delta z^2} + \frac{q(x, y, x, t)}{\lambda_c} \right] \quad [D.1]$$

with:

$T(x,y,z,t)$ = temperature of a centerpoint of an element [K]

t = time [hrs]

λ_c = coefficient of thermal conductivity [W/m.K]

c_c	= specific heat of the concrete [kJ/kg.K]
ρ_c	= density of the concrete [kg/m ³]
$q(x,y,z,t)$	= heat source [kJ/m ³ .h]

The temperature field can be used to calculate the thermal deformations, which can be determined by multiplying the temperature increment by the actual Thermal Dilation Coefficient (TDC):

$$\Delta\varepsilon_T = \Delta T_i * \alpha_T \quad [D.2]$$

with:

$\Delta\varepsilon_T$	= thermal strain increment [-]
ΔT	= temperature increment [K]
α_T	= thermal dilation coefficient [1/K]

In general, the TDC of concrete can be determined from the individual components concrete is composed of:

$$\alpha_T(t) = \sum_i^n \alpha_{T,i} \cdot V_i \quad [D.3]$$

with:

α_T	= thermal dilation coefficient [1/K]
t	= time [hrs]
$\alpha_{T,i}$	= thermal dilation coefficient of the component i [1/K]
V_i	= volume of the component i [m ³ /m ³] (aggregate, sand, cement, water)

For hardened concrete, the TDC is assumed to be constant and can be calculated from the TDC of the components of the concrete. At early ages, the TDC is not a constant value. At very early ages it starts at very high values before it drops significantly during cement hydration (Figure D.2). This is believed to be attributed to the water phase which dominates the fresh state with a very high TDC compared to solids [Bjøntegaard, 1999]. After the formation of a skeleton, it has a solid behaviour with a much lower TDC. For hardening concrete in particular, Hamfler

Appendix D

proposed to calculate the thermal dilation coefficient as a function of relative humidity [Hamfler, 1988]:

$$\alpha_T(\text{RH}) = \alpha_{T0} + 4 \cdot 10^{-6} \text{RH} \quad [\text{D.4}]$$

with:

- α_T = thermal dilation coefficient [1/K]
- α_{T0} = $8 \cdot 10^{-6}$ (dependent of mix design) [1/K]
- RH = relative humidity [%]

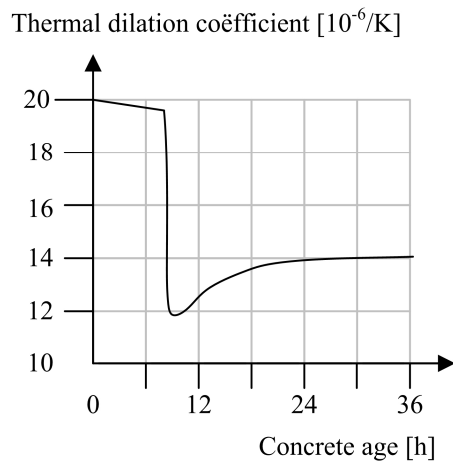


Figure D.2 Thermal dilation coefficient [Nolting, 1989]

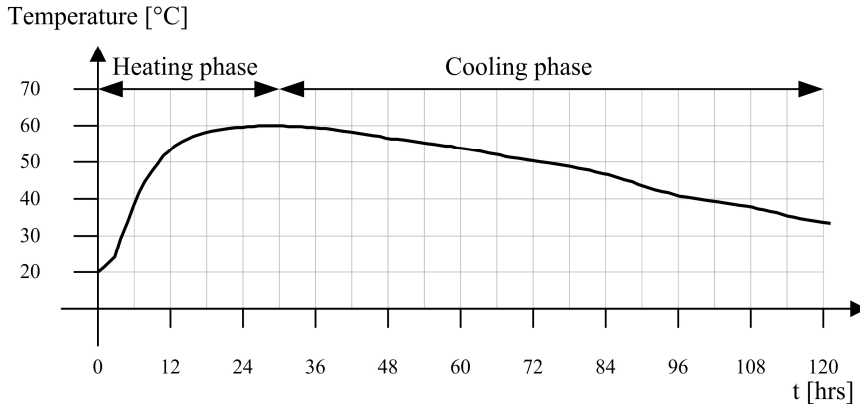


Figure D.3 Simulated temperature development versus time for the observation point

Temperature simulations are carried out for the example of the new concrete wall casted on an existing concrete slab (Figure D.3). The initial temperature was 20°C and during the hardening period, when the hydration process proceeds rapidly, the temperature of the concrete at the observation point reached 60°C after 30 hours of hardening. After reaching the maximum temperature, the structure cools down to the ambient temperature. During the cooling phase, the influence of the ambient temperature on the temperatures at the observation point can be observed.

D.4 Early-age volume changes

Hardening deformations can be divided into chemical shrinkage and autogenous deformations. Both deformations are caused by a changing moisture state in the hardening mixture. Chemical shrinkage is caused by the chemical reaction between the cement and the water. The reaction product has a smaller volume than the volume of its original components. Because chemical shrinkage results in empty pores, it doesn't cause any major damage to the structure.

Autogenous deformations are caused by internal water consumption due to cement hydration. Autogenous deformations can be generally defined as the bulk

Appendix D

deformation of a closed (sealed), isothermal (constant temperature), cementitious material system that is not subjected to external forces [Jensen, 2001]. More theoretical, autogenous deformations are defined as a volume reduction of a hardening element that finds its origin in the fact that the self-desiccation of hardening cement-based material is accompanied by an increase of the capillary forces.

A general, phenomenological, approach to describe autogenous deformations has been developed by Müller [fib, 1999]:

$$\varepsilon_{as}(t) = \varepsilon_{as0}(f_{cm}) \cdot \beta_{as}(t) \quad [D.5]$$

$$\varepsilon_{as0}(f_{cm}) = -\alpha_{as} \cdot \left(\frac{f_{cm}/f_{cm0}}{6 + f_{cm}/f_{cm0}} \right)^{2.5} \cdot 10^{-6} \quad [D.6]$$

$$\beta_{as}(t) = 1 - \exp\left(-0.2 \cdot \left(\frac{t}{t_1}\right)^{0.5}\right) \quad [D.7]$$

with:

- $\varepsilon_{as}(t)$ = autogenous shrinkage at time t [-]
- t = concrete age, or equivalent concrete age t_e [days]
- ε_{as0} = notional autogenous shrinkage coefficient [-]
- $\beta_{as}(t)$ = development of autogenous shrinkage with time [-]
- f_{cm} = mean compressive strength after 28 days ($f_{cm0}=10$ MPa)
- α_{as} = coefficient which depends on the type of cement [-]
600 -700-800 for rapid, normal and slow hardening cement, respectively
- t_1 = 1 day

The Müller approach correlates the autogenous deformations very practical to the type of cement by the coefficient α_{as} . Rapid hardening cement results in higher temperatures and increased autogenous deformations.

D.5 Elasticity

If the thermal deformations and hardening shrinkage are restrained (degree of restraint 'R') instantaneous stress increments will develop. The relation between the deformation and the stress increment is linear and its behaviour can be compared with a mechanical spring. The actual phenomenon is dependent of the age of the concrete when a load is applied. The elastic stress increment, or time independent stress increment, can be calculated directly using the modulus of elasticity. The modulus of elasticity is mostly described as a function of the evolution of the compressive strength, like in CEB-FIP Model Code 1990. In that code the modulus of elasticity is described by empirical relations based on the cube compressive strength development and the maturity concept by:

$$E(t) = \left[\exp \left\{ s \cdot \left[1 - \left(\frac{28}{t} \right)^{1/2} \right] \right\} \right]^{1/2} \cdot \alpha_E \cdot E_{c0} \cdot \left(\frac{f_{cm}}{f_{cm0}} \right)^{1/3} \quad [D.8]$$

with:

- E = modulus of elasticity [MPa]
- t = equivalent concrete age [days]
- s = factor depending on the type of cement (0.2-0.38) [-]
- α_E = coefficient which accounts for the E-modulus of the used aggregate [-]
- E_{c0} = 21500 MPa
- f_{cm} = mean compressive strength after 28 days ($f_{cm0}=10$ MPa)

It is generally accepted that the modulus of elasticity in tension is slightly larger compared to compression [Onken, 1995] [Hagihara, 2002] [Altrushi, 2003]. The measured ratio between both moduli of elasticity varies between 1.05 and 1.2 (Figure D.4), however, for practical applications, both moduli are assumed to be equal.

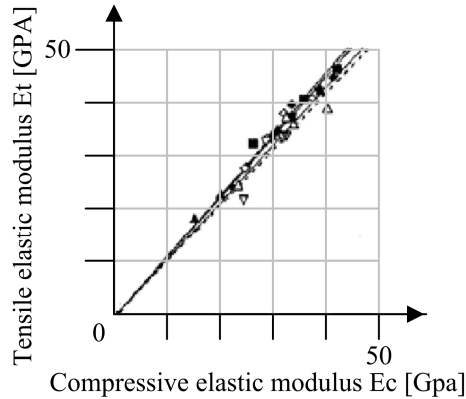


Figure D.4 Relation between modulus of elasticity in tension and compression [Hagihari, 2002]

D.6 Visco-elasticity

Besides the methods presented in paragraph 2.3, a practical method is prescribed in CEB-FIP Model Code 1990, which directs visco-elasticity towards creep of concrete subjected to compressive stresses, although it is accepted that the scope of the model also extends to concrete in tension. The model is valid for ordinary structural concrete ($12 \text{ MPa} < f_{ck} \leq 80 \text{ MPa}$) subjected to a compressive stress $|\sigma_c| \leq 0.4f_{cm}(t_0)$ at an age of loading t_0 and exposed to mean relative humidity's in the range of 40 to 100% at mean temperatures from 5°C to 30°C . Within this range, creep is assumed to be linearly related to stress. The model predicts the mean behaviour of a concrete cross-section.

$$\varphi(t, t') = \varphi_0 \cdot \beta_c(t, t') = \varphi_{RH} \cdot \beta(f_{cm}) \cdot \beta(t_0) \cdot \beta_c(t, t') \quad [\text{D.9}]$$

with:

- φ_0 = notional creep, includes effects of relative humidity loading time and age
- β_c = development of creep after loading, includes cement type and temperature effects

Another practical method is the instant creep method, where creep is taken into account as an instant effect on the stress increments. Stress increments are multiplied by a stress reduction factor. This results in an effective stress increment. The reduction factor applies to both early-age as long term stresses and is taken to reduce stresses by up to 50 per cent [Altoubat, 2001] while a 35 per cent reduction may be more typical [Bamforth, 1982, Vitherana, 1995]. For the practical application described in this chapter, equation 2.8 is applied for each element separately.

D.7 Stress development

The simulated stress development for the observation point is given in Figure D.5. Maximum compressive stresses are reached after 18 hours of hardening during the heating phase of the structure. The shift between the time of maximum temperature and maximum compressive stress is due to the autogenous shrinkage and relaxation of stresses. After reaching the maximum compressive stress for the observation point, stresses starts to decrease. The sign of stresses change from compression into tension after about 54 hours and the element wil crack if tensile stresses become to heigh. Fromt then, crack widths can be controlled by adding reinforcement.

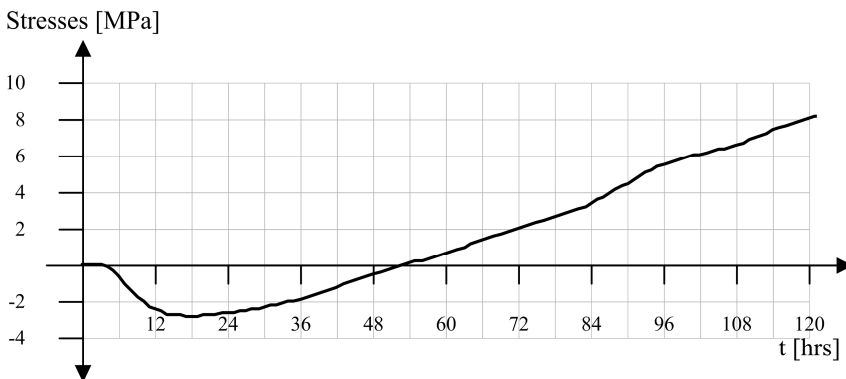


Figure D.5 Simulated stress development versus time for the observation point

D.8 Calculating reinforcement

To determine a reinforcement ratio to control the crack widths in the wall, a criterion has to be adopted, which marks the moment of cracking of an element. This criterion is defined as the cracking criterion. Several cracking criteria can be distinguished, like a temperature criterion, a strain criterion, energy criterion and a stress criterion. Bernander recommended to focus on the stress related criteria because of its reliability [Bernander, 1973, 1982, 1994]. The stress criterion is the ratio between the stress level in the concrete at the moment of cracking and the actual tensile strength of the concrete:

$$\xi = \frac{\sigma(t)}{f_{ctm;spl}(t)} \quad [D.10]$$

with:

- ξ = stress based cracking criterion [-]
- $\sigma(t)$ = actual stress at time 't' [N/mm²]
- $f_{ctm;spl}(t)$ = actual tensile splitting strength at time 't' [N/mm²]

Following values for the cracking criterion for plain concrete are developed in previous research:

- $\xi = 0.75$ normal strength concrete [Lokhorst, 2001]
- $\xi = 0.6$ high strength concrete [Sule, 2003]
- $\xi = 0.5$ [Emborg, 1994]
- $\xi = 0.45$ practice [Sule, 2003]

The influence of reinforcement on stress development and cracking can be taken into account by a cracking criterion which marks the beginning of micro-cracking [Sule, 2003]. The micro-cracking criterion is determined by:

$$\xi_{mc} = \left(\frac{c}{h} + \frac{\phi}{\omega} \right) \quad [D.11]$$

with:
156

- ζ_{mc} = micro-cracking criterion [-]
 c = concrete cover [m]
 h = side length of concrete prism surrounding a rebar [m]
 ϕ = diameter of reinforcement bars [m]
 ω = reinforcement ratio [-]

After the stresses in the concrete exceed the micro-cracking criterion, the micro cracks start to develop. Due to the micro-cracks, the concrete loses stiffness, what is taken into account by multiplying the stress increment by a reduction factor k :

$$k = \frac{c \cdot \omega}{\phi} \cdot k_1 \quad [D.12]$$

with:

- k = reduction factor for stress increments after micro-cracking [-]
 c = concrete cover [m]
 ω = reinforcement ratio [-]
 ϕ = diameter of reinforcement bars [m]
 k_1 = factor dependent of concrete cover, 0.0010 for $c = 20\text{mm}$, 0.0015 for $c = 37.5\text{mm}$ and 0.0025 for $c = 42\text{mm}$

If a not completely developed cracking pattern is assumed (most likely for cracking induced by restrained deformations), the crack width can be calculated from the strain difference between the concrete and the reinforcement at the moment of cracking of the concrete. For the crack width, it holds that [Noakowski, 1978]:

$$w = \frac{\phi}{4 \cdot \omega_s \cdot E_s} \cdot \left[\sigma_{scr} - \frac{f_{ctm}}{2} \left(\frac{1}{\omega_s} + n \right) \right] \quad [D.13]$$

with:

- w = crack width [mm]
 ϕ = diameter of the reinforcement bars [mm]
 ω_s = reinforcement ratio [%]

Appendix D

- E_s = modulus of elasticity of the reinforcement [MPa]
- σ_{scr} = steel stress in the crack [MPa]
- f_{ctm} = tensile strength of the concrete [MPa]
- n = ratio between elastic modulus of concrete and reinforcement [-]

The steel stress in the crack can be calculated based on equilibrium at the moment of cracking:

$$\sigma_{scr} = f_{ctm} \cdot \left(\frac{1}{\omega_s} + n \right) \quad [D.14]$$

If, for example, for an actual tensile strength at the moment of cracking (2.5 MPa) and actual modulus of elasticity at the moment of cracking (36,7 GPa), the reinforcement ratio, needed to control the maximum crack width at an arbitrary value of 0.20mm, is calculated at a value of 0.966% for reinforcement bars of $\phi 12$ mm. Since the cracking criterion, the moment of cracking, the actual tensile strength and the modulus of elasticity are correlated; the cracking criterion and the reinforcement ratio are correlated as well. For a representative range of cracking criterions, ranging from 0 to 1, the minimum required reinforcement has been calculated. The results are presented in Figure D.6.

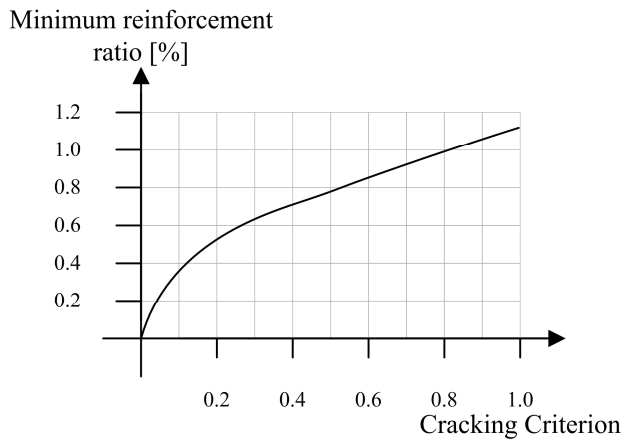


Figure D.6 Reinforcement ratio as a function of cracking criterion.

It is observed that the lower the value of the cracking criterion, the lower the values of the required reinforcement ratio, needed to obey the ultimate crack width of 0.20mm (arbitrary). This can be attributed to the lower tensile strength and modulus of elasticity at younger ages of the concrete. So, in case it is uncertain which cracking criterion should be adopted to calculate the reinforcement ratio, it is recommended to use a higher cracking criterion, which implicitly results in a higher reinforcement ratio.

D.9 Probability of cracking

The probability of cracking can be deduced from the development of stresses in an element and the development of the strength of that element. In general, three levels of calculation procedures are distinguished for probability estimations:

Level I	Deterministic design formulas;
Level II	Linearization of the reliability function;
Level III	Consideration of probability density functions of all load and resistance variables.

Nowak [Nowak, 2000] distinguished also a fourth level, where the total expected cost of a design is used as an optimization criterion, however, this level is not considered in this thesis.

D.9.1 Level 1: Deterministic design formulas

A probabilistic calculation on the first level is a design-based method, based on local codes, which assumes an element sufficiently reliable against cracking if a certain margin exist between representative values of strength and stresses. In this case no real probabilities of cracking are calculated. The margin will be achieved by taking into account partial safety factors. The values of the safety factors can be determined on higher levels of calculation (Level II or Level III). Based on level II calculations, Lokhorst developed a design graph (Figure D.7) which relates the required probability of cracking to an allowable maximum stress/strength ratio [Lokhorst, 2001].

Appendix D

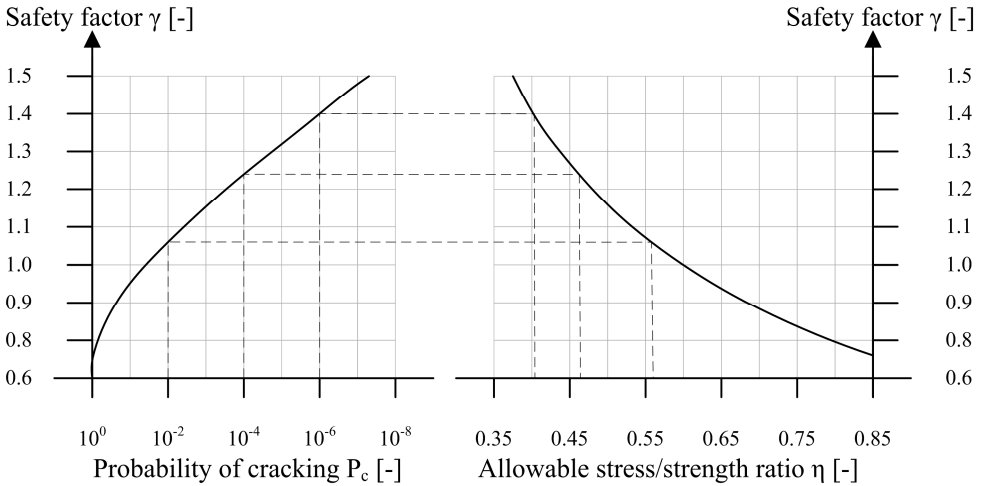


Figure D.7 Design graph for the determination of the maximum allowable stress/strength ratio in a hardening concrete structure. The allowable stress/strength ratio is coupled with a chosen probability of cracking [Lokhorst, 2001]

D.9.2 Level II: First Order Second Moment

Because of its simplicity, the first order second moment method is a frequently used method to calculate the probability of cracking for hardening concrete structures. Since only stress (Q) and strength (R) developments are taken into account, the first order second moment method can be solved analytical. The first two moments of stress and strength development (mean value and standard deviation) are applied to calculate the probability of cracking by using a standard normal distribution. The probability of cracking is calculated by:

$$P(R - Q < 0) = \Phi(-\beta) \quad [D.15]$$

Where β is the reliability index of the system:

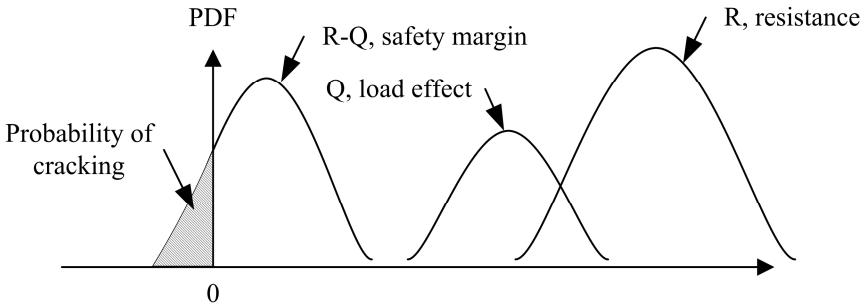


Figure D.8 Probability density functions of load, resistance and safety margin

$$\beta = \frac{\mu_{R-Q}}{\sigma_{R-Q}} \quad [D.16]$$

with:

$$\mu_{R-Q} = \text{safety margin of the system } \mu_{R-Q} = \mu_R - \mu_Q \quad (\text{Figure D.8}) \quad [D.17]$$

$$\sigma_{R-Q} = \text{standard deviation of limit state function } \sigma_{R-Q} = \sqrt{\sigma_R^2 + \sigma_Q^2} \quad [D.18]$$

D.9.3 Level III: Crude Monte Carlo approach

The Crude Monte Carlo approach is a technique that can be used to generate numerical results without doing any actually physical testing. The Monte Carlo approach is based on repetitions. A lot of simulations are performed, where the input parameters are varied for each simulation separately according to particular probability density functions. Results of previous tests, values from literature and other information can be used to establish the probability density functions of the input parameters of the early age cracking problem. Next, this probability distribution information can be used to generate samples of numerical data. The amount of simulations depends on the required accuracy of the result. The basic steps of the crude Monte Carlo approach are as follows:

Appendix D

1. determine the required number of simulations to obtain a sufficient reliable result (required reliability 95% ($V_p=0.05$), maximum relative error 0.1)

$$n > 400 \cdot \left(\frac{1}{P_f} - 1 \right) \quad [D.19]$$

2. randomly generate a set of input parameters using probability density functions of the input parameters
3. calculate safety margin $Y = R - Q = \text{strength (R)} - \text{stress (Q)}$
4. store the calculated safety margin
5. repeat steps 2-4 until a sufficient number (n) of Y values have been generated
6. calculate the probability of failure ' P_f ':

$$P_f = \frac{\text{number of times } Y < 0}{\text{total numbers of simulated } Y \text{ values}} \quad [D.20]$$

Disadvantage of the Crude Monte Carlo approach is the incapability of the models which predict temperature development and mechanical properties included in the calculation procedure like development of strength, stiffness and shrinkage to predict variation the results accurately. Variation of the input parameters into the models, results in an underestimation of variation of those properties (Table D.1). The model which describes e.g. the development of the tensile strength, results in an underestimated variation of the development of the tensile strength (7%) compared to variation of tensile strength as found in the literature (20%). An under estimation of variation of included models will directly result in an under estimation of variation of probability of cracking. Incapability of models can be ascribed to model uncertainties. Mathematical models are generated by use of idealized models, in which physical variables are neglected. Reason that some physical parameters are neglected can be either that they are unknown or they are identified to have quantitatively unknown influence and interact with other variables [Ditlevsen, 2005]. Those idealised mathematical models are fitted to experimental observations of some samples and induce a systematic error at any

162

given location of the failure surface, which can be decreased by a more detailed model formulation, but a systematic error of unknown size, due to fluctuations inherent of the observation method, will always be present. It should be taken into account quantitatively in the reliability analysis by use of suitable judgemental variables.

Since the existing models which are implemented in the Crude Monte Carlo approach are not capable to describe the variation of properties of hardening concrete sufficiently reliable, there is need for models which are able to describe the variation. To bridge this gap, a Simplified Monte Carlo approach is developed. In this Simplified Monte Carlo approach all input parameters are applied as constant values. Instead of variation of all input parameters, now the results of models for mechanical properties, concrete deformations and degree of restrained are varied, according to e.g. test results of Round Robin test programs (Table D.1). The difference of implementation between the Crude Monte Carlo approach and Simplified Monte Carlo approach is shown in Figure D.9.

Table D.1 Coefficients of variations according to literature versus values determined by the Crude Monte Carlo approach

	Literature	Monte Carlo approach
Temperature	20%	5%
Compressive strength	10%	2%
Tensile strength	20%	7%
Modulus of elasticity	15%	8%
Autogenous deformations	30%	11%

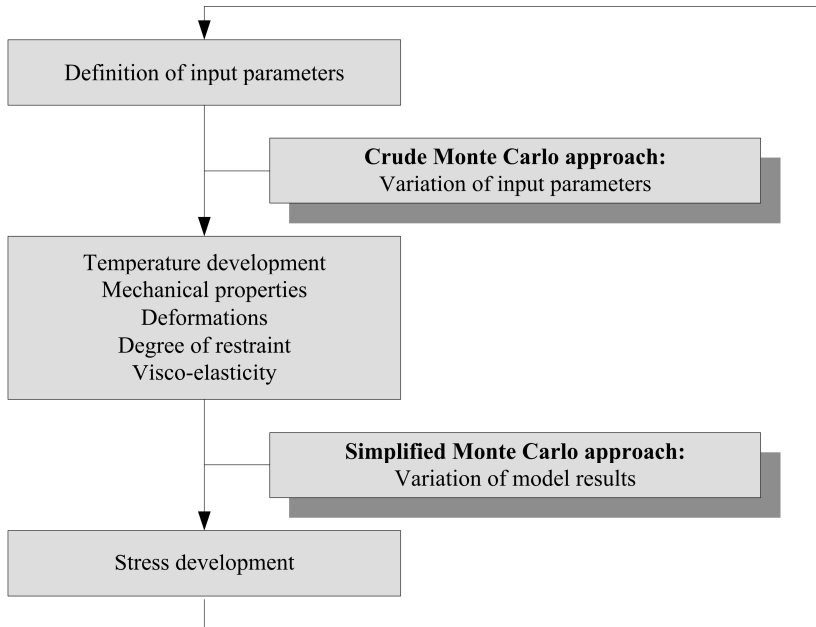


Figure D.9 Difference between Crude Monte Carlo approach and Simplified Monte Carlo approach

D.10 Discussion

Comparing the three levels of probabilistic methods, it must be mentioned that the first level does not result in a purely probability of cracking. The level I calculation indicates whenever the structure is assumed to be sufficient reliable against cracking. In this case, this is until 77 hours of hardening. Comparing the probability of cracking for the level III and level II calculation (Figure D.10), the results show a slight deviation, especially for the lower and higher probabilities of failure. Around the average values, the probabilities are the same, which indicates that differences in probabilistic behaviour of structures might exist when considering parameter values other than the average value. Differences between the probabilities of failure calculated according to the level II and III methods turned out to reach a maximum increase of about 17% with respect to the value of the probability of crack occurrence. When considering the moment of cracking, for all three methods, i.e. Level I, II and III, a mean value of 88 hours is predicted. When

examining the moment of cracking in more detail a time window indicated by the higher level probabilistic approach methods (II and III) it turns out that ranges of likelihood can be calculated for the moment of cracking (Table D.2). These methods provide more insight of the development of the probability of cracking in relation to the likelihoods of crack occurrence. For the building practice, this information can be very favourable.

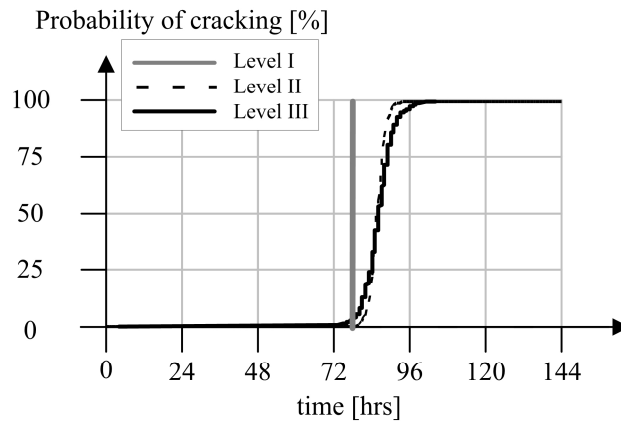


Figure D.10 Comparison of results of probabilistic methods

Table D.2 Overview of the results of the probabilistic methods

Method	Range for moment of cracking [hrs]	Note:
Level I, PSF	77 and 88	$\gamma_R \times \gamma_S = 0.75$ and 1.00 resp.
Level II, FOSM	Between 76 and 100	For $P_f = 0\%$ to 100%
Level III, MC	Between 72 and 102	Based on 400 simulations

Summary

Microstructure and transport phenomena in visco-elastic modelling of hardening cementitious materials.

Since the durability depends, among other things, on the quality of the concrete and presence of cracks, it is necessary to calculate the probability of cracking in hardening concrete as reliable as possible in case of durability predictions. In this thesis, it is investigated how the accuracy of stress prediction in hardening concrete can be improved by a more detailed description of microstructural and transport phenomena.

First it is described how hydration of cement and the microstructural development can be described. Two basically different models for cement hydration are explained, which introduced the possibility to couple results and information from the simulations with accurately property development of hardening concrete (strength, stiffness, porosity), however, the relation between visco-elastic behavior of hardening concrete and the microstructural development is still under development.

Some history of development of visco-elastic models is presented, from which it turned out that there is a need for a step forward in understanding and explicit modeling of visco-elastic behavior of hardening concrete, by taking into account the microstructural development of hardening cement paste and moisture movements in order to make stress predictions in hardening concrete elements more accurate and reliable.

Summary

The moisture state is modeled explicitly in the solidification theory by including hollow permeable shells in a microstructural hydration model. A hollow shell, or annular space, is defined as the zone between an anhydrous cement grain and the gel shell. This space is filled with water. The Shell Deformation Model (SDM) as developed in this thesis relates the time dependent deformations of a loaded cement paste to the transport of load bearing water inside the shell of cement gel to the capillary pores. The model assumes equal time dependent deformations for cement paste loaded in tension and compression. From the simulated results, it turned out that the fineness of cement does not influence the visco-elastic behavior of hardening concrete.

In order to obtain reliable and accurate results from the proposed model, the moisture state in the capillary pores is considered accurately. For this purpose, moisture movements are modeled at microlevel. Due to the inhomogeneous distribution of cement particles in the cement paste between the aggregates, pressure differences exist between water in the pores of cement paste located near the aggregates and the water in the pores of cement paste in-between the aggregates. A model is developed which describe pressure driven moisture movements based on the conservation of volume. The influence of capillary water transport on visco-elastic behaviour of hardening cement paste is studied. Taking those movements into account, an influence up to 8% on the visco-elastic behaviour is observed. The differences are bigger for higher water/cement ratio's and arise earlier for higher Blaine values of the used cement.

As a first validation of the proposed model, two test series are performed. First test serie contains sustained loading experiments. The results are used to study the influence of the cement fineness and to study the influence of the load sign. Result of this program is that no influence on the visco-elastic behaviour can be ascribed to both parameters. Second test serie contains degree of restraint experiments to validate the Shell Deformation Model. For three mixtures with different cement finenesses, it turned out that stress predictions are predicted more accurate by using the proposed Shell Deformation Model (SDM) compared to a model previously proposed.

Samenvatting

Microstructuur en transport fenomenen bij het modelleren van visco-elastisch gedrag van verhardende cementgebonden materialen.

Aangezien de duurzaamheid van betonnen constructies vooral afhangt van de kwaliteit van het beton en de aanwezigheid van scheuren, is het noodzakelijk voor duurzaamheidsvoorspellingen de kans op scheuren zo nauwkeurig mogelijk te berekenen. In dit proefschrift is onderzocht hoe de nauwkeurigheid van het berekenen van spanningen in verhardend beton kan worden verbeterd door het gebruik van meer gedetailleerde microstructuur en transport fenomenen.

Om te beginnen is beschreven hoe de hydratatie van cement en de ontwikkeling van microstructuren kan worden beschreven. Twee in de basis verschillende modellen voor cement hydratatie worden beschreven, welke de mogelijkheid geven om resultaten en informatie van de simulaties te koppelen aan accuraat beschreven ontwikkeling van de eigenschappen van verhardend beton (sterkte, stijfheid, porositeit etc). De relatie tussen visco-elastisch gedrag van verhardend beton en de ontwikkeling van microstructuren is echter nog in ontwikkeling.

De geschiedenis van de ontwikkeling van visco-elastische modellen is weergegeven, waaruit volgt dat er behoefte is om een stap vooruit te maken in het beter begrijpen en expliciet modelleren van visco-elastisch gedrag van verhardend beton, door de ontwikkeling van microstructuren en vochttransport hierin te betrekken. Zo worden simulaties van spanningen in verhardend beton betrouwbaarder en accurater.

Samenvatting

De vochthuishouding is expliciet gemodelleerd in de solidificatie theorie door het in rekening brengen van holle schalen in een microstructureel hydratatie model. Een holle schaal is gedefinieerd als de zone tussen een ongehydrateerde cement korrel en het hydratatie product. Deze ruimte is gevuld met water. Het in deze thesis ontwikkelde “Shell Deformation Model” (SDM) relateert de tijdsafhankelijke vervormingen van een belast cement pasta aan het transport van gespannen water in de schaal naar de capillaire poriën. Er is aangenomen dat een gelijk tijdsafhankelijk gedrag optreedt voor cement pasta belast onder trek en voor cement pasta belast onder druk. Uit de gesimuleerde resultaten blijkt ondermeer dat de fijnheid van het cement geen invloed heeft op het visco-elastische gedrag van beton.

Om betrouwbare en accurate resultaten te verkrijgen met het voorgestelde model, is het van belang de vochthuishouding in de capillaire poriën nauwkeurig te beschrijven. Voor dit doeleinde zijn vochttransporten op microniveau beschreven. Door de niet homogene verdeling van cement pasta tussen het toeslagmateriaal, ontstaan drukverschillen tussen water in de poriën nabij toeslagmateriaal en water in de poriën tussen het toeslagmateriaal. Een vochttransport model is ontwikkeld gebaseerd op de wet van behoud van volume wat door drukverschillen aangedreven vochttransport beschrijft. De invloed van vochttransport op het visco-elastisch gedrag van verhardende cement pasta is bestudeerd. Het in rekening brengen van deze vocht verplaatsingen geeft een tot 8% gewijzigd visco-elastisch gedrag. De verschillen zijn groter voor hogere water/cement factoren en ontstaan in een vroeger stadium voor grotere fijnheden van het cement.

Als eerste validatie van de ontwikkelde modellen zijn twee test series uitgevoerd. De eerste serie bestond uit proefstukken onder een constante belasting. Hiermee is de invloed van de fijnheid van het cement en de aard van belastingen (trek of druk) bestudeerd. Resultaat is dat geen invloed van een van deze parameters kan worden toegeschreven op het visco-elastische gedrag. De tweede serie zijn de experimenten aan proefstukken van verhardend beton onder verhinderde vervorming om het “Shell Deformation Model” te valideren. Voor drie verschillende mengsels met verschillende cement fijnheden blijkt dat de spanningsontwikkeling met het ontwikkelde Shell Deformation Model (SDM) beter beschreven kan worden dan met een eerder ontwikkeld model.

Acknowledgements

This chapter of my thesis is the shortest, but probably also the most important chapter of all. This is the chapter where I have the possibility to thank all the people who made it possible for me to finish my PhD and to come to this result.

The research is carried out at the section of Materials and Environment, Faculty of Civil Engineering and Geosciences at Delft university of Technology, financed by Delft Cluster, the Ministry of Infrastructure and Environment and TNO DIANA b.v. I would like to thank my supervisors, my colleagues and the people from the laboratory for there help, discussions and collaboration during these years. The experiments of this study could not have been performed without the help and technical expertise of the laboratory personnel, as of Ron Mulder, Ton Blom, Eric Horeweg, Edwin Scharp, Fred Schilperoort, Ger Nagtegaal and master student Ralph Goed, for the casting of the specimens and conducting the experiments. Especially thanks to Eric Horeweg († 2007), for his diligence and dedication to my experiments, I won't forget you.

Thanks to all my colleagues I met at the university, and especially the PhD researchers. Thanks for the social and non technical discussions, coffee breaks and drinks. Thanks Sonja, Ilse, Yuguang, Hooman, Bas, Lena, Petra, Eelke, Cees, Eddie, Roy. Without you all, I would never had such a nice time at university.

Thanks to the people, who encouraged me during my study time. First of all, my mom and dad, but also Wil Peperkamp and Ane de Boer.

Thanks also to my family and friends, for your support during my study. Especially at the end, I wasn't always involved in family live, but you all accepted that and helped me through.

Finally I want to thank my girlfriend Silvia. I want to apologize for all the nights, weekends and holidays I spent to my research and for the time I wasn't that happy and social. I promis I will compensate for this. I hope it was al worth it!

Acknowledgements

Curriculum vitae



Name: Herbert Wenceslaus Maria van der Ham
Date of Birth: September 28, 1978
Place of Birth: Teteringen, the Netherlands

- 1990-1994 High School, St. Jozef MAVO, Breda.
MAVO diploma, 1994
- 1994-1998 Civil Engineering, Middelbaar Technische School, Koning Willem I college, 's-Hertogenbosch, the Netherlands.
MTS Diploma, 1998
- 1998-2001 Civil Engineering, Technische Hogeschool 's-Hertogenbosch, the Netherlands. Main disciplines: Structural mechanics, steel and concrete structures, Thesis on highrise buildings.
Diploma Bachelor of Structures, 2001
- 2001-2004 Civil Engineering, Delft University of Technology, the Netherlands. Main disciplines: Structural mechanics, materials and concrete structures, Thesis on reinforcement optimisation in skew plate bridges, Diploma Master of Science, 2004
- 2004-2005 Iv-Infra b.v., Nieuwegein, the Netherlands
Structural engineer of concrete structures
- 2005-2010 Materials and Environment, Faculty of Civil Engineering and Geosciences, Delft University of Technology, the Netherlands.
PhD study on microstructure and transport phenomena in visco-elastic modelling of hardening cementitious materials
- 2009-present Iv-Infra b.v., Nieuwegein, the Netherlands
Scientific researcher concrete structures

Publications related to this research

Ham, H.W.M. van der, Koenders, E.A.B., Breugel, K. van, (2006): “Monte Carlo Calculations for Hardening Concrete”. European Symposium on Service Life and Serviceability of Concrete Structures ESCS-2006, Concrete Association of Finland, Espoo, Finland, ISBN 952-5075-79-6, pp. 189-194

Ham, H.W.M. van der, Koenders, E.A.B., Breugel, K. van, (2006): “Level III calculations for hardening concrete elements”, ASRANet, Integrating Structural Analysis, Risk & Reliability, Glasgow, UK, ISBN 0-9553550-0-1

Braam, C.R., Ham, H.W.M. van der, Koenders, E.A.B., (2006): “Early-age shrinkage control and strength development of concrete”, Volume Changes of Hardening Concrete: Testing and Mitigation, Lyngby, Denmark, ISBN 2-35158-004-4, pp. 185-194

Ham, H.W.M. van der, Koenders, E.A.B., Breugel, K. van, (2006): “Visco-elastic model evaluation in view of crack risk assessments for hardening concrete elements”, Service Life Design for Underground Structures, Shanghai, China, ISBN 7-5608-2659-8, pp. 316-324

Ham, H.W.M. van der, Koenders, E.A.B., Breugel, K. van, (2007): “Experimental study on scatter of input parameters for MC calculations for hardening concrete elements”, CONSEC Fifth International Conference on Concrete under Severe Conditions Environment and. Loading, Tours, France, ISSN 1626-4704, pp. 1053-1060

Ham, H.W.M. van der, Koenders, E.A.B., Breugel, K. van, (2007): “Mitigating autogenous shrinkage of hardening concrete, FRaMCoS 6th International Conference on Fracture Mechanics of Concrete and Concrete Structures, Catania, Italy, ISBN 978-0-415-44617-4, pp. 1319-1325

Koenders, E.A.B., Ham, H.W.M. van der, Breugel, K. van, (2007): “Modern statistical methods for accessing the hardening process of concrete”, Springer publishers, Stuttgart, Germany, ISBN 978-3-540-72447-6, pp. 471-478

Ham, H.W.M. van der, Koenders, E.A.B., Breugel, K. van, (2007): “Mitigating autogenous shrinkage in hardening cement paste by SAP” SEMC2007 The third international conference on structural engineering, mechanics and computation, Cape Town, South Africa, ISBN 978-90-5966-054-0

Ham, H.W.M. van der, Koenders, E.A.B., Breugel, K. van, (2007): “Stochastic variability of input parameters for crack calculations of hardening concrete elements”, The fourth International Structural Engineering & Construction Conference, Melbourne, Australia, ISBN 978-0-415-45756-9, pp. 489-496

Ham, H.W.M. van der, Koenders, E.A.B., Breugel, K. van, (2008): “Inter-particle moisture movement during cement hydration”, Conference on Concrete Modelling, Delft, The Netherlands, ISBN 978-2-35158-060-8, pp. 611-618

Ham, H.W.M. van der, Koenders, E.A.B., Breugel, K. van, (2008): “Cracking criterions for hardening concrete structures analysed by a probabilistic approach”, ASRANet, Integrating Structural Analysis, Risk & Reliability, Athens, Greece, ISBN 978-0-9553550-2-8

Ham, H.W.M. van der, Koenders, E.A.B., Breugel, K. van, (2008): “Visco-elastic properties of concrete mixtures including Super-Absorbent-Polymers”, 8th International Conference on Creep, Shrinkage and Durability of Concrete and Concrete Structures, Shima City, Japan

Ham, H.W.M. van der, Koenders, E.A.B., Breugel, K. van, (2008): “Creep model uncertainties in early-age concrete simulations”, 8th International Conference on Creep, Shrinkage and Durability of Concrete and Concrete Structures, Shima City, Japan

Ham, H.W.M. van der, Koenders, E.A.B., Breugel, K. van, (2010): “Visco-elastic model for hardening concrete based on a confined water theory”, Conference on Concrete Modelling, Lausanne, Switzerland

Stellingen

Behorend bij het proefschrift

“microstructuur en transport fenomenen bij het modelleren van visco-elastisch gedrag van verhardende cementgebonden materialen”

H.W.M. van der Ham

7 februari 2011

- 1 In verhardend beton wordt het visco-elastisch gedrag gedomineerd door andere mechanismen dan in verhard beton. *(dit proefschrift)*
- 2 De ontwikkeling van de microstructuur in combinatie met de veranderende vochtthuishouding vormen sleutelparameters voor de beschrijving van het visco-elastisch gedrag van verhardende cementgebonden materialen. *(dit proefschrift)*
- 3 Behalve invloed op de ontwikkeling van de hydratatiegraad, heeft de fijnheid van het cement geen invloed op het visco-elastisch gedrag van verhardend beton. *(dit proefschrift)*
- 4 De invloed van vochttransport tussen cementpasta nabij het toeslagmateriaal (ITZ) en de cementpasta tussen toeslagkorrels (bulk) op de eigenschappen van beton is groter als er meer water in het mengsel aanwezig is. *(dit proefschrift)*
- 5 Door in het begin van het ontwerpproces van een betonconstructie meer aandacht te besteden aan het verhardingsproces van beton, kunnen duurzamer betonconstructies worden verkregen.
- 6 Paradigma's kunnen niet minderwaardig zijn ten opzichte van elkaar, ze kunnen echter wel verschillen ten gevolge van een ander denkkader.
- 7 Door het stellen van de juiste vragen ben ik wetenschapper geworden. [Isidor I. Rabi (1898-1988), Nobelprijswinnaar Natuurkunde]
- 8 Ook al lijkt het overdag dat we alles onder controle hebben, 's nachts kan het toch behoorlijk spoken.
- 9 Devaluatie van diploma's wordt veroorzaakt door het terugdringen van voortijdige uitval van studenten.
- 10 Teneinde ervan verzekerd te zijn dat studenten rijp zijn voor de praktijk, dienen docenten te beschikken over voldoende praktische ervaring.

Deze stellingen worden opponeerbaar en verdedigbaar geacht en zijn als zodanig goedgekeurd door de promotor, prof. dr. ir. K. van Breugel.

Propositions

Accompanying the Ph.D. Thesis

“Microstructure and transport phenomena in visco-elastic modelling of hardening cementitious materials”

H.W.M. van der Ham

February 7th, 2011

- 1 The visco-elastic behaviour of hardening concrete is dominated by other mechanisms compared to the visco-elastic behaviour of hardened concrete. (*this thesis*)
- 2 Microstructure development combined with the changing moisture state are key parameters in the description of the visco-elastic behaviour of hardening cementitious materials. (*this thesis*)
- 3 Except its influence on the degree of hydration, the cement fineness has no influence on the visco-elastic behaviour of hardening concrete. (*this thesis*)
- 4 The influence of moisture transport between ITZ and bulk paste on concrete properties is more pronounced if more water is available in the mixture. (*this thesis*)
- 5 Giving more attention to the hardening process of concrete in the begin stage of the engineering process, results in more durable concrete structures.
- 6 Paradigms cannot be inferior to each other, however they can be different related to a different conception.
[Thomas S. Kuhn (1922-1996)]
- 7 Asking the right questions made me a scientist.
[Isidor I. Rabi (1898-1988), Nobel Prize for Physics]
- 8 Although it seems we have everything under control in daytime, at night, it can be very haunted.
- 9 Devaluation of diplomas is caused by pushing back the premature loss of students.
- 10 To be sure that students are competent for practice, teachers should have sufficient practical experience.

These propositions are regarded as opposable and defendable, and have been approved as such by the supervisor, prof. dr. ir. K. van Breugel.